Tropical Sea Surface Temperatures following the Middle Miocene Climate Transition from Laser-Ablation ICP-MS analysis of glassy foraminifera

Michael Grahame Nairn[1,1], Caroline H. Lear[1,1], Sindia Sosdian[1,1], Trevor Bailey[2,2], and Simon Beavington-Penney[3,3]

[1]Cardiff University
[2]National Museums and Galleries of Wales
[3]University of Manchester

December 1, 2022

Abstract

The mid-to-late Miocene is proposed as a key interval in the transition of the Earth's climate state towards that of the modern-day. However, it remains a poorly understood interval in the evolution of Cenozoic climate, and the sparse proxy-based climate reconstructions are associated with large uncertainties. In particular, tropical sea surface temperature (SST) estimates largely rely on the unsaturated alkenone Uk37 proxy, which fails to record temperatures higher than 29@C, the TEX86 proxy which has challenges around its calibration, and Mg/Ca ratios of poorly preserved foraminifera. We reconstruct robust, absolute, SSTs between 13.5 Ma and 9.5 Ma from the South West Indian Ocean (paleolatitude ~5.5@S) using Laser-Ablation (LA-) ICP-MS microanalysis of glassy planktic foraminiferal Mg/Ca. Employing this microanalytical technique, and stringent screening criteria, permits the reconstruction of paleotemperatures using foraminifera which although glassy, are contaminated by authigenic coatings. Our absolute estimates of 24-310C suggest that SST in the tropical Indian Ocean was relatively constant between 13.5 and 9.5 Ma, similar to those reconstructed from the tropics using the Uk37 alkenone proxy. This finding suggests an interval of enhanced polar amplification between 10 and 7.5 Ma, immediately prior to the global late Miocene Cooling.

Michael G. Nairn[1], Caroline H. Lear[1], Sindia M. Sosdian[1], Trevor R Bailey[2], and Simon Beavington-Penney[3]

[1]School of Earth and Environmental Sciences, Cardiff University, Cardiff, UK,

[2]Department of Natural Sciences, Amgueddfa Cymru, National Museum Wales, Cathays Park, Cardiff,

[3]BG Group, 100 Thames Valley Park Drive, Reading, RG6 1PT, UK*

Corresponding author: Michael G. Nairn (NairnMG@cardiff.ac.uk)

*Current address: Department of Earth and Environmental Sciences, The University of Manchester, Williamson Building, Oxford Road, Manchester, M13 9PL, UK.

Key Points:

- Laser-Ablation ICP-MS facilitates absolute sea surface temperature reconstructions using foraminifera with diagenetic coatings.
- Tropical sea surface temperatures remained relatively stable at 24-31°C following the Miocene Climate Transition.
- Development of an increased latitudinal temperature gradient began prior to the Late Miocene Cooling.

Abstract

The mid-to-late Miocene is proposed as a key interval in the transition of the Earth's climate state towards that of the modern-day. However, it remains a poorly understood interval in the evolution of Cenozoic climate, and the sparse proxy-based climate reconstructions are associated with large uncertainties. In particular, tropical sea surface temperature (SST) estimates largely rely on the unsaturated alkenone $U^{k}{}_{37}$ proxy, which fails to record temperatures higher than 29@C, the TEX_{86} proxy which has challenges around its calibration, and Mg/Ca ratios of poorly preserved foraminifera. We reconstruct robust, absolute, SSTs between 13.5 Ma and 9.5 Ma from the South West Indian Ocean (paleolatitude ~5.5@S) using Laser-Ablation (LA-) ICP-MS microanalysis of glassy planktic foraminiferal Mg/Ca. Employing this microanalytical technique, and stringent screening criteria, permits the reconstruction of paleotemperatures using foraminifera which although glassy, are contaminated by authigenic coatings. Our absolute estimates of 24-310C suggest that SST in the tropical Indian Ocean was relatively constant between 13.5 and 9.5 Ma, similar to those reconstructed from the tropics using the $U^{k}{}_{37}$ alkenone proxy. This finding suggests an interval of enhanced polar amplification between 10 and 7.5 Ma, immediately prior to the global late Miocene Cooling.

1 Introduction

The mid-late Miocene is an important interval in the evolution of global climate through the Cenozoic, representing a key period in the transition out of the warm, dynamic climate state of the Miocene Climatic Optimum (MCO) into a more stable unipolar icehouse world (*Badger et al.* , 2013; *Foster et al.* , 2012; *Greenop et al.* , 2014; *Sosdian et al.* , 2018). Despite being characterized by similar to modern day atmospheric CO_2 concentrations (*Foster et al.* , 2012; *Sosdian et al.* , 2018; *Super et al.* , 2018), middle Miocene mean global temperatures were likely significantly warmer than the modern day (*Pound et al.* , 2011;*Rousselle et al.* , 2013). This has been used to suggest a decoupling of global temperature and atmospheric CO_2forcing (*LaRiviere et al.* , 2012; *Pagani et al.* , 1999), a characteristic which general circulation models struggle to simulate (*Knorr et al.* , 2011; *von der Heydt and Dijkstra* , 2006). It has also been suggested that the late Miocene was an additional important key step in the transition to our modern climate state, as high latitudes cooled more than low latitudes, leading to a marked steepening of latitudinal temperature gradients (*Herbert et al.* , 2016).

The late Miocene Cooling (LMC) between ~ 7.5 and 5.5 Ma was a global phenomenon (*Herbert et al.* , 2016) perhaps associated with decreasing atmospheric pCO_2 (*Stoll et al.* , 2019). The increase in the equator to pole surface temperature gradients was not associated with an increase in the benthic foraminiferal oxygen isotope record, implying that it occurred in the absence of a large increase in continental ice volume (*Herbert et al.* , 2016). Polar amplification in the LMC is consistent with estimates for other time intervals (e.g., *Cramwinckel et al.* (2018)). However, the LMC was also preceded by a significant cooling of mid to high southern and northern latitudes, a heterogenous cooling at high northern latitudes, and a muted, limited cooling in the tropics (*Herbert et al.* , 2016). This heterogenous cooling perhaps suggests an unusually high polar amplification factor for the interval immediately preceding the LMC. Potential changes in the Earth System that could impact the magnitude of polar amplification include sea ice extent, vegetation induced changes in albedo, cloud cover, or ocean-atmosphere heat transport. Constraining the magnitude and timing of the steepening of latitudinal temperature gradients is therefore important for understanding the factors driving the late Miocene surface cooling specifically, and Earth System feedbacks more generally. Ideally, this would be achieved through a combined data-modelling approach using multi-proxy temperature reconstructions spanning a range of latitudes to increase confidence in calculated changes in temperature gradients.

Despite the significance of this climate interval, the evolution of global sea surface temperatures (SST) and hence temperature gradients during the mid-late Miocene is relatively poorly constrained due to a paucity of complete well-preserved sedimentary successions (*Lunt et al.* , 2008). The widespread carbonate dissolution, which dramatically reduced the sediment carbonate content and preservation quality in deep marine sediments, is termed the middle-late Miocene carbonate crash (*Farrell et al.* , 1995; *Jiang et al.* , 2007; *Keller and Barron* , 1987; *Lübbers et al.* , 2019; *Lyle et al.* , 1995). In addition to these dissolution issues, the majority of foraminifera-bearing Miocene sections are comprised of carbonate rich sediments which have undergone some degree of recrystallisation. The oxygen isotopic composition of planktic foraminifera that have undergone recrystallisation in seafloor sediments has been shown to be biased to colder temperatures (*Pearson et al.* , 2001). While planktic foraminiferal Mg/Ca appears to be less affected than $\delta^{18}O$, the impact of recrystallisation on reconstructed Mg/Ca sea surface temperatures remains an additional source of uncertainty (*Sexton et al.* , 2006). As a consequence, many mid-late Miocene absolute sea surface temperature reconstructions are restricted to estimates based on the unsaturated alkenone proxy and the TEX_{86} proxy (*Herbert et al.* , 2016; *Huang et al.* , 2007; *LaRiviere et al.* , 2012; *Rousselle et al.* , 2013; *Seki et al.* , 2012; *Zhang et al.* , 2014). These records show a cooling in the late Miocene which begins around 10 Ma at high northern and southern latitudes. However, significant cooling in the tropics is not apparent in the alkenone records until ˜7.5 Ma, while atmospheric pCO_2reconstructions also suggest a significant decline from this time (*Sosdian et al.* , 2018; *Stoll et al.* , 2019). At face value therefore, these records imply an interval of enhanced polar amplification between 10 Ma and 7.5 Ma in the absence of significant drawdown of CO_2 or increase in ice volume (*Herbert et al.* , 2016; *Sosdian et al.* , 2018). One significant caveat to this interpretation is that the Uk_{37} alkenone proxy becomes saturated above 280C (*Müller et al.* , 1998) and the late Miocene tropical SSTs prior to 7.5 Ma are at this limit (*Herbert et al.* , 2016). Therefore, an alternative interpretation of the data would be that the high latitudes and the tropics cooled synchronously from ˜10 Ma, but the initial cooling in the tropics was not able to be recorded by the Uk_{37} alkenone proxy. Corroboration of the absolute Uk_{37} alkenone temperatures by an independent proxy would therefore confirm the timing of the global late Miocene Cooling and the possible interval of enhanced polar amplification between 10 Ma and 7.5 Ma.

Here we present a new planktic foraminiferal Mg/Ca record from the Sunbird-1 industry well cored offshore Kenya by BG Group. Critically, middle to late Miocene sediments in Sunbird-1 are hemipelagic clays, which has resulted in glassy preservation of the foraminifera. However, the foraminifera are coated with metal-rich authigenic coatings, which are not removed by standard cleaning techniques. Planktic foraminifera were therefore analyzed by laser ablation ICP-MS to obtain Mg/Ca from the primary foraminiferal test and hence enable estimation of absolute SSTs.

2 Materials and Methods

2.1 Site location, stratigraphy, and age control

This study utilizes 91 cuttings, spanning 273 meters at burial depths ranging from 630 m to 903 m, recovered by BG Group from the Sunbird-1 well offshore Kenya (04° 18' 13.268" S, 39° 58' 29.936" E; 723.3 m water depth) (Figure 1, Supplementary Table S1). Sedimentation at Sunbird-1 through the studied interval (9.5-13.5 Ma) is dominated by clays; the fraction of the sediment >63µm averages 11.5% (Supplementary Table S1), much lower than typical carbonate-rich deep-water sites. The impermeable nature and chemical composition of clay-rich sediment reduces diagenetic alteration of primary foraminiferal calcite, making them ideal targets for geochemical analysis (*Pearson et al.* , 2001; *Sexton et al.* , 2006). Tests displaying the desired exceptional preservation appear glassy and translucent under reflected light, and SEM imaging shows retention of the foraminiferal original microstructure (*Pearson and Burgess* , 2008). This style of preferential glassy preservation, as displayed in the Sunbird-1 well, is rare to absent in published records from Miocene foraminifera.

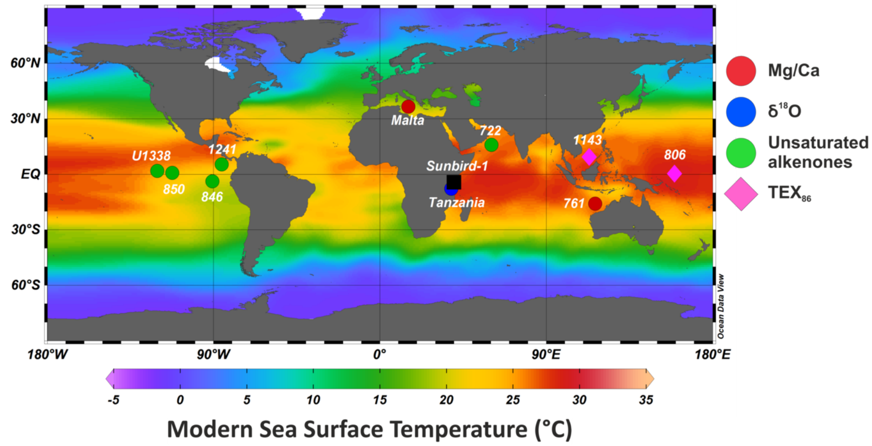

Figure 1: Location of the Sunbird-1 study site (black square). Other sites for which there are mid to late Miocene sea surface temperature reconstructions from Mg/Ca (red circles), ^{18}O (blue circles), unsaturated alkenones (green circles) and TEX_{86} (pink diamonds) are shown. Figure produced using Ocean Data Viewer (*Schlitzer, R.,* 2018) using modern-day mean annual sea surface temperature data from the World Ocean Database.

Micropaleontological and calcareous nannoplankton assemblages for Sunbird-1 were analyzed by Haydon Bailey and Liam Gallagher of Network Stratigraphic Consulting. Biostratigraphic datums, correlated with the astronomical timescale of *Raffi et al.* (2020), are based on the planktic foraminifera zonations of *Wade et al.* (2011) and calcareous nanofossil zonations of *Backman et al.* (2012). An age model was constructed by linear interpolation between these biostratigraphic datums (Supplementary Figure S1). Sedimentation rates were ˜3 cm/kyr immediately following the middle Miocene Climate Transition (MMCT), and subsequently increased to ˜17 cm/kyr between 11.8 and 11.5 Ma, before decreasing to ˜8 cm/kyr until 9.5 Ma.

2.2 Foraminiferal stable isotope analysis

Up to 12 individual tests of the planktic foraminifer*Globigerinoides obliquus* showing glassy preservation were used.*G. obliquus* is an extinct, symbiont-bearing species with a tropical to subtropical paleogeographical distribution, and is interpreted as a surface mixed-layer dweller (*Aze et al.* , 2011;*Keller* , 1985). The assertion that *G. obliquus* inhabits and calcifies in the surface mixed layer (*Aze et al.* , 2011;*Keller* , 1985) is supported by multispecies analyses from a 10.0 Ma sediment sample from the Indian Ocean offshore Tanzania showing*G. obliquus* to have the most negative δ^{18}O (-2.5communication, 2019). Tests were crushed between two glass plates ensuring all chambers were opened. Any visible infill was removed using a fine paintbrush under a binocular microscope. Fine clays and other detrital material on the outer surface of the test were removed by rinsing three times in 18.2 M DI water, ultrasonicating for 5-10 seconds in analytical grade methanol, and finally rinsing a further time in 18.2 M DI water. Samples were analyzed at Cardiff University on a ThermoFinnigan MAT253 with online sample preparation using an automated Kiel IV carbonate device. Results are reported relative to Vienna Pee Dee Belemnite, and long-term uncertainty based on repeat analysis of NBS-19 is ±0.08 of BCT63 is +-0.07 Supplementary Table S2.

2.3 Solution ICP-MS trace metal analysis

Between 10 and 15 individuals of the planktic foraminifer*Dentoglobigerina altispira* from the 250 – 355 µm size fraction were picked and weighed on a six-decimal-place balance to determine average test weight. Individual tests were then crushed between two glass plates ensuring all chambers were opened. Due to the low foraminiferal abundance it was not possible to analyze the same species for stable isotope and trace metal composition. Any visible infill was removed using a fine paintbrush under a binocular microscope. Fragments were cleaned to remove clays and organic matter following the standard protocol (*Barker et al.*

, 2003; *Boyle and Keigwin* , 1985). Due to the clay-rich nature of the sediment the clay removal procedure was conducted twice. To test for the possible presence of metal oxides half of the samples were reductively cleaned between the clay removal and oxidative cleaning steps. Samples were dissolved in trace metal pure 0.065 M HNO_3 and diluted with trace metal pure 0.5M HNO_3 to a final volume of 350 µl. Samples were analyzed at Cardiff University on a Thermo Element XR ICP-MS using standards with matched calcium concentrations to reduce matrix effects (*Lear et al.* , 2010; *Lear et al.* , 2002). Together with Mg/Ca, several other ratios (Al/Ca, Mn/Ca, and U/Ca) were analyzed to screen for potential contaminant phases. Data are available in Supplementary Table S3. Long-term analytical precision for Mg/Ca throughout the study is better than 2%.

2.4 Laser ablation-ICP-MS analysis

Direct sampling of solid phase material via laser ablation (LA-) allows for geochemical analyses through individual foraminiferal tests at the sub-micron scale when coupled to an inductively-coupled-plasma mass spectrometer (ICP-MS) (*Detlef et al.* , 2019; *Eggins et al.* , 2004; *Evans et al.* , 2015a; *Fehrenbacher et al.* , 2015;*Hines et al.* , 2017; *Petersen et al.* , 2018; *Reichart et al.* , 2003). A key advantage of analyzing the trace element composition of foraminifera using LA-ICP-MS over the more traditional solution-based ICP-MS is the ability to recognize the diagenetically altered portions of the tests, allowing identification of the primary calcite (*Creech et al.* , 2010; *Hasenfratz et al.* , 2016;*Pena et al.* , 2005). The elemental composition of this primary calcite can provide important information about palaeotemperature (*Nooijer et al.* , 2017; *Eggins et al.* , 2003; *Pena et al.* , 2005) and other paleo-environmental conditions such as pH (*Mayk et al.* , 2020; *Thil et al.* , 2016) and oxygenation (*Koho et al.* , 2015; *Petersen et al.* , 2018).

Up to six specimens of *D. altispira* per sample were selected from 44 depth intervals through the Sunbird-1 core for LA-ICP-MS analysis. Foraminiferal sample preparation included the removal of fine clays and other detrital material on the outer surface of the test using DI water and methanol, but the more aggressive oxidative and reductive steps (*Barker et al.* , 2003; *Boyle and Keigwin* , 1985), were not required for laser ablation analysis (*Vetter et al.* , 2013). The cleaned tests were mounted onto glass slides using double sided carbon tape and were allowed to dry before being mounted into the sample cell (*Evans et al.* , 2015b; *Fehrenbacher et al.* , 2015;*Hines et al.* , 2017).

Analyses were performed using an ArF excimer (193nm) LA- system with dual-volume laser-ablation cell (RESOlution S-155, Australian Scientific Instruments) coupled to a Thermo Element XR ICP-MS. Optimized ablation parameters and analytical settings determined for analyzing foraminifera in the Cardiff University CELTIC laboratory (Supplementary Table S4; (*Detlef et al.* , 2019; *Nairn* , 2018)) were used for this study. Three cleaning pulses to remove any contaminant on the outer ˜0.5 µm of the test surface were included prior to analysis. We analyzed ^{25}Mg, ^{27}Al,^{43}Ca, ^{55}Mn and^{88}Sr, each isotope having a constant 50 ms dwell time. Typically, intervals with elevated Mn and Al in concert with elevated Mg are interpreted as being contaminant phases (e.g., Fe-Mn oxides-hydroxides or clays), and are commonly found on the inner and outer test surface (*Barker et al.* , 2003; *de Nooijer et al.* , 2014; *Hasenfratz et al.* , 2016; *Koho et al.* , 2015;*Pena et al.* , 2005).

Where possible, three laser spot depth profiles were collected on each of the penultimate (f-1) and previous (f-2) chambers by ablating with 100 consecutive laser pulses in one position on the test. Assuming that each laser pulse only ablates a ˜0.1 µm layer of calcite (*Eggins et al.* , 2003), we estimate the profile to represent a transect through the test wall approximately 15 µm long. However, in some cases older chambers were required to ensure six laser profiles per specimen were analyzed (*Nairn* , 2018). NIST SRM 610 glass standard was measured between every six laser profiles, and NIST SRM 612 at the beginning and end of analyses from each sample depth. The reference values for elemental concentrations in both silicate glass standards are taken from the GEOREM website (http://georem.mpch-mainz.gwdg.de/sample_query_pref.asp), updated from *Jochum et al.* (2011a). NIST SRM 612 was used to determine long term external reproducibility using NIST SRM 610. For Mg/Ca, NIST 612 (n=90) had an accuracy of 12.0% and a precision of 3.7% relative to the reported value. A similar ˜12% negative offset relative to the reported value of NIST 610-calibrated NIST 612 has been observed over a much longer period of data collection (*Evans and Müller* , 2018). To supplement this assessment, we also conducted accuracy tests using the GOR-132 and KL-2 MPI-DING glasses (*Jochum et al.* , 2011b). For this, GOR-132 and KL2 were treated as unknowns, with both NIST 610 and NIST 612 as calibration standards. For Mg/Ca, GOR-132 (n=25) had an accuracy of 1.1% and a precision of 3.2% relative to the reported value, and KL-2 (n=25) had an accuracy of 0.6% and a precision of 2.6% relative to the reported value when calibrated using NIST 610. These values increased to 10.9% and 9.4% for GOR-132, and 8.2% and 5.4% for KL-2 when calibrated using NIST 612. The NIST 610-calibrated data presented here supports the determination of*Evans et al.,* (2015a) that the Mg values for NIST 612 requires reassessment.

An important issue related to accuracy is that because a well-characterized, homogenous calcite reference material is not currently available for laser ablation use, the glass standards we used have a different matrix to the calcite foraminifera tests (*Evans et al.* , 2015a; *Evans and Müller* , 2018; *Fehrenbacher et al.* , 2015). Therefore, while we have high confidence in the accuracy of the intra-and inter-specimen geochemical variability described in Section 2.6, we must consider the possibility of an analytical bias in the absolute geochemical composition of foraminiferal tests determined by laser ablation ICP-MS. One way to assess the magnitude of such potential bias is to analyse foraminiferal samples by both solution and laser ablation ICP-MS. However, it is important to note that the corrosive cleaning protocol for solution analysis tends to slightly lower primary test calcite Mg/Ca, an issue that is routinely circumvented by employing the same cleaning on calibration samples for paleotemperature reconstructions (*Barker et al.,* 2003). For the purpose of this study, it is therefore important that our LA-ICP-MS technique gives values that are consistent with our samples analysed by solution ICP-MS. We are able to make a direct comparison of our youngest samples in this way, because these do not have significant authigenic coatings biasing the solution analyses. For these samples, our solution and laser ablation results are in excellent agreement, which gives us confidence in the LA-ICP-MS values for the older samples, where we know the solution ICP-MS results are compromised by authigenic coatings (Supplementary Figure S2). Furthermore, we note that if future work indicates a consistent offset between laser ablation Mg/Ca analyses of carbonates and silicate glasses, owing to their differing matrices, our standard values reported above will allow our data to be corrected to obtain an accurate composition of the uncleaned foraminiferal calcite.

2.5 LA-ICP-MS data processing and screening

Each individual laser ablation profile was carefully inspected and processed using the SILLS data reduction software package (*Guillong et al.* , 2008) following the established protocol outlined in *Longerich et al.* (1996). Profiles generally followed one of two patterns: (i) a rise from background values to a transient peak, followed by a somewhat lower plateau, or (ii) a rise from background values to a general plateau (Figure 2). There are two likely explanations for the initial transient peak in some isotope profiles: ablation of authigenic coatings enriched in some trace metals, or laser ablation induced isotope fractionation (so-called “pit effects”). We favor the first explanation because we used the same operating parameters on every profile, and would therefore expect any “pit effects” to be consistent among the profiles. Furthermore, profiles containing the transient peaks were more prevalent in the older part of the record, where our solution Mn/Ca analyses demonstrate the presence of authigenic coatings. Therefore, we assume the transient peaks represent contaminated portions of the test and exclude those regions. The integration interval for the profile was selected based upon the following three criteria: (i) stable ^{43}Ca counts, indicating ablation of calcite, (ii) stable Mg/Ca signal, indicating a consistent primary calcite phase, (iii) flat Mn/Ca and Al/Ca signals, avoiding any peaks indicating intervals of contamination (Figure 2).

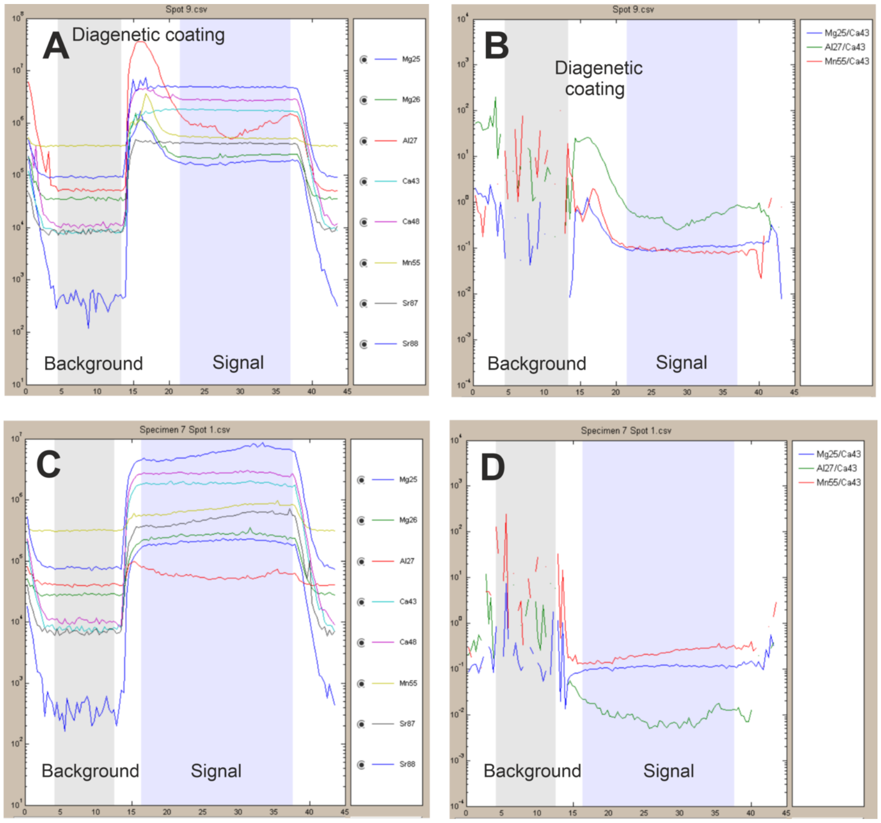

Figure 2: Representative LA-ICP-MS Mg, Al, and Mn profiles demonstrating the selection of background (grey panel) and sample (blue panel) signals for a profile with an authigenic coating (A, B) and for a profile without an authigenic coating (C, D). Both examples are shown in raw isotopic counts (A, C), and ratios mode (B, D) where the isotopes of interest are relative to ^{43}Ca, the internal standard. In both examples the x axis is analysis time (seconds), and the y axis is the raw intensity of the isotopes or ratios on a log scale. The sample interval is selected to avoid the elevated Mg/Ca, Mn/Ca, and Al/Ca at the outer surface of the test.

Individual depth profiles were corrected by first subtracting the mean background signal (determined from ~15 seconds of data acquired when the laser was turned off prior to ablation). The repeated analysis of the NIST 610 standard reference material was used to linearly correct for any instrumental drift. Typically, this is small, <2%, because of the good counting statistics and stable data acquisition during ablation. The ablation profiles were normalized to^{43}Ca as the internal standard and elemental concentrations (TM/Ca) were calculated, assuming 40 wt % for $CaCO_3$.

Following data processing, rigorous screening of the Mg/Ca ratios for the influence of intratest contamination was conducted. It is important to recognise that Mn/Mg and Al/Mg of contaminant phases vary greatly, such that there is no single universal threshold for these elements that can be applied in every situation (*Lear et al* ., 2015). For the Sunbird-1 samples we examined co-variation of Mg/Ca and Mn/Ca and chose to exclude all samples above a Mn/Ca threshold of 200 µmol/mol (Supplementary Figure S3). Consideration of Al/Ca was more complex, as some samples with extremely high Al/Ca (>1000 µmol/mol) was not associated with markedly elevated Mg/Ca. This result demonstrates that aluminum is sporadically present in foraminiferal tests in variable phases (with differing Al/Mg). We therefore used a dual-pronged approach, considering both Al/Ca and intra-sample heterogeneity. We excluded profiles where two conditions were met: (i) Al/Ca was >100 µmol/mol, and (ii) the associated Mg/Ca was substantially elevated relative to the other depth profiles from the same sample.

2.6 Determination of mean foraminiferal test Mg/Ca by laser ablation

Geochemical heterogeneity exists both within an individual foraminiferal test and between foraminiferal tests from the same sample (*Eggins et al.* , 2004; *Fehrenbacher and Martin* , 2014; *Sadekov et al.* , 2008; *Sadekov et al.* , 2005). Therefore, several laser ablation profiles are required to produce a consistent Mg/Ca ratio for temperature reconstructions. Here we analyzed ten depth profiles through each of ten individual *D. altispira* tests from the 1551-1554 m (11.74 Ma) sample to determine representative inter-specimen variability for these samples (Figure 3). Approximately one third (n=28) of the 100 depth profiles were excluded during screening for elevated Al/Ca and Mn/Ca indicative of diagenetic contamination. The Mg/Ca value of individual depth profiles in *D. altispira* from the 1551-1554 m sample ranges from 2.67 mmol/mol to 5.23 mmol/mol, with a mean of 3.63 $\pm$ 0.14 mmol/mol (n=72) (Figure 3a; Supplementary Table S5). The mean Mg/Ca value from four specimens, a total of 28 profiles, is 3.41 $\pm$ 0.18 mmol/mol (Figure 3a). Averaging profiles from ten individual tests did therefore not produce significantly better accuracy or precision than averaging profiles from four individual tests (Figure 3b). Therefore, for a Mg/Ca ratio to be considered representative it must represent an average of at least 28 laser ablation profiles, from at least four specimens, with the analytical uncertainty (2 SE) indicating the intra- and inter-specimen variability this incorporates. To account for depth profiles excluded due to contamination, where possible the number of measurements per sample was increased to 36, six depth profiles per specimen and six specimens per sample. This result is in line with other LA-ICP-MS studies (*Rathmann et al.* , 2004; *Sadekov et al.* , 2008). Future studies are advised to conduct similar testing to determine the number of measurements required for a mean sample Mg/Ca to be representative, as this will likely be site dependent.

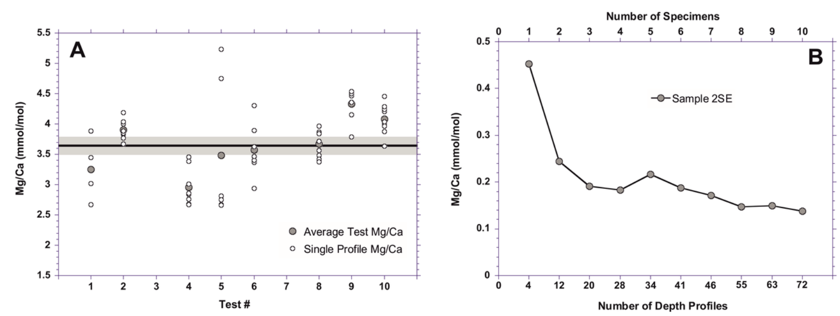

Figure 3: Distribution of *D. altispira* Mg/Ca values from LA-ICP-MS profiles of the 1551-1554 m sample. (A) A summary of all Mg/Ca values, where open circles denote individual measurements, and filled circles denote mean Mg/Ca values for each specimen. The horizontal black line is the mean of all depth profiles from the sample, and the gray bar the $\pm$2 SE sample uncertainty. (B) The evolution of the sample 2 SE with increasing specimens. Only profiles that passed data screening are included (n=72). Data is provided in Supplementary Table S5.

2.7 Mg/Ca paleo-sea surface temperature calculations

The influence of calcification temperature (T) on the Mg/Ca ratio of foraminiferal calcite can be explained by an exponential curve of general form Mg/Ca = $\mathrm{Bexp}^{\mathrm{AT}}$ where the pre-exponential constant (B) and exponential constant (A) are species specific (*Anand et al.* , 2003; *Lear et al.* , 2002; *Nürnberg et al.* , 1996; *Rosenthal et al.* , 1997). To convert raw Mg/Ca ratios to absolute temperatures, several secondary controls on Mg/Ca must be considered, and accounted for (*Gray et al.* , 2018; *Hollis et al.* , 2019; *Holland et al.,* 2020).

In this study we use Mg/Ca values from *D. altispira* , a near surface dweller present from the Oligocene to the Pliocene. Since this is not an extant species, we consider two approaches to calculating SST: (i) using the multi-species calibration equation from *Anand et al.* (2003) and (ii) using the *Globigerinoides ruber* Mg/Ca-SST equation and pH correction from *Evans et al.* 2016.

In scenario (i), we apply a compilation of nine modern planktic foraminifera (*Anand et al.,* 2003). This calibration is commonly applied to extinct planktic foraminiferal species such as *D. altispira* and applies a power law relationship, where H is a constant that describes the sensitivity of $Mg/Ca_{CALCITE}$ to seawater Mg/Ca (Mg/Ca_{SW}) (*Hasiuk and Lohmann,*2010; *Cramer et al.,* 2011; *Evans and Müller* , 2012) (Equation 1).

$$\frac{\textbf{Equation 1}: \quad \mathrm{Mg}}{\mathrm{Ca}} = \frac{\mathbf{B}}{\frac{\mathrm{Mg}}{\mathrm{Ca}}{}_{\mathrm{SW}}^{\mathbf{t=0^H}}} \text{ x } \frac{\mathrm{Mg}}{\mathrm{Ca}}{}_{\mathrm{SW}}^{\mathbf{t=t^H}} \; \mathrm{ex}\mathbf{p}^{\mathrm{AT}}$$

Fluxes of Mg^{2+} and Ca^{2+} into and out of the oceans leads to secular variation in Mg/Ca_{sw}. This variability must be accounted for when determining absolute sea surface temperatures on Cenozoic timescales (*Hollis et al.* , 2019). Reconstructions of Mg/Ca_{sw} based on large benthic foraminifera (*Evans et al.* , 2018), calcite veins (*Coggon et al.* , 2010), fluid inclusions (*Horita et al.* , 2002), and echinoderms (*Dickson* , 2002) have constrained this variability through the Cenozoic (Supplementary Figure S4). The Eocene-Oligocene demonstrates relatively stable values of 2.0-2.5 mol/mol (*Coggon et al.* , 2010; *Evans et al.* , 2018). However, only one data point exists from the Miocene, through which Mg/Ca_{sw} more than doubles from ˜2.2 mol/mol in the late Oligocene (*Coggon et al.* , 2010) to the well constrained value of 5.2 mol/mol in the modern ocean (*Broecker et al.* , 1982;*Dickson* , 2002; *Horita et al.* , 2002; *Kısakürek et al.* , 2008). Therefore, the method of *Lear et al.* (2015) is followed by fitting the fourth-order polynomial curve fit through the compiled Mg/Ca_{sw} proxy records (Supplementary Figure S4). We use a ±0.5 mol/mol uncertainty window in the following temperature calculations, this error envelope incorporating the majority of the spread in the proxy data.

The power law function negates the assumption that the temperature sensitivity remains constant, independent of changing Mg/Ca_{SW} through the Cenozoic era. We apply a power law constant of H=0.41, similar to the value applied for *T. trilobus* , a symbiont-bearing, mixed layer dweller (*Delaney et al.,* 1985;*Evans and Müller* , 2012). Adapting Equation 1 to include our H value, a modern-day Mg/Ca_{sw} value of 5.2 mol/mol, and the calibration constants of *Anand et al.,* (2003) derives Equation (2).

Equation 2 :

$$\frac{\mathrm{Mg}}{\mathrm{Ca}} = \frac{\mathbf{0.38 \pm 0.02}}{\mathbf{5.2^{0.41}}} \text{ x } \mathbf{Mg/Ca_{sw}}^{\mathbf{0.41}} \; \mathrm{ex}\mathbf{p}^{(\mathbf{0.090 \pm 0.003 \text{ x } SST})}$$

This first calibration approach assumes that foraminiferal Mg/Ca is not influenced by changes in the carbonate system. However, studies have shown that planktic foraminiferal Mg/Ca is influenced by changes in the carbonate system, the ratio increasing with decreased pH and/or Δ[῝O_3^{2-}] (*Εανς ετ αλ.* , 2016· *Γραψ ανδ Εανς* , 2019· *Γραψ ετ αλ.* , 2018·*Ρυσσελλ ετ αλ.* , 2004· *Ψυ ανδ Ελδερφιελδ* , 2008). Ηοωεερ, τηε υλτιματε δριερ οφ τηις εφφεςτ ις νοτ ςερταιν ανδ σομε σπεςιες αρε ινσενσιτιε το ςηανγες ιν τηε ςαρβονατε σψστεμ. Φυρτηερ, ιτ ηας βεεν σηοων τηατ φορ *Ορβυλινα υνιερσα* δισσολεδ ινοργανις ςαρβον (ΔΙ῝) πλαψς α ρολε ιν τεστ Μγ/῝α αριαβιλιτψ (*Ηολλανδ ετ αλ.* , 2020). Ωε φολλοω ρεςεντ ρεσυλτς ωηιςη ιντερπρετ πΗ, ας οπποσεδ το Δ[῝O_3^{2-}] ορ ΔΙ῝, ας τηε παραμετερ ωηιςη ςοντρολς τηε ςαρβονατε σψστεμ΄ς ινφλυενςε ον Μγ/῝α (*Εανς ετ αλ.* , 2016· *Γραψ ετ αλ.* , 2018). Φυρτηερμορε, υνλικε ωιτη ειτηερ ΔΙ῝ ορ Δ[῝O_3^{2-}], ιτ ις ποσσιβλε το ρεςονστρυςτ πΗ τηρουγη τηε Νεογενε υσινγ βορον ισοτοπες ιν φοραμινιφερα (*Φοστερ ανδ Ραε* , 2015· *Γρεενοπ ετ αλ.* , 2014· *Ηενεηαν ετ αλ.* , 2013· *Σοσδιαν ετ αλ.* , 2018). Φορ τηεσε ρεασονς ωε υσε τηε ρεςεντ Νεογενε βορον ισοτοπε ςομπιλατιον οφ *Σοσδιαν ετ αλ.*(2018), ωηιςη προιδες ωελλ ςονστραινεδ εστιματες οφ πΗ αςροσς τηις τιμε ιντεραλ (Συππλεμενταρψ Φιγυρε Σ5· Συππλεμενταρψ Ταβλε Σ9). Λινεαρ ιντερπολατιον βετωεεν τηεσε πΗ αλυες αλλοως υς το εστιματε α μεαν πΗ αλυε, ανδ ασσοςιατεδ υνςερταιντψ ενελοπε, φορ εαςη Συνβιρδ-1 σαμπλε, ωηερε τηε υνςερταιντψ ενελοπε ις μαξιμυμ ανδ μινιμυμ πΗ ατ τηε 17% ανδ 83% ςονφιδενςε ιντεραλ (˜± 0.06 pH units).

Therefore, in addition to scenario (i) we also consider the approach from *Evans et al* . (2016) which corrects for pH changes using the interpolated Neogene pH record of *Sosdian et al.* (2018) (Supplementary Figure S5). Measured planktic foraminiferal Mg/Ca values are corrected for this influence of pH using the equation of *Evans et al.* (2016) (Equation 3).

$$\textbf{Equation 3}: \quad \frac{\mathbf{Mg}}{\mathrm{Ca}_{\mathrm{CORRECTED}}} = \frac{\frac{\mathrm{Mg}}{\mathrm{Ca}_{\mathrm{MEASURED}}}}{\frac{\mathbf{0.66}}{\mathbf{1+exp(6.9(pH-8.0))}}+\mathbf{0.76}}$$

The preferred equation of *Evans et al.* (2016) is used to account for the influence of changing Mg/Ca_{sw} when estimating SST. These authors determined that the best fit to culture-derived calibration lines is when both the pre-exponential (B) and exponential (A) coefficients vary quadratically with Mg/Ca_{sw}(Equation 4 and 5).

Equation 4: $B = (0.019 \times Mg/Ca_{sw}{}^2) - (0.16 \times Mg/Ca_{sw}) + 0.804$

Equation 5: $A = (-0.0029 \times Mg/Ca_{sw}{}^2) + (0.032 \times Mg/Ca_{sw})$

We substitute these equations into the general exponential calibration, $Mg/Ca = B\exp^{AT}$, to account for changing Mg/Ca_{sw}. Although the *Evans et al.* (2016) equation is specific to *G. ruber* , this species inhabits a shallow water depth of 0-50m (*Schiebel and Hemleben* , 2017) similar to the inferred mixed-layer habitat depth *D. altispira* (*Aze et al.* , 2011). Furthermore, as with *G. ruber* , *D. altispira*was a tropical/subtropical species, with symbionts (*Aze et al.* , 2011).

Salinity can exert a secondary effect on foraminiferal Mg/Ca, sensitivity measurements from culture and core-top studies show this to be ˜3-5% per practical salinity unit (psu) (*Gray et al.* , 2018; *Hollis et al.* , 2019; *Hönisch et al.* , 2013;*Kısakürek et al.* , 2008). In the absence of a robust, independent salinity proxy (although we do note the promise of Na/Ca (*Bertlich et al.* , 2018; *Geerken et al.* , 2018)) and the relatively minor effect of salinity on foraminiferal Mg/Ca, this potential secondary control is not empirically accounted for. Sunbird-1 was located in a coastal setting and likely experienced a highly variable hydrological cycle due to changes in the position of the ITCZ making it susceptible to changes in salinity. Therefore, an error of ± 0.50C is incorporated into the final sea surface temperature estimates, equivalent to an assumed salinity variability of ˜± 1 PSU.

Mg/Ca-derived sea surface temperature estimates calculated using both approaches (i) and (ii) yield extremely similar trends (Supplementary Figure S6). Across the time interval of the Sunbird-1 dataset (˜13.5 Ma – 9.5 Ma) pH changes by a small amount and thus the choice of approach has little influence on the Sunbird-1 absolute SST record. In our discussion below, we adopt approach (i); the multi-species calibration equation from *Anand et al.* (2003) without a pH correction. This approach avoids any potential species-specific effects from applying the *Evans et al.* (2016) calibration specific to *G. ruber* to the extinct *D. altispira* used in this study. Furthermore, *D. altispira* has been considered to be symbiont bearing, so may demonstrate a muted response to changes in pH and insensitivity to pH changes, similar to *Trilobatus trilobus* (*Gray and Evans* , 2019).

The uncertainties (± 2SE) associated with the conversion from Mg/Ca to absolute SST estimates incorporate the uncertainty on the Mg/Ca_{sw} record, and the potential uncertainty due to varying salinity. Additionally, scenario (i) incorporates the uncertainty in the calibration of *Anand et al.* (2003) (Equation 2), and scenario (ii) using the approach of *Evans et al. (* 2016) incorporates the uncertainty in the pH correction. These combined are termed the calibration uncertainty and are considerably greater than the independent analytical uncertainty, which only incorporates the intra- and inter- specimen variability (±2 SE). Absolute sea surface temperature estimates, and associated uncertainties, calculated using approach (i) and (ii) are available in Table 1 and Supplementary Table S9 respectively

Age (Ma)	Minimum Age (Ma)	Maximum Age (Ma)	Temperature (°C)	Maximum Temperature (°C)	Minimum Ter
9.53	9.43	9.62	27.73	31.08	24.64
9.86	9.86	9.86	28.15	31.86	24.68
10.19	10.05	10.33	29.54	33.49	25.81
10.43	10.43	10.43	26.82	30.55	23.32
10.48	10.48	10.48	28.13	31.58	24.94
10.57	10.57	10.57	27.81	31.47	24.41
10.62	10.62	10.62	24.88	28.12	21.90
10.78	10.73	10.89	29.48	33.14	26.09
10.92	10.92	10.92	28.95	32.78	25.36
11.13	10.98	11.28	28.42	32.47	24.58
11.40	11.40	11.40	28.18	31.50	25.15
11.50	11.46	11.55	29.36	32.85	26.15
11.61	11.10	11.61	26.78	30.39	23.44
11.63	11.63	11.63	26.65	30.34	23.21
11.64	11.64	11.64	29.57	33.29	26.11
11.67	11.67	11.67	25.44	29.02	22.12
11.72	11.69	11.74	28.19	31.84	24.81
11.77	11.77	11.77	26.89	30.09	23.96
11.82	11.82	11.82	26.39	29.69	23.37
11.87	11.87	11.87	28.84	32.47	25.47
12.03	12.03	12.03	28.10	31.66	24.82
12.71	12.57	12.85	29.14	32.80	25.77
13.23	13.13	13.33	28.85	32.54	25.43

Table 1. Sunbird-1 LA-ICP-MS Mg/Ca derived SST using the approach of *Anand et al.* (2003) without a pH correction. Minimum and maximum age refer to the age range of the pooled samples (Supplementary Table S7). Maximum and Minimum temperatures refer to the full range of absolute temperatures derived incorporating the analytical and calibration uncertainty, whereas Analytical Error Only Maximum and Minimum temperatures refer to the range of temperatures derived from the analytical uncertainty only.

2.8 $\delta^{18}O$ paleo-sea surface temperature calculations

Due to the limited sampling resolution of the trace metal data, SST is also calculated using foraminiferal $\delta^{18}O$. Foraminiferal $\delta^{18}O$ ($\delta^{18}O_{calcite}$) is converted to temperature (T) using the palaeotemperature equation of *Bemis et al.* (1998) (Equation 4), changes in global ice volume being corrected using the $\delta^{18}O_{sw}$ value from the nearest 0.1 Myr time interval in the compilation of *Cramer et al.*(2011).

$$\textbf{Equation 4}: \ \left(\delta^{\mathbf{18}}\mathbf{O}_{\text{calcite}} \ \ \delta^{\mathbf{18}}\mathbf{O}_{\text{sw}} \ \mathbf{+0.27}\right) = \ \mathbf{-0.21} \ \pm \mathbf{0.003} \ \mathbf{T} \ + \ \mathbf{3.10} \ \pm \mathbf{0.07}$$

The absence of a robust, independent salinity proxy makes any quantitative attribution of its influence on foraminiferal $\delta^{18}O$ challenging. Therefore, we incorporate potential $\delta^{18}O$ variability due to salinity into any temperature estimate uncertainty. Salinity of the upper water column in a 0.75° x 0.75° grid square around the modern-day study site varies between 34.9 and 35.4 PSU (*Boyer et al.* , 2013). Using the Indian Ocean $\delta^{18}O_{sw}$-salinity relationship of*LeGrande and Schmidt* (2006) (Equation 5) this equates to a maximum $\delta^{18}O_{sw}$ uncertainty of ±0.091Using Equation 4 this equates to a 0.4 0C uncertainty in the calculated surface temperature.

$$\textbf{Equation 5}: \ \delta^{\mathbf{18}}\mathbf{O}_{\text{sw}} \, (\text{SMOW}) = (\mathbf{0.16} \pm \mathbf{0.004 \ x \ Salinity}) \, \mathbf{-5.31 \pm 0.135}$$

We acknowledge the likelihood of variability in sea surface salinity in this downcore record. We use the paleolatitude calculator of *van Hinsbergen et al.* (2015) to calculate a paleolatitude for Sunbird-1 at 10 Ma of approximately 5.5 °S. The latitudinal correction of*Zachos et al.* (1994) gives a $\delta^{18}O_{sw}$ of 0.1The absence of a significant offset from SMOW (0will have a negligible influence on the isotopic SST reconstructions.

3 Results

3.1 Solution ICP-MS trace element chemistry

D. altispira Mg/Ca measured by solution ICP-MS ranges from 3.15 ± 0.1 to 40.2 ± 0.2 mmol/mol (Figure 4a), translating to unrealistically high reconstructed sea surface temperatures. The high Mg/Ca ratios strongly suggest the addition of magnesium from a secondary, post-depositional source, prior to 11.75 Ma. The elevated Mg/Ca ratios are associated with correspondingly high Mn/Ca, Al/Ca, and U/Ca (Figure 4b-d). Six of the sixteen Mn/Ca ratios are in excess of the proposed 200 µmol/mol threshold, from our LA-ICP-MS analysis, above which Mg/Ca ratios are excluded due to contamination (Supplementary Figure S3). Furthermore, every foraminiferal U/Ca ratio is considerably higher than typical U/Ca ratios of primary foraminiferal calcite, which range from ~3-23 nmol/mol (*Chen et al.* , 2017; *Raitzsch et al.* , 2011; *Russell et al.* , 2004). In addition, foraminiferal Al/Ca exceeds the commonly applied 100 µmol/mol threshold in all but the four youngest samples.

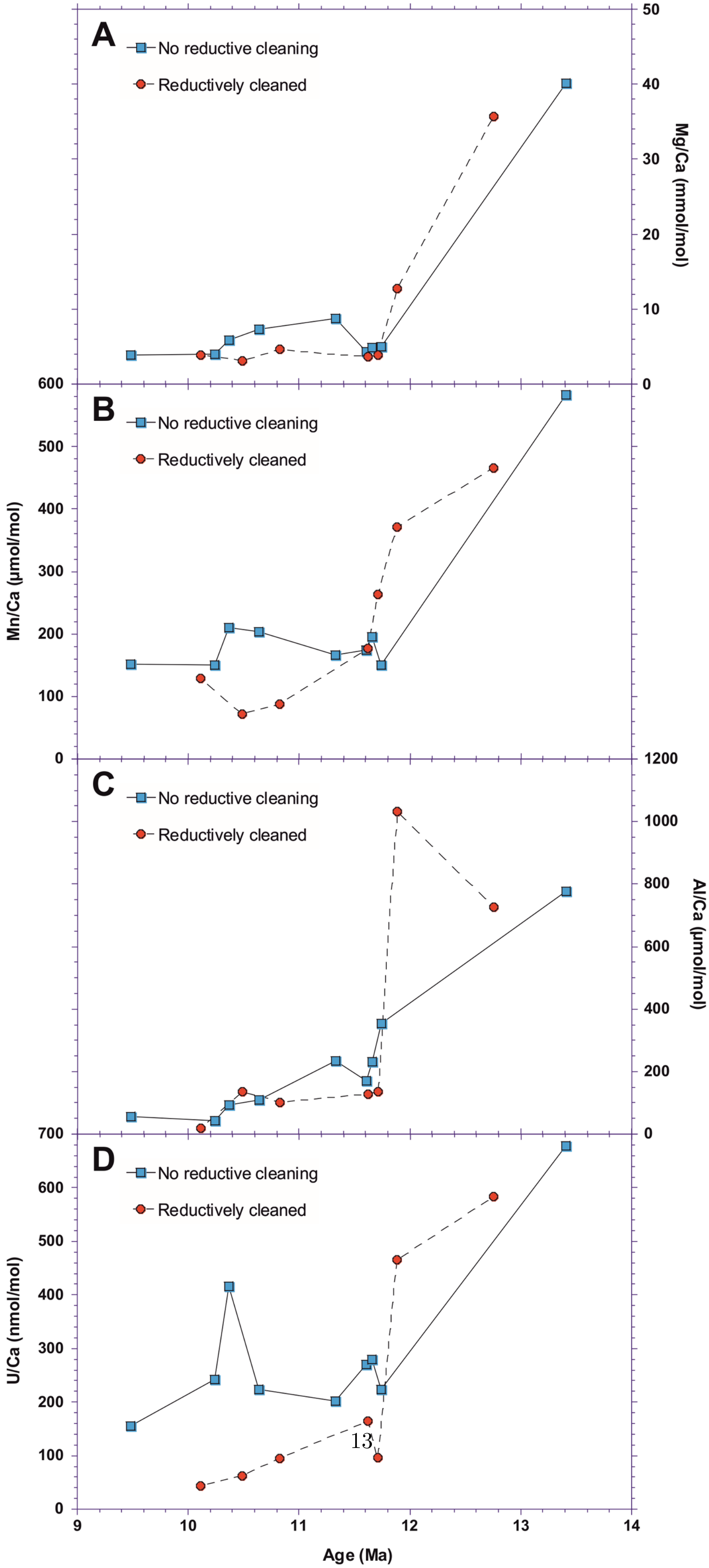
A
No reductive cleaning
Reductively cleaned
Mg/Ca (mmol/mol)
B
Mn/Ca (µmol/mol)
C
Al/Ca (µmol/mol)
D
U/Ca (nmol/mol)
Age (Ma)

Figure 4: Downcore solution ICP-MS (a) Mg/Ca, (b) Mn/Ca, (C) U/Ca, and (d) Al/Ca records for *D. altispira* in the Sunbird-1 core, distinguishing between sample that were reductively cleaned (red circles) and those that were not (blue squares).

The presence of elevated foraminiferal Mn/Ca, Al/Ca, and U/Ca ratios does not necessarily mean that the Mg/Ca ratios are contaminated. However, the downcore, point to point correlation (Figure 4) and covariance (Supplementary Figure S7) between Mg/Ca and contaminant indicators suggest a strong association. This downcore association between Mg/Ca and contaminant indicators, despite a rigorous chemical cleaning protocol, suggests one of two things; (i) the chemical cleaning protocol is not fully effective at removing contaminant coatings, and/or (ii) an Mg-rich contaminant phase is pervasive throughout the calcite test.

Including the reductive cleaning step lowers Mg/Ca, Mn/Ca, and U/Ca ratios in the post 11.8 Ma portion of the record, but has a negligible effect on Al/Ca. Neither cleaning protocol is effective at removing the authigenic coatings on the Sunbird-1 foraminifera in the pre 11.8 Ma portion of the record (Figure 4). For this reason, we also analyzed Sunbird-1 planktic foraminifera by laser ablation ICP-MS.

3.2 Downcore Laser Ablation ICP-MS Mg/Ca

Our laser ablation profiles clearly demonstrate that the metal-rich contaminant is present as an authigenic surface coating on the glassy foraminifera (e.g., Figure 2a-b). Because the alteration is not pervasive throughout the calcite test, laser ablation ICP-MS is an ideal approach to determine primary test Mg/Ca on these coated samples (section 2.6). *D. altispira* Mg/Ca determined by laser-ablation ICP-MS ranges from 3.03 to 5.07 mmol/mol, with an average value of 4.18 $\pm$ 0.40 mmol/mol, and errors ($\pm$2SE) range from 0.10 to 1.04 mmol/mol (Supplementary Table S6). However, due to elevated Al/Ca and Mn/Ca ratios, only 14 of the 44 samples are represented by at least 28 laser profiles. To alleviate this problem, adjacent samples have been combined into longer time slices to ensure that the absolute mean Mg/Ca measurements are robust (Supplementary Table S7). Samples comprising the mean of at least 28 laser profiles are termed "un-pooled samples". Samples pooled to achieve a minimum of 28 laser profiles are termed "pooled samples". It is acknowledged that combining adjacent samples, which span up to 420 kyr, could incorporate orbital scale climatic variability into these pooled samples. However, we do not infer climatic variability on orbital timescales because the coarse sampling resolution could incorporate aliasing of any precessional or obliquital periodicity into longer term eccentricity cycles (*Pisias and Mix* , 1988). Combining adjacent samples to generate a representative mean Mg/Ca for a longer time-slice could smooth orbital scale variability, could reduce uncertainty and assist the interpretation of longer-term climatic trends.

The mean Mg/Ca of representative samples after incorporating the nine pooled Mg/Ca samples with the 14 un-pooled samples ranges from 3.08 to 4.70 mmol/mol, with an average value of 4.04 $\pm$ 0.29 mmol/mol, and errors ($\pm$2SE) range from 0.14 to 0.48 mmol/mol (Supplementary Table S8). These values are in good agreement with the reductively cleaned solution ICP-MS data for the post-11.8 Ma portion of the record (Supplementary Figure S2), coinciding with the interval when contaminant indicators (Mn/Ca, Al/Ca, and U/Ca) are substantially lower (Figure 4b-d). This agreement between Mg/Ca values obtained by LA-ICP-MS and solution ICP-MS following effective reductive-cleaning supports the suitability of the LA-ICP-MS analyses. Because we can be more confident that the laser ablation data are not biased by authigenic coatings, the laser-ablation approach has the advantage that we can also determine original test Mg/Ca in the older part of the record.

There is no obvious long-term trend in Mg/Ca through the interval (Figure 5a). Between 11.8 Ma and 11.7 Ma there is a 0.7-0.8 mmol/mol decrease in Mg/Ca followed by a recovery to approximately previous values at 11.5-11.4 Ma. There is a Mg/Ca decrease of similar magnitude from between 10.7 Ma and 10.36 Ma, recovering by 9.85 Ma. We acknowledge that the coarse sampling frequency, and the combining of samples could be obscuring similar variability through the rest of the record.

3.3 *G. obliquus* $\delta^{18}O$

G. obliquus $\delta^{18}O$ ranges from -3.63with a mean value of -2.92very little variability, values remaining stable at -3.4positive 0.65b). The low variability translates to a stable δ18O SST record, temperatures ranging between 27°C and 31°C with the only distinctive trend being a ~3°C decrease between ~12.7 Ma and 12.0 Ma. The coeval positive 0.3seawater δ18O (*Cramer et al.* , 2011) dampens the influence on the SST estimate of the positive 0.6obliquus δ18O at ~12.5 Ma.

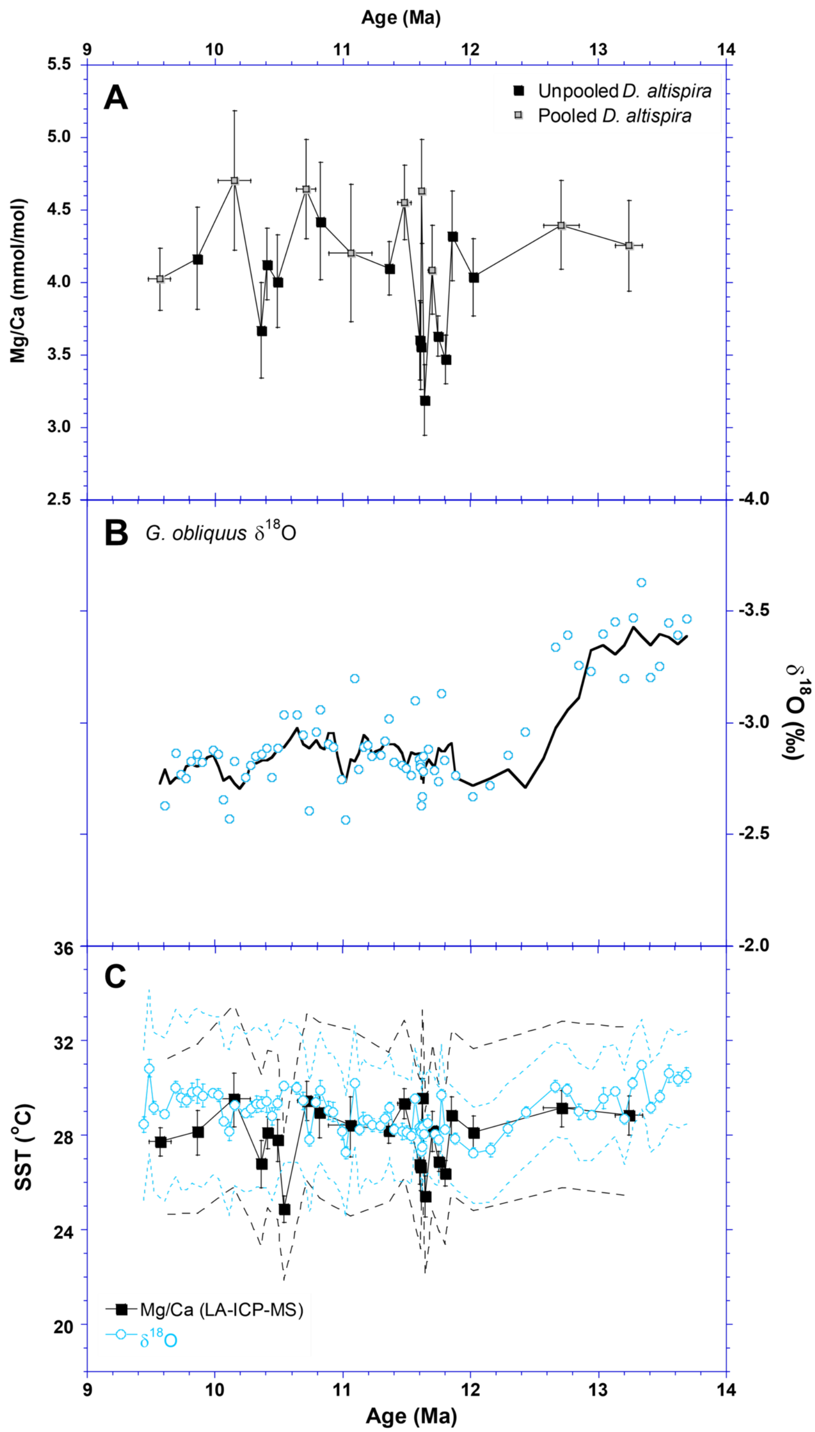

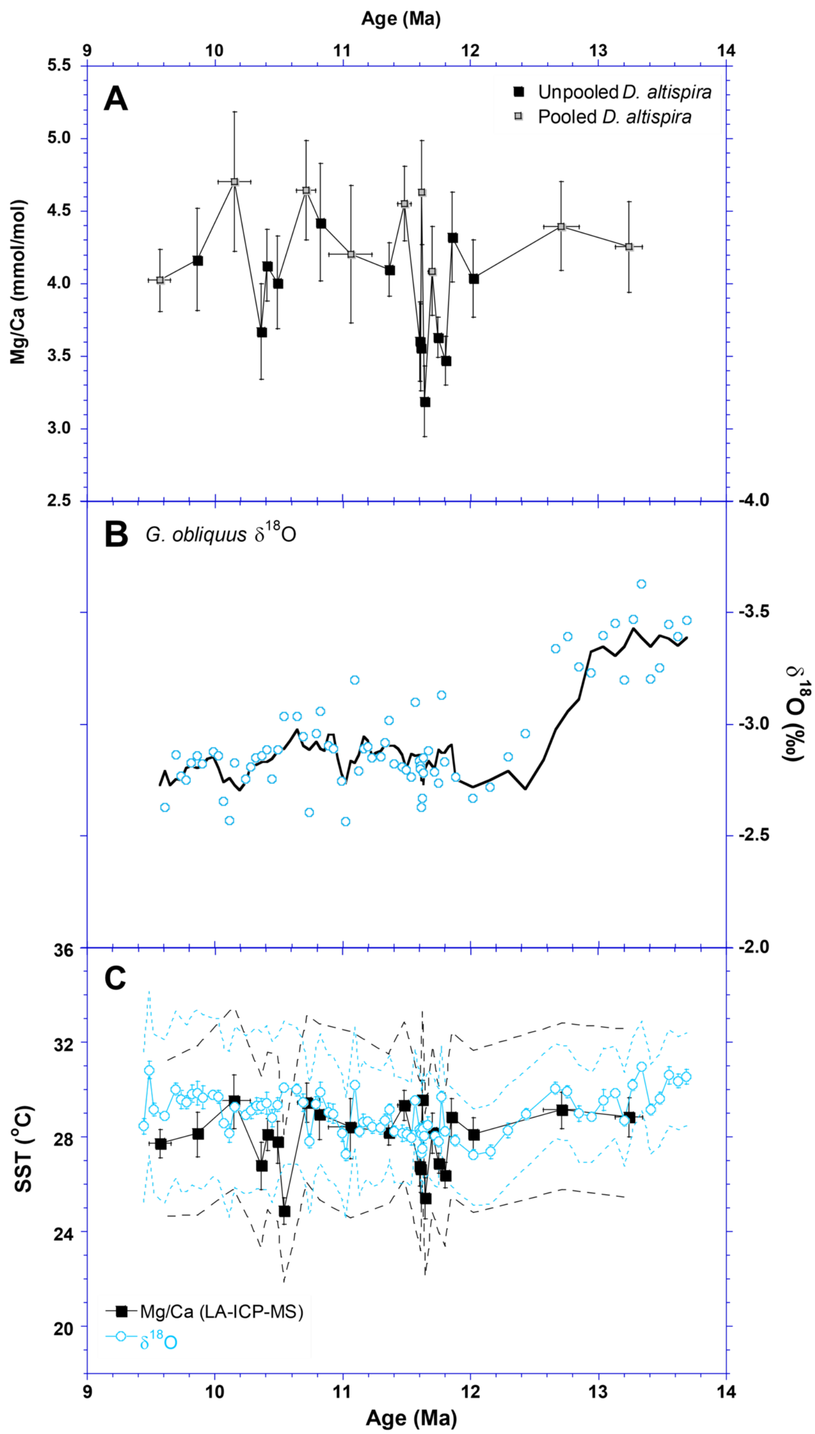

Figure 5: (a) Mean *D. altispira* LA-ICP-MS Mg/Ca ratios (mmol/mol) for unpooled (black squares) and pooled (grey squares) samples from Sunbird-1. Error bars denote the age range for pooled samples, and the ± 2SE of Mg/Ca from all depth profiles in the sample. (b) *G. obliquus* $\delta^{18}O$ from Sunbird-1. Solid line is a five-point moving average. (c) Sea surface temperature records at Sunbird-1 from planktic foraminiferal $\delta^{18}O$,

and LA-ICP-MS Mg/Ca using our preferred approach that applies the calibration of *Anand et al.* (2003) without a pH correction. Symbols are the same as in (a) and (b). Error bars on the $\delta^{18}O$ record denote the analytical uncertainty (± 2SD), and error bars on the Mg/Ca record denote the sample uncertainty (± 2SE). As in (a), pooled Mg/Ca samples also have horizontal error bars denoting the sample age range. Dashed blue and black lines denote the full uncertainty on the temperature estimates, including that derived from the calibration uncertainty, for $\delta^{18}O$ and LA-ICP-MS Mg/Ca respectively. Supplementary Figure S8 provides LA-ICP-MS Mg/Ca sea surface temperatures using the alternative approach of*Evans et al.* , (2016).

4 Discussion

4.1 Reconstructing sea surface temperature from diagenetically altered foraminifera using laser ablation ICP-MS

Robust paleotemperature reconstructions using foraminiferal Mg/Ca ratios are reliant upon the Mg/Ca ratio recording a primary environmental signal, unaltered by diagenetic alteration. Despite employing a thorough cleaning protocol (*Barker et al.* , 2003; *Boyle and Keigwin* , 1985), our Mg/Ca ratios from solution-based ICP-MS analysis in the >11.8 Ma portion of the record are clearly influenced by a diagenetic contaminant phase containing elevated magnesium (Figure 4). This finding demonstrates that foraminifera with a glassy appearance under the light microscope are not necessarily free from the influence of all modes of diagenetic alteration. We therefore emphasize the importance of complementary trace metal ratios indicative of contamination (i.e. Al/Ca, Mn/Ca, U/Ca) to assess the reliability of foraminiferal Mg/Ca ratios (Figure 4). The application of LA-ICP-MS to collect high resolution elemental profiles through the foraminiferal tests, excluding regions displaying diagenetic contamination, has facilitated the identification of what we interpret to be primary paleotemperatures from diagenetically altered foraminifera (*Hines et al.* , 2017; *Hollis et al.* , 2015).

The Sunbird-1 $\delta^{18}O_{PF}$ SST record from*G. obliquus* reconstructs very similar absolute temperatures to the planktic foraminiferal Mg/Ca SST record (Figure 5c). Mean SST from the Sunbird-1 $\delta^{18}O_{PF}$ record (290C) is 20C higher than mean SST from the Mg/Ca record (270C), although with the exception of the two transient decreases in Mg/Ca reconstructed SST initiating at 11.8 Ma and 10.7 Ma the records are within error. The similarity of the absolute SSTs reconstructed by the two proxies strengthens the case for the LA-ICP-MS Mg/Ca SST record recording a primary temperature signal, and that these absolute sea surface temperatures at Sunbird-1 should be considered primary.

The majority of the uncertainty in the absolute temperature estimates is derived from the uncertainties incorporated from the relevant calibrations, in particular the seawater Mg/Ca and seawater $\delta^{18}O$ records (Figure 5c). This is true for both LA-ICP-MS Mg/Ca (Table 1 and Supplementary Table S9) and $\delta^{18}O$ (Supplementary Table S10). Therefore, despite being appreciable, the uncertainty resulting from the geochemical heterogeneity both within an individual foraminiferal test and between foraminiferal tests from the same sample (Figure 3) is not the primary contributor to the final absolute temperature uncertainty.

4.2 Mid-late Miocene sea surface temperatures in the equatorial Indian Ocean

The results from Sunbird-1 indicate that SST in the equatorial Indian Ocean remained stable at ˜270C-290C through the 13.3 Ma to 9.5 Ma interval (Figure 5c). This finding suggests that tropical climate was relatively stable following the global cooling associated with the expansion of the East Antarctic Ice Sheet across the MMCT. These records from Sunbird-1 supports the robustness of contemporaneous alkenone based studies which exhibit similar absolute tropical SST estimates (*Herbert et al.* , 2016; *Huang et al.* , 2007;*Rousselle et al.* , 2013; *Seki et al.* , 2012; *Zhang et al.* , 2014) (Figure 6a). The $U^{k}{}_{37}$ SST calibration fails to reconstruct SST>290C (*Müller et al.* , 1998) but these results using Mg/Ca paleo-thermometry suggest that outside the western Pacific warm pool this restriction does not apply to this time interval, unlike the preceding Miocene Climatic Optimum during which Mg/Ca temperature estimates are higher than those estimated with the $U^{k}{}_{37}$ proxy (*Badger et al.* , 2013).

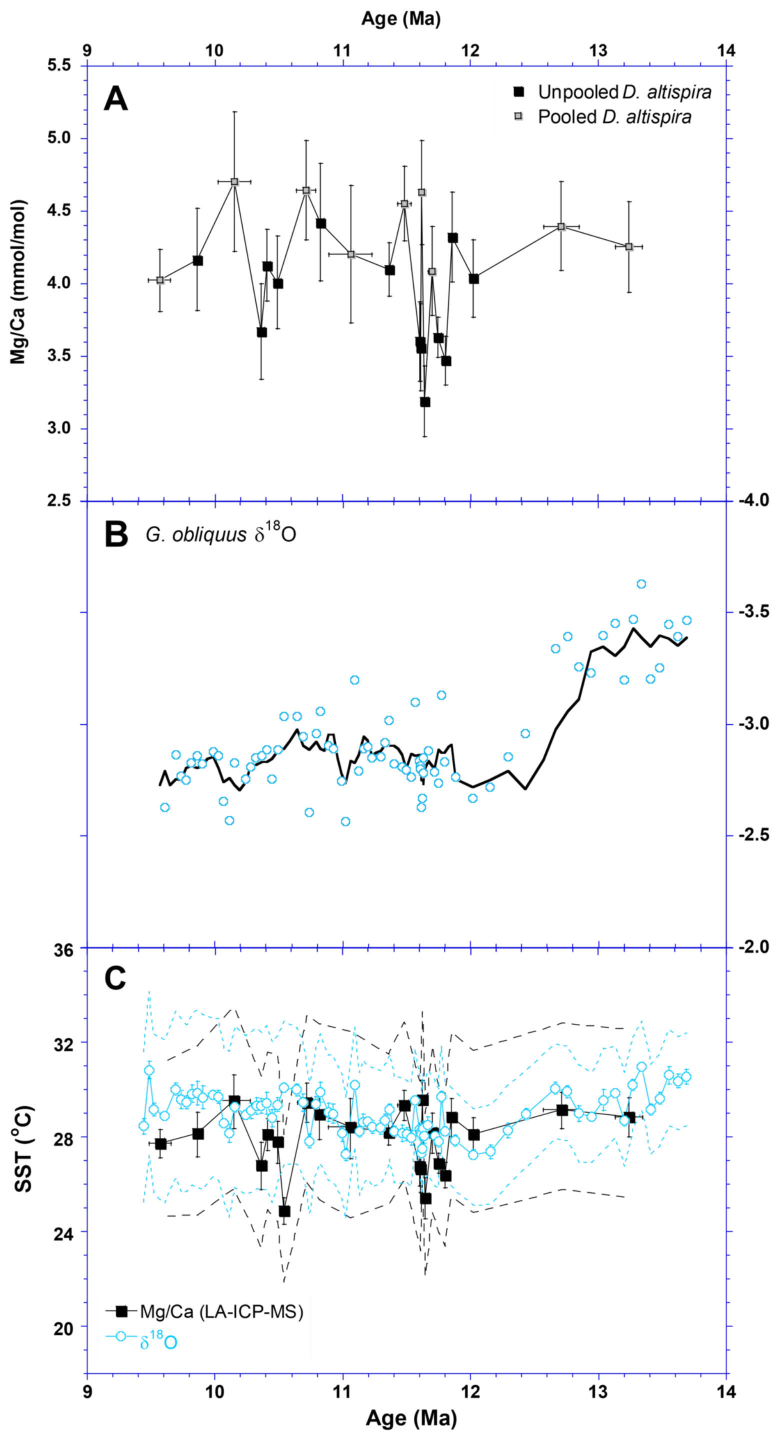

Figure 6: Sunbird-1 LA-ICP-MS Mg/Ca derived SST using the approach of *Anand et al.* (2003) without a pH correction compared to and SST estimates at contemporaneous sites from (a) U^{k}_{37}, and (b) foraminiferal geochemistry. Estimates applying $U^{k}_{37}$are from ODP Site 722 (*Huang et al.,* 2007) in the Arabian Sea, ODP & IODP Sites 846 (*Herbert et al.,* 2016), 850 (*Zhang et al.,* 2014), 1241 (*Seki et al.,* 2012), and U1338

(*Rousselle et al.,* 2013) in the Eastern Equatorial Pacific, terrestrial outcrops in Malta (*Badger et al.,* 2013). Estimates applying the foraminiferal Mg/Ca proxy are from ODP Sites 761 (*Sosdian and Lear,* 2020) and terrestrial outcrops in Malta (*Badger et al.,*2013). ODP Site 761 data is displayed on an alternative axis as SST anomalies relative to the baseline average from 16.0 – 15.5 Ma. Two temperature estimates using the $\delta^{18}O$ of exceptionally preserved foraminifera from Tanzania are also shown (*Stewart et al.,* 2004). The upper limit for the $U^{k}{}_{37}$ proxy (290C) is marked by the thick dashed black line. All previously published records used for comparison are kept on their original age models. Supplementary Figure S9 provides LA-ICP-MS Mg/Ca sea surface temperatures using the alternative approach of *Evans et al.* , (2016).

Although not a true tropical location, and consisting of only three data points, the *Badger et al.* (2013) Mg/Ca record from the Mediterranean estimates SST of ˜27.50C between 13.5 and 13 Ma, within the Sunbird-1 SST uncertainty envelope (Figure 6b). Mg/Ca-SST records based on less well-preserved planktic foraminifera also suggest stable tropical SST between 13.8 and 11.4 Ma (*Sosdian and Lear,* 2020) (Figure 6b). Furthermore, well preserved planktic foraminifera from clay-rich sediments of coastal Tanzania yield Indian Ocean sea surface temperatures of 270C at 12.2 Ma and 290C at 11.55 Ma using the $\delta^{18}O$ paleothermometer (*Stewart et al.* , 2004), again in agreement with the Sunbird-1 temperature estimates (Figure 6b). It is worth noting that this study, as well as the tropical SST records of *Herbert et al.* (2016) and references therein, do not sample the warm pool of the Western Pacific. Sea surface temperature estimates for the western equatorial Pacific using the TEX_{86} paleothermometer suggest a slight, ˜1°C, SST decrease between 12 Ma and 9 Ma, whilst those for the eastern equatorial Pacific are more or less constant across the same interval (*Zhang et al.,* 2014).

Although the estimates provided by the Sunbird-1 record suggest absolute tropical sea surface temperatures remained relatively stable through the mid-late Miocene, some temporal variability does persist. Between 11.8 Ma and 11.7 Ma SST drops sharply by ˜30C. Excluding one value of 28.60C at 11.62 Ma, this decrease in SST to ˜24-250C persists for ˜300 kyr before recovering to pre excursion values by 11.5 Ma. However, no transient decrease in sea surface temperature is recorded from contemporaneous alkenone based estimates of tropical SST utilizing the $U^{k}{}_{37}$ proxy from the Arabian Sea (*Huang et al.* , 2007), and the Eastern Equatorial Pacific (*Herbert et al.* , 2016; *Rousselle et al.* , 2013; *Seki et al.* , 2012; *Zhang et al.* , 2014) (Figure 6a). We therefore suggest that the observed transient ˜30C SST decrease is not the result of a global driver, and supports a mechanism causing local ocean cooling of the surface waters at Sunbird-1. An alternative hypothesis is that an unaccounted increase in local salinity and/or pH, lowering foraminiferal Mg/Ca ratios, caused a bias to cooler temperatures between ˜11.8 and 11.5 Ma. Assuming constant SST, the observed ˜0.7 mmol/mol decrease in Mg/Ca would require a salinity increase on the order of 5.0 PSU (*Hönisch et al.* , 2013; *Gray et al.* , 2018). This salinity increase equates to a 0.8 Indian Ocean $\delta^{18}O_{sw}$-salinity relationship of *LeGrande and Schmidt* (2006) (Equation 5). As well as being an extremely large change in salinity, the planktic foraminiferal $\delta^{18}O$ record does not support such a significant change in sea surface salinity between ˜11.8 and 11.5 Ma (Figure 5b). However, we do acknowledge that a contribution from increased salinity control cannot be discounted. Despite incorporating varying pH from a globally distributed set of open ocean sites (*Sosdian et al.* , 2018), a localized increase in pH at Sunbird-1 cannot be ruled out. This possibility may be particularly relevant considering the land-proximal, tectonically active nature of the study site. A further possibility is that selective dissolution of foraminiferal chambers precipitated during warmer seasons occurred during post-burial diagenetic alteration, causing an apparent ˜3°C lowering of SST between 11.8 Ma and 11.5 Ma. However, mean *D. altispira* test weights suggest that there was no increased dissolution of the foraminiferal tests through this interval of lower LA-ICP-MS Mg/Ca derived SST (Supplementary Table S11 and Supplementary Figure S10).

Therefore, our preferred interpretation is for a local cooling between ˜11.8 and 11.5 Ma. The lack of a marked increase in the planktic $\delta^{18}O$ record at this time implies that the cooling was associated with a freshening of surface waters (Figure 5c). Interestingly, this interval corresponds to a period of very high sedimentation rates (Supplementary Figure S1), which might be consistent with enhanced precipitation and runoff, lowering regional surface salinity.

4.3 Implications for the global climate state during the mid-late Miocene

Previous studies utilizing the $U^{k}{}_{37}$proxy suggest a substantial cooling of sea surface temperature at mid-to-high latitudes in both hemispheres between 10 and 5.5 Ma, whilst tropical sea surface temperatures show limited cooling in the late Miocene prior to ~7 Ma (*Herbert et al.* , 2016;*LaRiviere et al.* , 2012). The absolute tropical SST record reported in this study supports the finding that the latitudinal temperature gradient steepened from ~10 Ma, as the climate system transitioned towards its modern-day state. Furthermore, support for the absolute temperatures reconstructed by the alkenone proxy suggests that the interval between 10 and 7.5 Ma was associated with enhanced polar amplification, significantly greater than that calculated for the greenhouse climate of the Eocene (*Cramwinckel et al.* , 2018). There is little evidence for a significant change in pCO_2 in this interval (*Sosdian et al.* , 2018;*Stoll et al.* , 2019) (Figure 7). We speculate that the marked regional cooling between 10 and 7.5 Ma perhaps reflects processes internal to the climate system, involving for example ocean-atmospheric heat transport, sea ice extent, or changes in regional cloud cover. A combined data-modelling approach would help constrain possible factors and explore potential relationships between this highly heterogenous cooling and the CO_2 drawdown that was associated with the subsequent global late Miocene Cooling starting ~7.5 Ma (Figure 7).

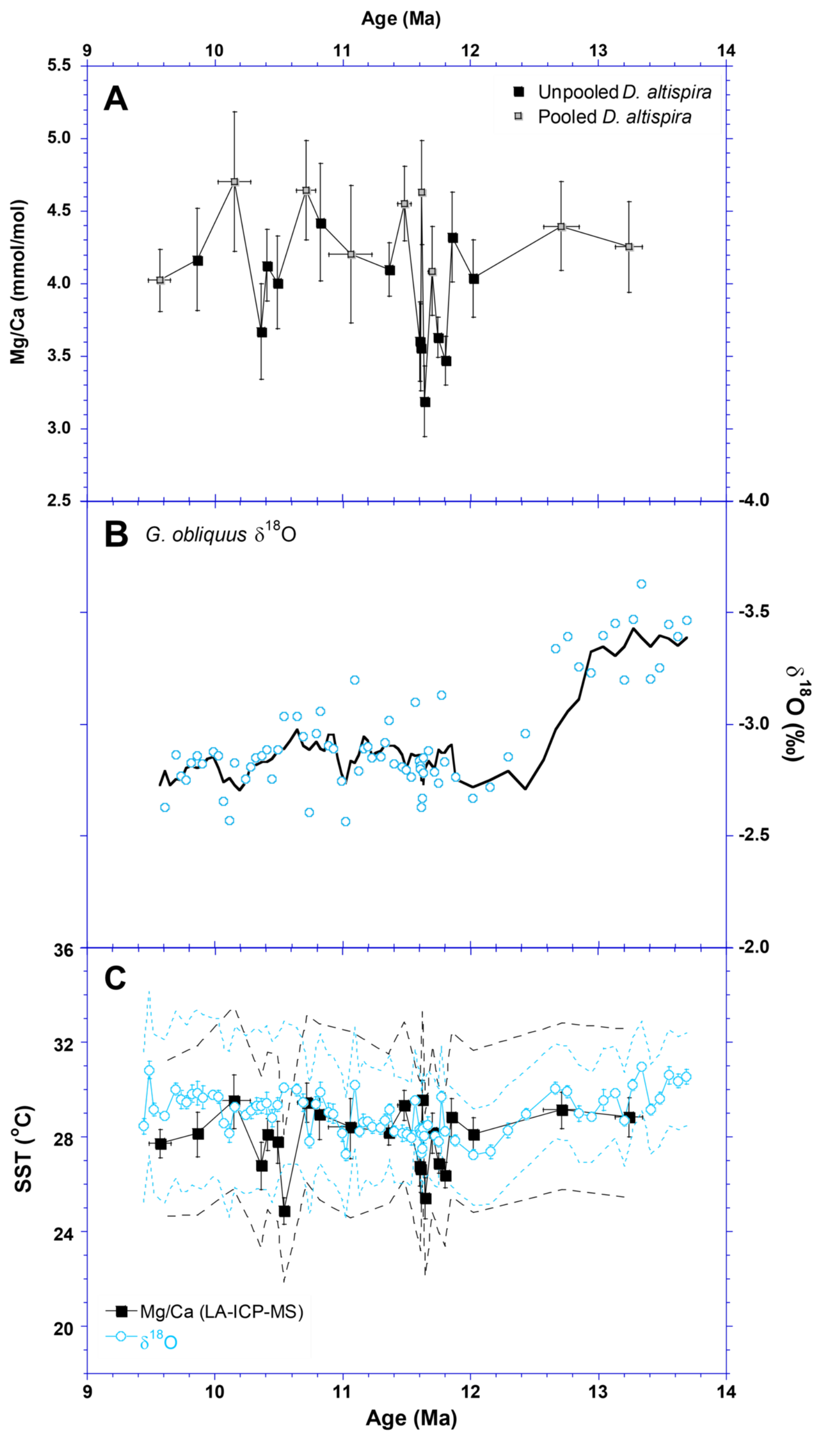

Figure 7 : Summary of global climate through the mid-to-late Miocene. (a) Sea surface temperature estimates from Sunbird-1, fellow low latitude ODP sites 850 (*Zhang et al.* , 2014) and 761 (*Sosdian and Lear,* 2020), mid latitude Northern Hemisphere ODP site 1021 (*LaRiviere et al.,* 2012), and mid-latitude Southern Hemisphere site 1125 (*Herbert et al.,* 2016), and high-latitude Northern Hemisphere ODP Site 982

(*Herbert et al.* , 2016). ODP Site 761 data is displayed on an alternative axis as SST anomalies relative to the baseline average from 16.0 – 15.5 Ma. (b) pCO_2reconstructions, with Y axis on a log scale, of *Sosdian et al.*(2018) applying the CCD reconstruction of *Pälike et al.* (2012) and the $\delta^{11}B_{SW}$ scenario of*Greenop et al.* (2017), and *Stoll et al.* (2019) applying temperature estimates from *Bolton et al.* (2016) and *Zhang et al.* (2013). Confidence intervals (95%) are displayed as dashed lines and error bars respectively. (c) Composite benthic $\delta^{18}O$ record showing data that have been smoothed by a locally weighted function over 20 kyr (blue curve) and 1 Myr (red curve) (*Westerhold et al.* , 2020). Blue, yellow, and gray panels indicate intervals of ice sheet expansion across the Mid Miocene Climate Transition (MMCT) associated with CO_2 decline, the steepening of latitudinal temperature gradeints in the absence of a CO_2 trend, and the Late Miocene Cooling (LMC).

5 Conclusions

Our Sunbird-1 sea surface temperature estimates from LA-ICP-MS Mg/Ca analyses are in good agreement with those using the $\delta^{18}O$ paleo-thermometer on glassy foraminifera, supporting the use of LA-ICP-MS micro-analysis across multiple specimens for reconstructing paleotemperatures. This analytical technique has allowed the reconstruction of reliable Mg/Ca derived paleotemperatures using foraminifera whose bulk trace element ratios demonstrate diagenetic contamination by authigenic coatings. This finding opens the potential for Mg/Ca paleothermometry on other challenging time intervals, and locations, where contaminant coatings have previously inhibited the geochemical analysis of primary foraminiferal calcite. We present new sea surface temperature records from planktic foraminiferal Mg/Ca for the south west Indian Ocean between 13.5 Ma and 9.5 Ma. Absolute estimates of 24-310C suggest that sea surface temperature was relatively constant through the interval, although our record also suggests two intervals of regional cooling and freshening of surface waters at 11.8 and 10.7 Ma. The late Miocene represented a key interval in the transition of Earth's climate to its modern state, including the development of stronger latitudinal temperature gradients. Our new temperature record suggests that different mechanisms may have been responsible for this cooling. The initial cooling from ˜10 Ma at mid to high latitudes in both hemispheres was not associated with significant cooling at low latitudes. On the other hand, the late Miocene cooling between ˜7.5 and 5.5 Ma was global in nature and associated with a drawdown in pCO_2. Further work should therefore explore the mechanisms responsible for the enhanced polar amplification between 10 and 7.5 Ma, and the possibility of carbon cycle feedbacks contributing to the subsequent late Miocene Cooling.

Acknowledgments, Samples, and Data

This study uses samples from the Sunbird-1 core provided by BG-Group. All data from this study can be found in Table 1 and Supplementary Tables S1 to S11,and aredeposited in the Zenodo online data repository http://doi.org/10.5281/zenodo.4472994. We thank Alexandra Nederbragt and Anabel Morte-Rodeñas for laboratory assistance. We thank the reviewers and editor for their insightful comments that improved the manuscript. This research was supported by NERC iCASE studentship BW/22003105 (M.G.N.), and NE/L009633/1 grant to C.H.L.

References

Anand, P., Elderfield, H., & Conte, M. H. (2003). Calibration of Mg/Ca thermometry in planktonic foraminifera from a sediment trap time series.*Paleoceanography, 18* (2). https://doi.org/10.1029/2002PA000846

Aze, T., Ezard, T. H., Purvis, A., Coxall, H. K., Stewart, D. R., Wade, B. S., & Pearson, P. N. (2011). A phylogeny of Cenozoic macroperforate planktonic foraminifera from fossil data. *Biological Reviews, 86* (4), 900-927. https://doi.org/10.1111/j.1469-185X.2011.00178.x

Backman, J., Raffi, I., Rio, D., Fornaciari, E., & Pälike, H. (2012). Biozonation and biochronology of Miocene through Pleistocene calcareous nannofossils from low and middle latitudes. *Newsletters on Stratigraphy, 45* (3), 221-244. 10.1127/0078-0421/2012/0022

Badger, M. P., Lear, C. H., Pancost, R. D., Foster, G. L., Bailey, T. R., Leng, M. J., & Abels, H. A. (2013). CO2 drawdown following the middle Miocene expansion of the Antarctic Ice Sheet.*Paleoceanography, 28* (1), 42-53. https://doi.org/10.1002/palo.20015

Barker, S., Greaves, M., & Elderfield, H. (2003). A study of cleaning procedures used for foraminiferal Mg/Ca paleothermometry.*Geochemistry, Geophysics, Geosystems, 4* (9). https://doi.org/10.1029/2003GC000559

Bemis, B. E., Spero, H. J., Bijma, J., & Lea, D. W. (1998). Reevaluation of the oxygen isotopic composition of planktonic foraminifera: Experimental results and revised paleotemperature equations. *Paleoceanography, 13* (2), 150-160. https://doi.org/10.1029/98PA00070

Bertlich, J., Nürnberg, D., Hathorne, E. C., De Nooijer, L. J., Mezger, E. M., Kienast, M., et al. (2018). Salinity control on Na incorporation into calcite tests of the planktonic foraminifera Trilobatus sacculifer–evidence from culture experiments and surface sediments.*Biogeosciences (BG), 15* (20), 5991-6018. http://dx.doi.org/10.5194/bg-2018-164

Boyer, T. P., Antonov, J. I., Baranova, O. K., Coleman, C., Garcia, H. E., Grodsky, A., et al. (2013). World Ocean Database 2013.

Boyle, E., & Keigwin, L. (1985). Comparison of Atlantic and Pacific paleochemical records for the last 215,000 years: Changes in deep ocean circulation and chemical inventories. *Earth and Planetary Science Letters, 76* (1), 135-150. http://doi.org/0012-821x/85/$03.30

Boyle, E. A. (1983). Manganese carbonate overgrowths on foraminifera tests. *Geochimica et Cosmochimica Acta, 47* (10), 1815-1819. https://doi.org/10.1016/0016-7037(83)90029-7

Broecker, W. S., Peng, T.-H., & Beng, Z. (1982). *Tracers in the Sea* : Lamont-Doherty Geological Observatory, Columbia University.

Chen, P., Yu, J., & Jin, Z. (2017). An evaluation of benthic foraminiferal U/Ca and U/Mn proxies for deep ocean carbonate chemistry and redox conditions. *Geochemistry, Geophysics, Geosystems* . Article in Press. http://doi.org/10.1002/2016GC006730

Coggon, R. M., Teagle, D. A., Smith-Duque, C. E., Alt, J. C., & Cooper, M. J. (2010). Reconstructing past seawater Mg/Ca and Sr/Ca from mid-ocean ridge flank calcium carbonate veins. *Science, 327* (5969), 1114-1117. http://doi.org/10.1126/science.1182252

Cramer, B., Miller, K., Barrett, P., & Wright, J. (2011). Late Cretaceous–Neogene trends in deep ocean temperature and continental ice volume: reconciling records of benthic foraminiferal geochemistry (δ18O and Mg/Ca) with sea level history. *Journal of Geophysical Research: Oceans (1978–2012), 116* (C12). https://doi.org/10.1029/2011JC007255

Cramwinckel, M. J., Huber, M., Kocken, I. J., Agnini, C., Bijl, P. K., Bohaty, S. M., et al. (2018). Synchronous tropical and polar temperature evolution in the Eocene. *Nature, 559* (7714), 382-386. http://doi.org/10.1038/s41586-018-0272-2

Creech, J. B., Baker, J. A., Hollis, C. J., Morgans, H. E. G., & Smith, E. G. C. (2010). Eocene sea temperatures for the mid-latitude southwest Pacific from Mg/Ca ratios in planktonic and benthic foraminifera.*Earth and Planetary Science Letters, 299* (3–4), 483-495. http://dx.doi.org/10.1016/j.epsl.2010.09.039

de Nooijer, L. J., Hathorne, E. C., Reichart, G.-J., Langer, G., & Bijma, J. (2014). Variability in calcitic Mg/Ca and Sr/Ca ratios in clones of the benthic foraminifer Ammonia tepida. *Marine Micropaleontology, 107* , 32-43. https://doi.org/10.1016/j.marmicro.2014.02.002

de Nooijer, L. J., van Dijk, I., Toyofuku, T., & Reichart, G. J. (2017). The Impacts of Seawater Mg/Ca and Temperature on Element Incorporation in Benthic Foraminiferal Calcite. *Geochemistry, Geophysics, Geosystems, 18* (10), 3617-3630. http://doi.org/10.1002/2017GC007183Delaney, M. L., Be, A. W. H., & Boyle, E. A. (1985). Li, Sr, Mg, and Na in foraminiferal calcite shelss from laboratory culture sediment traps, and sediment cores.*Geochim. Cosmochim. Acta, 49* (6), 1327-1341. https://doi.org/10.1016/0016-7037(85)90284-4

Detlef, H., Sosdian, S. M., Kender, S., Lear, C. H., & Hall, I. R. (2019). Multi-elemental composition of authigenic carbonates in benthic foraminifera from the eastern Bering Sea continental margin (International Ocean Discovery Program Site U1343). *Geochimica et Cosmochimica Acta* . https://doi.org/10.1016/j.gca.2019.09.025

Dickson, J. A. D. (2002). Fossil Echinoderms As Monitor of the Mg/Ca Ratio of Phanerozoic Oceans. *Science, 298* (5596), 1222-1224. http://doi.org/10.1126/science.1075882

Eggins, S., De Deckker, P., & Marshall, J. (2003). Mg/Ca variation in planktonic foraminifera tests: implications for reconstructing palaeo-seawater temperature and habitat migration. *Earth and Planetary Science Letters, 212* (3), 291-306. https://doi.org/10.1016/S0012-821X(03)00283-8

Eggins, S. M., Sadekov, A., & De Deckker, P. (2004). Modulation and daily banding of Mg/Ca in Orbulina universa tests by symbiont photosynthesis and respiration: a complication for seawater thermometry? *Earth and Planetary Science Letters, 225* (3), 411-419. https://doi.org/10.1016/j.epsl.2004.06.019

Evans, D. and Müller, W. (2012). Deep time foraminifera Mg/Ca paleothermometry: Nonlinear correction for secular change in seawater Mg/Ca. *Paleoceanography, 27(4).*https://doi.org/10.1029/2012PA002315

Evans, D., Erez, J., Oron, S. and Müller, W., (2015a). Mg/Ca-temperature and seawater-test chemistry relationships in the shallow-dwelling large benthic foraminifera Operculina ammonoides. Geochimica et Cosmochimica Acta, 148, pp.325-342. https://doi.org/10.1016/j.gca.2014.09.039

Evans, D., Bhatia, R., Stoll, H., & Müller, W. (2015b). LA-ICPMS Ba/Ca analyses of planktic foraminifera from the Bay of Bengal: Implications for late Pleistocene orbital control on monsoon freshwater flux. *Geochemistry, Geophysics, Geosystems, 16* (8), 2598-2618. https://doi.org/10.1002/2015GC005822

Evans, D., Brierley, C., Raymo, M. E., Erez, J., & Muller, W. (2016). Planktic foraminifera shell chemistry response to seawater chemistry: Pliocene-Pleistocene seawater Mg/Ca, temperature and sea level change. *Earth and Planetary Science Letters* . Article in Press. http://doi.org/10.1016/j.epsl.2016.01.013

Evans, D., & Muller, W. (2018). Automated Extraction of a Five-Year LA-ICP-MS Trace Element Dataset of Ten Common Glass and Carbonate Reference Materials: Long-Term Data Quality, Optimisation and Laser Cell Homogeneity. *Geostandards and Geoanalytical Research* . https://doi.org/10.1111/ggr.12204

Evans, D., Sagoo, N., Renema, W., Cotton, L. J., Muller, W., Todd, J. A., et al. (2018). Eocene greenhouse climate revealed by coupled clumped isotope-Mg/Ca thermometry. *Proceedings of the National Academy of Sciences of the United States of America, 115* (6), 1174-1179. Article. http://doi.org/10.1073/pnas.1714744115

Evans, D., Wade, B. S., Henehan, M., Erez, J., & Muller, W. (2016). Revisiting carbonate chemistry controls on planktic foraminifera Mg / Ca: Implications for sea surface temperature and hydrology shifts over the Paleocene-Eocene Thermal Maximum and Eocene-Oligocene transition. *Climate of the Past, 12* (4), 819-835. Article. http://doi.org/10.5194/cp-12-819-2016

Farrell, J. W., Raffi, I., Janecek, T. R., Murray, D. W., Levitan, M., Dadey, K. A., et al. (1995). 35. LATE NEOGENE SEDIMENTATION PATTERNS IN THE EASTERN EQUATORIAL PACIFIC OCEAN1.

Fehrenbacher, J. S., & Martin, P. A. (2014). Exploring the dissolution effect on the intrashell Mg/Ca variability of the planktic foraminifer Globigerinoides ruber. *Paleoceanography, 29* (9), 854-868. https://doi.org/10.1002/2013PA002571

Fehrenbacher, J. S., Spero, H. J., Russell, A. D., Vetter, L., & Eggins, S. (2015). Optimizing LA-ICP-MS analytical procedures for elemental depth profiling of foraminifera shells. *Chemical Geology, 407-408* , 2-9. http://doi.org/10.1016/j.chemgeo.2015.04.007

Foster, G. L., Lear, C. H., & Rae, J. W. B. (2012). The evolution of pCO2, ice volume and climate during the middle Miocene. *Earth and Planetary Science Letters, 341–344* (0), 243-254.

http://dx.doi.org/10.1016/j.epsl.2012.06.007

Foster, G. L., & Rae, J. W. (2015). Reconstructing Ocean pH with Boron Isotopes in Foraminifera. *Annual Review of Earth and Planetary Sciences* (0). https://www.annualreviews.org/doi/full/10.1146/annurev-earth-060115-012226#_i63

Geerken, E., De Nooijer, L. J., Van DIjk, I., & Reichart, G.-J. (2018). Impact of salinity on element incorporation in two benthic foraminiferal species with contrasting magnesium contents. *Biogeosciences, 15* (7), 2205-2218. https://doi.org/10.5194/bg-15-2205-2018

Gray, W. R., & Evans, D. (2019). Nonthermal influences on Mg/Ca in planktonic foraminifera: a review of culture studies and application to the Last Glacial Maximum. *Paleoceanography and Paleoclimatology, 34* (3), 306-315. https://doi.org/10.1029/2018PA003517

Gray, W. R., Weldeab, S., Lea, D. W., Rosenthal, Y., Gruber, N., Donner, B., & Fischer, G. (2018). The effects of temperature, salinity, and the carbonate system on Mg/Ca in Globigerinoides ruber (white): A global sediment trap calibration. *Earth and Planetary Science Letters, 482* , 607-620. Article. http://doi.org/10.1016/j.epsl.2017.11.026

Greenop, R., Foster, G. L., Wilson, P. A., & Lear, C. H. (2014). Middle Miocene climate instability associated with high-amplitude CO2 variability. *Paleoceanography, 29* (9), 845-853. https://doi.org/10.1002/2014PA002653

Greenop, R., Hain, M. P., Sosdian, S. M., Oliver, K. I. C., Goodwin, P., Chalk, T. B., et al. (2017). A record of Neogene seawater δ11B reconstructed from paired δ11B analyses on benthic and planktic foraminifera. *Climate of the Past, 13* (2), 149-170. Article. https://doi.org/10.5194/cp-13-149-2017

Guillong, M., L. Meier, D., Allan, M., A. Heinrich, C., & Yardley, B. (2008). *SILLS: A MATLAB-based program for the reduction of laser ablation ICP-MS data of homogeneous materials and inclusions* (Vol. 40).

Hasenfratz, A. P., Martínez-García, A., Jaccard, S. L., Vance, D., Wälle, M., Greaves, M., & Haug, G. H. (2016). Determination of the Mg/Mn ratio in foraminiferal coatings: An approach to correct Mg/Ca temperatures for Mn-rich contaminant phases. *Earth and Planetary Science Letters* . http://dx.doi.org/10.1016/j.epsl.2016.10.004

Hasiuk, F.J. and Lohmann, K.C., 2010. Application of calcite Mg partitioning functions to the reconstruction of paleocean Mg/Ca. Geochimica et Cosmochimica Acta, 74(23), pp.6751-6763. https://doi.org/10.1016/j.gca.2010.07.030

Henehan, M. J., Rae, J. W. B., Foster, G. L., Erez, J., Prentice, K. C., Kucera, M., et al. (2013). Calibration of the boron isotope proxy in the planktonic foraminifera Globigerinoides ruber for use in palaeo-CO2 reconstruction. *Earth and Planetary Science Letters, 364* , 111-122. https://doi.org/10.1016/j.epsl.2012.12.029

Herbert, T. D., Lawrence, K. T., Tzanova, A., Peterson, L. C., Caballero-Gill, R., & Kelly, C. S. (2016). Late Miocene global cooling and the rise of modern ecosystems. *Nature Geoscience* . https://doi.org/10.1038/ngeo2813

Hines, B. R., Hollis, C. J., Atkins, C. B., Baker, J. A., Morgans, H. E. G., & Strong, P. C. (2017). Reduction of oceanic temperature gradients in the early Eocene Southwest Pacific Ocean. *Palaeogeography, Palaeoclimatology, Palaeoecology, 475* , 41-54. https://doi.org/10.1016/j.palaeo.2017.02.037

Holland, K., Branson, O., Haynes, L. L., Hönisch, B., Allen, K. A., Russell, A. D., et al. (2020). Constraining multiple controls on planktic foraminifera Mg/Ca. *Geochimica et Cosmochimica Acta, 273* , 116-136. Article. https://doi.org/10.1016/j.gca.2020.01.015

Hollis, C., Dunkley Jones, T., Anagnostou, E., Bijl, P., Cramwinckel, M., Cui, Y., et al. (2019). The DeepMIP contribution to PMIP4: methodologies for selection, compilation and analysis of latest Paleocene and early Eocene climate proxy data, incorporating version 0.1 of the DeepMIP database. *Geoscientific Model Development Discussions, 2019* , 1-98. http://dx.doi.org/10.5194/gmd-12-3149-2019

Hollis, C., Hines, B., Littler, K., Villasante-Marcos, V., Kulhanek, D., Strong, C., et al. (2015). The Paleocene–Eocene Thermal Maximum at DSDP Site 277, Campbell Plateau, southern Pacific Ocean. https://doi.org/10.5194/cp-11-1009-2015

Hönisch, B., Allen, K. A., Lea, D. W., Spero, H. J., Eggins, S. M., Arbuszewski, J., et al. (2013). The influence of salinity on Mg/Ca in planktic foraminifers–Evidence from cultures, core-top sediments and complementary δ18O. *Geochimica et Cosmochimica Acta, 121* , 196-213. https://doi.org/10.1016/j.gca.2013.07.028

Horita, J., Zimmermann, H., & Holland, H. D. (2002). Chemical evolution of seawater during the Phanerozoic: Implications from the record of marine evaporites. *Geochimica et Cosmochimica Acta, 66* (21), 3733-3756. https://doi.org/10.1016/S0016-7037(01)00884-5

Huang, Y., Clemens, S. C., Liu, W., Wang, Y., & Prell, W. L. (2007). Large-scale hydrological change drove the late Miocene C4 plant expansion in the Himalayan foreland and Arabian Peninsula. *Geology, 35* (6), 531-534. https://doi.org/10.1130/G23666A.1

Hut, G. (1987). Consultants' group meeting on stable isotope reference samples for geochemical and hydrological investigations.

Jiang, S., Wise, S., & Wang, Y. (2007). *Cause of the middle/late Miocene carbonate crash: dissolution or low productivity.* Paper presented at the Proceedings of the Ocean Drilling Program. Scientific Results.

Jochum, K. P., Weis, U., Stoll, B., Kuzmin, D., Yang, Q., Raczek, I., et al. (2011a). Determination of reference values for NIST SRM 610–617 glasses following ISO guidelines. *Geostandards and Geoanalytical Research, 35* (4), 397-429. https://doi.org/10.1111/j.1751-908X.2011.00120.x

Jochum, K.P., Wilson, S.A., Abouchami, W., Amini, M., Chmeleff, J., Eisenhauer, A., Hegner, E., Iaccheri, L.M., Kieffer, B., Krause, J. and McDonough, W.F., (2011b). GSD-1G and MPI-DING reference glasses for in situ and bulk isotopic determination. Geostandards and Geoanalytical Research, 35(2), pp.193-226. https://doi.org/10.1111/j.1751-908X.2010.00114.x

Keller, G. (1985). Depth stratification of planktonic foraminifers in the Miocene ocean. *The Miocene ocean: paleoceanography and biogeography, 163* , 177-196.

Keller, G., & Barron, J. A. (1987). Paleodepth distribution of Neocene deep-sea hiatuses. *Paleoceanography, 2* (6), 697-713. https://doi.org/10.1029/PA002i006p00697

Kısakürek, B., Eisenhauer, A., Böhm, F., Garbe-Schönberg, D., & Erez, J. (2008). Controls on shell Mg/Ca and Sr/Ca in cultured planktonic foraminiferan, Globigerinoides ruber (white). *Earth and Planetary Science Letters, 273* (3-4), 260-269. https://doi.org/10.1016/j.epsl.2008.06.026

Knorr, G., Butzin, M., Micheels, A., & Lohmann, G. (2011). A warm Miocene climate at low atmospheric CO2 levels. *Geophysical Research Letters, 38* (20). https://doi.org/10.1029/2011GL048873

Koho, K., de Nooijer, L., & Reichart, G. (2015). Combining benthic foraminiferal ecology and shell Mn/Ca to deconvolve past bottom water oxygenation and paleoproductivity. *Geochimica et Cosmochimica Acta, 165* , 294-306. https://doi.org/10.1016/j.gca.2015.06.003

LaRiviere, J. P., Ravelo, A. C., Crimmins, A., Dekens, P. S., Ford, H. L., Lyle, M., & Wara, M. W. (2012). Late Miocene decoupling of oceanic warmth and atmospheric carbon dioxide forcing. *Nature, 486* (7401), 97. https://doi.org/10.1038/nature11200

Lear, C. H., Coxall, H. K., Foster, G. L., Lunt, D. J., Mawbey, E. M., Rosenthal, Y., et al. (2015). Neogene ice volume and ocean temperatures: Insights from infaunal foraminiferal Mg/Ca paleothermometry. *Paleoceanography* . https://doi.org/10.1002/2015PA002833

Lear, C. H., Mawbey, E. M., & Rosenthal, Y. (2010). Cenozoic benthic foraminiferal Mg/Ca and Li/Ca records: Toward unlocking temperatures and saturation states. *Paleoceanography, 25* (4). https://doi.org/10.1029/2009pa001880

Lear, C. H., Rosenthal, Y., & Slowey, N. (2002). Benthic foraminiferal Mg/Ca-paleothermometry: A revised core-top calibration. *Geochimica et Cosmochimica Acta, 66* (19), 3375-3387. https://doi.org/10.1016/S0016-7037(02)00941-9

LeGrande, A. N., & Schmidt, G. A. (2006). Global gridded data set of the oxygen isotopic composition in seawater. *Geophysical Research Letters, 33* (12). https://doi.org/10.1029/2006GL026011

Lemarchand, D., Gaillardet, J., Lewin, E., & Allegre, C. (2002). Boron isotope systematics in large rivers: implications for the marine boron budget and paleo-pH reconstruction over the Cenozoic. *Chemical Geology, 190* (1), 123-140. https://doi.org/10.1016/S0009-2541(02)00114-6

Longerich, H. P., Jackson, S. E., & Günther, D. (1996). Inter-laboratory note. Laser ablation inductively coupled plasma mass spectrometric transient signal data acquisition and analyte concentration calculation. *Journal of analytical atomic spectrometry, 11* (9), 899-904. https://doi.org/10.1039/JA9961100899

Lübbers, J., Kuhnt, W., Holbourn, A. E., Bolton, C. T., Gray, E., Usui, Y., et al. (2019). The middle to late Miocene "Carbonate Crash" in the equatorial Indian Ocean. *Paleoceanography and Paleoclimatology, 34* (5), 813-832. https://doi.org/10.1029/2018PA003482

Lunt, D. J., Flecker, R., Valdes, P. J., Salzmann, U., Gladstone, R., & Haywood, A. M. (2008). A methodology for targeting palaeo proxy data acquisition: A case study for the terrestrial late Miocene. *Earth and Planetary Science Letters, 271* (1), 53-62. https://doi.org/10.1016/j.epsl.2008.03.035

Lyle, M., Dadey, K. A., & Farrell, J. W. (1995). 42. The Late Miocene (11–8 Ma) Eastern Pacific Carbonate Crash: evidence for reorganization of deep-water Circulation by the closure of the Panama Gateway.*1995 Proceedings of the Ocean Drilling Program, Scientific Results, 138* .

Mayk, D., Fietzke, J., Anagnostou, E., & Paytan, A. (2020). LA-MC-ICP-MS study of boron isotopes in individual planktonic foraminifera: A novel approach to obtain seasonal variability patterns.*Chemical Geology, 531* . Article. https://doi.org/10.1016/j.chemgeo.2019.119351

Müller, P. J., Kirst, G., Ruhland, G., Von Storch, I., & Rosell-Melé, A. (1998). Calibration of the alkenone paleotemperature index U 37 K' based on core-tops from the eastern South Atlantic and the global ocean (60 N-60 S). *Geochimica et Cosmochimica Acta, 62* (10), 1757-1772. https://doi.org/10.1016/S0016-7037(98)00097-0

Nairn, M. (2018). *Mid-Late Miocene climate constrained by a new Laser Ablation ICP-MS set up.* Cardiff University,

Nurnberg, D., Bijma, J., & Hemleben, C. (1996). Assessing the reliability of magnesium in foraminiferal calcite as a proxy for water mass temperatures. *Geochimica et Cosmochimica Acta, 60* (5), 803-814.

Pagani, M., Freeman, K. H., & Arthur, M. A. (1999). Late Miocene Atmospheric CO₂ Concentrations and the Expansion of C₄ Grasses.*Science, 285* (5429), 876-879. https://doi.org/10.1126/science.285.5429.876

Pearson, P. N., & Burgess, C. E. (2008). Foraminifer test preservation and diagenesis: comparison of high latitude Eocene sites.*Geological Society, London, Special Publications, 303* (1), 59-72. https://doi.org/10.1144/SP303.5

Pearson, P. N., Ditchfield, P. W., Singano, J., Harcourt-Brown, K. G., Nicholas, C. J., Olsson, R. K., et al. (2001). Warm tropical sea surface temperatures in the Late Cretaceous and Eocene epochs. *Nature, 413* (6855), 481-487. https://doi.org/10.1038/35097000

Pena, L., Calvo, E., Cacho, I., Eggins, S., & Pelejero, C. (2005). Identification and removal of Mn-Mg-rich contaminant phases on foraminiferal tests: Implications for Mg/Ca past temperature reconstructions. *Geochemistry, Geophysics, Geosystems, 6* (9). https://doi.org/10.1029/2005GC000930

Petersen, J., Barras, C., Bezos, A., La, C., De Nooijer, L. J., Meysman, F. J. R., et al. (2018). Mn/Ca intra- and inter-test variability in the benthic foraminifer Ammonia tepida. *Biogeosciences, 15* (1), 331-348. Article. https://doi.org/10.5194/bg-15-331-2018

Pisias, N., & Mix, A. (1988). *Aliasing of the geologic record and the search for long-period Milankovitch cycles* (Vol. 3).

Pound, M. J., Haywood, A. M., Salzmann, U., Riding, J. B., Lunt, D. J., & Hunter, S. J. (2011). A Tortonian (Late Miocene, 11.61–7.25Ma) global vegetation reconstruction. *Palaeogeography, Palaeoclimatology, Palaeoecology, 300* (1), 29-45. https://doi.org/10.1016/j.palaeo.2010.11.029

Raffi, I., Wade, B.S., Palike, H., Beu, A.G., Cooper, R., Crundwell, M.P., Krijgsman, W., Moore, T., Raine, I., Sardella, R. and Vernyhorova, Y.V. (2020). The Neogene Period. In Geologic Time Scale 2020, (pp. 1141-1215). *Elsevier*.https://doi.org/10.1016/B978-0-12-824360-2.00029-2.

Raitzsch, M., & Honisch, B. (2013). Cenozoic boron isotope variations in benthic foraminifers. *Geology, 41* (5), 591-594. https://doi.org/10.1130/g34031.1

Raitzsch, M., Kuhnert, H., Hathorne, E. C., Groeneveld, J., & Bickert, T. (2011). U/Ca in benthic foraminifers: A proxy for the deep-sea carbonate saturation. *Geochemistry, Geophysics, Geosystems, 12* (6). https://doi.org/10.1029/2010GC003344

Rathmann, S., Hess, S., Kuhnert, H., & Mulitza, S. (2004). Mg/Ca ratios of the benthic foraminifera Oridorsalis umbonatus obtained by laser ablation from core top sediments: Relationship to bottom water temperature. *Geochemistry, Geophysics, Geosystems, 5* (12). https://doi.org/10.1029/2004gc000808

Reichart, G.-J., Jorissen, F., Anschutz, P., & Mason, P. R. (2003). Single foraminiferal test chemistry records the marine environment. *Geology, 31* (4), 355-358. https://doi.org/10.1130/0091-7613(2003)031<0355:SFTCRT>2.0.CO;2

Rosenthal, Y., Boyle, E. A., & Slowey, N. (1997). Temperature control on the incorporation of magnesium, strontium, fluorine, and cadmium into benthic foraminiferal shells from Little Bahama Bank: Prospects for thermocline paleoceanography. *Geochimica et Cosmochimica Acta, 61* (17), 3633-3643.

Rousselle, G., Beltran, C., Sicre, M.-A., Raffi, I., & De Rafelis, M. (2013). Changes in sea-surface conditions in the Equatorial Pacific during the middle Miocene–Pliocene as inferred from coccolith geochemistry. *Earth and Planetary Science Letters, 361* , 412-421. http://dx.doi.org/10.1016/j.epsl.2012.11.003

Russell, A. D., Honisch, B., Spero, H. J., & Lea, D. W. (2004). Effects of seawater carbonate ion concentration and temperature on shell U, Mg, and Sr in cultured planktonic foraminifera. *Geochimica et Cosmochimica Acta, 68* (21), 4347-4361. https://doi.org/10.1016/j.gca.2004.03.013

Sadekov, A., Eggins, S. M., De Deckker, P., & Kroon, D. (2008). Uncertainties in seawater thermometry deriving from intratest and intertest Mg/Ca variability in Globigerinoides ruber. *Paleoceanography, 23* (1). https://doi.org/10.1029/2007pa001452

Sadekov, A. Y., Eggins, S. M., & De Deckker, P. (2005). Characterization of Mg/Ca distributions in planktonic foraminifera species by electron microprobe mapping. *Geochemistry, Geophysics, Geosystems, 6* (12). https://doi.org/10.1029/2005GC000973

Schiebel, R., & Hemleben, C. (2017). *Planktic Foraminifers in the Modern Ocean* .

Schlitzer, R., Ocean Data View, odv.awi.de, (2018).

Seki, O., Schmidt, D., Schouten, S., C. Hopmans, E., Sinninghe-Damste, J., & D. Pancost, R. (2012). *Paleoceanographic changes in the Eastern Equatorial Pacific over the last 10 Myr* (Vol. 27).

Sexton, P. F., Wilson, P. A., & Pearson, P. N. (2006). Microstructural and geochemical perspectives on planktic foraminiferal preservation:"Glassy" versus "Frosty". *Geochemistry, Geophysics, Geosystems, 7* (12). https://doi.org/10.1029/2006GC001291

Sosdian, S. M., Greenop, R., Hain, M. P., Foster, G. L., Pearson, P. N., & Lear, C. H. (2018). Constraining the evolution of Neogene ocean carbonate chemistry using the boron isotope pH proxy. *Earth and Planetary Science Letters, 498* , 362-376. https://doi.org/10.1016/j.epsl.2018.06.017

Sosdian, S.M. and Lear, C.H. (2020). Initiation of the Western Pacific Warm Pool at the Middle Miocene Climate Transition?*Paleoceanography and Paleoclimatology, 35(12)* , e2020PA003920. https://doi.org/10.1029/2020PA003920

Stewart, D. R. M., Pearson, P. N., Ditchfield, P. W., & Singano, J. M. (2004). Miocene tropical Indian Ocean temperatures: evidence from three exceptionally preserved foraminiferal assemblages from Tanzania.*Journal of African Earth Sciences, 40* (3), 173-189. https://doi.org/10.1016/j.jafrearsci.2004.09.001

Stoll, H. M., Guitian, J., Hernandez-Almeida, I., Mejia, L. M., Phelps, S., Polissar, P., et al. (2019). Upregulation of phytoplankton carbon concentrating mechanisms during low CO2 glacial periods and implications for the phytoplankton pCO2 proxy. *Quaternary Science Reviews, 208* , 1-20. https://doi.org/10.1016/j.quascirev.2019.01.012

Super, J. R., Thomas, E., Pagani, M., Huber, M., O'Brien, C., & Hull, P. M. (2018). North Atlantic temperature and p CO2 coupling in the early-middle Miocene. *Geology, 46* (6), 519-522. https://doi.org/10.1130/G40228.1

Thil, F., Blamart, D., Assailly, C., Lazareth, C. E., Leblanc, T., Butsher, J., & Douville, E. (2016). Development of laser ablation multi-collector inductively coupled plasma mass spectrometry for boron isotopic measurement in marine biocarbonates: New improvements and application to a modern Porites coral. *Rapid Communications in Mass Spectrometry, 30* (3), 359-371. Article. https://doi.org/10.1002/rcm.7448

van Hinsbergen, D. J., de Groot, L. V., van Schaik, S. J., Spakman, W., Bijl, P. K., Sluijs, A., et al. (2015). A paleolatitude calculator for paleoclimate studies. *PloS one, 10* (6). https://doi.org/DOI:10.1371/journal.pone.0126946

Vetter, L., Kozdon, R., Mora, C. I., Eggins, S. M., Valley, J. W., Honisch, B., & Spero, H. J. (2013). Micron-scale intrashell oxygen isotope variation in cultured planktic foraminifers. *Geochimica et Cosmochimica Acta, 107* , 267-278. https://doi.org/10.1016/j.gca.2012.12.046

von der Heydt, A., & Dijkstra, H. A. (2006). Effect of ocean gateways on the global ocean circulation in the late Oligocene and early Miocene.*Paleoceanography, 21* (1). https://doi.org/10.1029/2005pa001149

Wade, B. S., Pearson, P. N., Berggren, W. A., & Palike, H. (2011). Review and revision of Cenozoic tropical planktonic foraminiferal biostratigraphy and calibration to the geomagnetic polarity and astronomical time scale. *Earth-Science Reviews, 104* (1), 111-142. https://doi.org/10.1016/j.earscirev.2010.09.003

Yu, J., & Elderfield, H. (2008). Mg/Ca in the benthic foraminifera< i> Cibicidoides wuellerstorfi</i> and< i> Cibicidoides mundulus</i>: Temperature versus carbonate ion saturation. *Earth and Planetary Science Letters, 276* (1), 129-139. https://doi.org/10.1016/j.epsl.2008.09.015

Zachos, J. C., Stott, L. D., & Lohmann, K. C. (1994). Evolution of early Cenozoic marine temperatures. *Paleoceanography, 9* (2), 353-387. https://doi.org/10.1029/93PA03266

Zhang, Y. G., Pagani, M., & Liu, Z. (2014). A 12-Million-Year Temperature History of the Tropical Pacific Ocean. *Science, 344* (6179), 84-87. https://doi.org/10.1126/science.1246172

Tropical Sea Surface Temperatures following the Middle Miocene Climate Transition from Laser-Ablation ICP-MS analysis of glassy foraminifera

Michael G. Nairn[1], Caroline H. Lear[1], Sindia M. Sosdian[1], Trevor R Bailey[2], and Simon Beavington-Penney[3]

[1]School of Earth and Environmental Sciences, Cardiff University, Cardiff, UK,

[2]Department of Natural Sciences, Amgueddfa Cymru, National Museum Wales, Cathays Park, Cardiff,

[3]BG Group, 100 Thames Valley Park Drive, Reading, RG6 1PT, UK*

Corresponding author: Michael G. Nairn (NairnMG@cardiff.ac.uk)

*Current address: Department of Earth and Environmental Sciences, The University of Manchester, Williamson Building, Oxford Road, Manchester, M13 9PL, UK.

Key Points:

- Laser-Ablation ICP-MS facilitates absolute sea surface temperature reconstructions using foraminifera with diagenetic coatings.
- Tropical sea surface temperatures remained relatively stable at 24-31°C following the Miocene Climate Transition.
- Development of an increased latitudinal temperature gradient began prior to the Late Miocene Cooling.

Abstract

The mid-to-late Miocene is proposed as a key interval in the transition of the Earth's climate state towards that of the modern-day. However, it remains a poorly understood interval in the evolution of Cenozoic climate, and the sparse proxy-based climate reconstructions are associated with large uncertainties. In particular, tropical sea surface temperature (SST) estimates largely rely on the unsaturated alkenone U^{k}_{37} proxy, which fails to record temperatures higher than 29˚C, the TEX_{86} proxy which has challenges around its calibration, and Mg/Ca ratios of poorly preserved foraminifera. We reconstruct robust, absolute, SSTs between 13.5 Ma and 9.5 Ma from the South West Indian Ocean (paleolatitude ~5.5˚S) using Laser-Ablation (LA-) ICP-MS microanalysis of glassy planktic foraminiferal Mg/Ca. Employing this microanalytical technique, and stringent screening criteria, permits the reconstruction of paleotemperatures using foraminifera which although glassy, are contaminated by authigenic coatings. Our absolute estimates of 24-31^{0}C suggest that SST in the tropical Indian Ocean was relatively constant between 13.5 and 9.5 Ma, similar to those reconstructed from the tropics using the U^{k}_{37} alkenone proxy. This finding suggests an interval of enhanced polar amplification between 10 and 7.5 Ma, immediately prior to the global late Miocene Cooling.

1 Introduction

The mid-late Miocene is an important interval in the evolution of global climate through the Cenozoic, representing a key period in the transition out of the warm, dynamic climate state of the Miocene Climatic Optimum (MCO) into a more stable unipolar icehouse world (*Badger et al.*, 2013; *Foster et al.*, 2012; *Greenop et al.*, 2014; *Sosdian et al.*, 2018). Despite being characterized by similar to modern day atmospheric CO_2 concentrations (*Foster et al.*, 2012; *Sosdian et al.*, 2018; *Super et al.*, 2018), middle Miocene mean global temperatures were likely significantly warmer than the modern day (*Pound et al.*, 2011; *Rousselle et al.*, 2013). This has been used to suggest a decoupling of global temperature and atmospheric CO_2 forcing (*LaRiviere et al.*, 2012; *Pagani et al.*, 1999), a characteristic which general circulation models struggle to simulate (*Knorr et al.*, 2011; *von der Heydt and Dijkstra*, 2006). It has also been suggested that the late Miocene was an additional important key step in the transition to our modern climate state, as high latitudes cooled more than low latitudes, leading to a marked steepening of latitudinal temperature gradients (*Herbert et al.*, 2016).

The late Miocene Cooling (LMC) between ~ 7.5 and 5.5 Ma was a global phenomenon (*Herbert et al.*, 2016) perhaps associated with decreasing atmospheric pCO_2 (*Stoll et al.*, 2019). The increase in the equator to pole surface temperature gradients was not associated with an increase in the benthic foraminiferal oxygen isotope record, implying that it occurred in the absence of a large increase in continental ice volume (*Herbert et al.*, 2016). Polar amplification in the LMC is consistent with estimates for other time intervals (e.g., *Cramwinckel et al.* (2018)). However, the LMC was also preceded by a significant cooling of mid to high southern and northern latitudes, a heterogenous cooling at high northern latitudes, and a muted, limited cooling in the tropics (*Herbert et al.*, 2016). This heterogenous cooling perhaps suggests an unusually high polar amplification factor for the interval immediately preceding the LMC.

Potential changes in the Earth System that could impact the magnitude of polar amplification include sea ice extent, vegetation induced changes in albedo, cloud cover, or ocean-atmosphere heat transport. Constraining the magnitude and timing of the steepening of latitudinal temperature gradients is therefore important for understanding the factors driving the late Miocene surface cooling specifically, and Earth System feedbacks more generally. Ideally, this would be achieved through a combined data-modelling approach using multi-proxy temperature reconstructions spanning a range of latitudes to increase confidence in calculated changes in temperature gradients.

Despite the significance of this climate interval, the evolution of global sea surface temperatures (SST) and hence temperature gradients during the mid-late Miocene is relatively poorly constrained due to a paucity of complete well-preserved sedimentary successions (*Lunt et al.*, 2008). The widespread carbonate dissolution, which dramatically reduced the sediment carbonate content and preservation quality in deep marine sediments, is termed the middle-late Miocene carbonate crash (*Farrell et al.*, 1995; *Jiang et al.*, 2007; *Keller and Barron*, 1987; *Lübbers et al.*, 2019; *Lyle et al.*, 1995). In addition to these dissolution issues, the majority of foraminifera-bearing Miocene sections are comprised of carbonate rich sediments which have undergone some degree of recrystallisation. The oxygen isotopic composition of planktic foraminifera that have undergone recrystallisation in seafloor sediments has been shown to be biased to colder temperatures (*Pearson et al.*, 2001). While planktic foraminiferal Mg/Ca appears to be less affected than $\delta^{18}O$, the impact of recrystallisation on reconstructed Mg/Ca sea surface temperatures remains an additional source of uncertainty (*Sexton et al.*, 2006). As a consequence, many mid-late Miocene absolute sea surface temperature reconstructions are restricted to estimates based on the unsaturated alkenone proxy and the TEX_{86} proxy (*Herbert et al.*, 2016; *Huang et al.*, 2007; *LaRiviere et al.*, 2012; *Rousselle et al.*, 2013; *Seki et al.*, 2012; *Zhang et al.*, 2014). These records show a cooling in the late Miocene which begins around 10 Ma at high northern and southern latitudes. However, significant cooling in the tropics is not apparent in the alkenone records until ~7.5 Ma, while atmospheric pCO_2 reconstructions also suggest a significant decline from this time (*Sosdian et al.*, 2018; *Stoll et al.*, 2019). At face value therefore, these records imply an interval of enhanced polar amplification between 10 Ma and 7.5 Ma in the absence of significant drawdown of CO_2 or increase in ice volume (*Herbert et al.*, 2016; *Sosdian et al.*, 2018). One significant caveat to this interpretation is that the Uk_{37} alkenone proxy becomes saturated above $28^{0}C$ (*Müller et al.*, 1998) and the late Miocene tropical SSTs prior to 7.5 Ma are at this limit (*Herbert et al.*, 2016). Therefore, an alternative interpretation of the data would be that the high latitudes and the tropics cooled synchronously from ~10 Ma, but the initial cooling in the tropics was not able to be recorded by the Uk_{37} alkenone proxy. Corroboration of the absolute Uk_{37} alkenone temperatures by an independent proxy would therefore confirm the timing of the global late Miocene Cooling and the possible interval of enhanced polar amplification between 10 Ma and 7.5 Ma.

Here we present a new planktic foraminiferal Mg/Ca record from the Sunbird-1 industry well cored offshore Kenya by BG Group. Critically, middle to late Miocene sediments in Sunbird-1 are hemipelagic clays, which has resulted in glassy preservation of the foraminifera. However, the foraminifera are coated with metal-rich authigenic coatings, which are not removed by standard cleaning techniques. Planktic foraminifera were therefore analyzed by laser ablation ICP-MS to obtain Mg/Ca from the primary foraminiferal test and hence enable estimation of absolute SSTs.

2 Materials and Methods

2.1 Site location, stratigraphy, and age control

This study utilizes 91 cuttings, spanning 273 meters at burial depths ranging from 630 m to 903 m, recovered by BG Group from the Sunbird-1 well offshore Kenya (04° 18' 13.268" S, 39° 58' 29.936" E; 723.3 m water depth) (Figure 1, Supplementary Table S1). Sedimentation at Sunbird-1 through the studied interval (9.5-13.5 Ma) is dominated by clays; the fraction of the sediment >63µm averages 11.5% (Supplementary Table S1), much lower than typical carbonate-rich deep-water sites. The impermeable nature and chemical composition of clay-rich sediment reduces diagenetic alteration of primary foraminiferal calcite, making them ideal targets for geochemical analysis (*Pearson et al.*, 2001; *Sexton et al.*, 2006). Tests displaying the desired exceptional preservation appear glassy and translucent under reflected light, and SEM imaging shows retention of the foraminiferal original microstructure (*Pearson and Burgess*, 2008). This style of preferential glassy preservation, as displayed in the Sunbird-1 well, is rare to absent in published records from Miocene foraminifera.

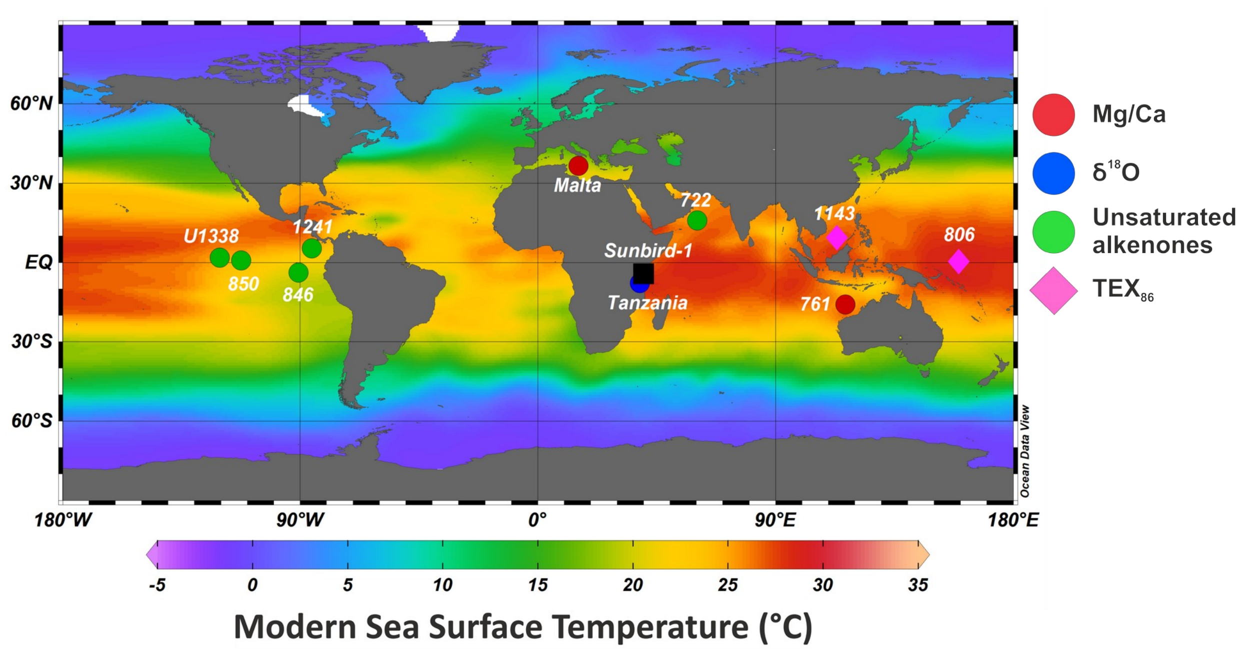

Figure 1: Location of the Sunbird-1 study site (black square). Other sites for which there are mid to late Miocene sea surface temperature reconstructions from Mg/Ca (red circles), $\delta^{18}O$ (blue circles), unsaturated alkenones (green circles) and TEX_{86} (pink diamonds) are shown. Figure produced using Ocean Data Viewer (*Schlitzer, R.,* 2018) using modern-day mean annual sea surface temperature data from the World Ocean Database.

Micropaleontological and calcareous nannoplankton assemblages for Sunbird-1 were analyzed by Haydon Bailey and Liam Gallagher of Network Stratigraphic Consulting. Biostratigraphic datums, correlated with the astronomical timescale of *Raffi et al.* (2020), are based on the planktic foraminifera zonations of *Wade et al.* (2011) and calcareous nanofossil zonations of *Backman et al.* (2012). An age model was constructed by linear interpolation between these biostratigraphic datums (Supplementary Figure S1). Sedimentation rates were ~3 cm/kyr immediately following the middle Miocene Climate Transition (MMCT), and subsequently increased to ~17 cm/kyr between 11.8 and 11.5 Ma, before decreasing to ~8 cm/kyr until 9.5 Ma.

2.2 Foraminiferal stable isotope analysis

Up to 12 individual tests of the planktic foraminifer *Globigerinoides obliquus* showing glassy preservation were used. *G. obliquus* is an extinct, symbiont-bearing species with a tropical to subtropical paleogeographical distribution, and is interpreted as a surface mixed-layer dweller (*Aze et al.*, 2011; *Keller*, 1985). The assertion that *G. obliquus* inhabits and calcifies in the surface mixed layer (*Aze et al.*, 2011; *Keller*, 1985) is supported by multispecies analyses from a 10.0 Ma sediment sample from the Indian Ocean offshore Tanzania showing *G. obliquus* to have the most negative $\delta^{18}O$ (-2.5‰) of all species (Paul Pearson, personal communication, 2019). Tests were crushed between two glass plates ensuring all chambers were opened. Any visible infill was removed using a fine paintbrush under a binocular microscope. Fine clays and other detrital material on the outer surface of the test were removed by rinsing three times in 18.2 MΩ DI water, ultrasonicating for 5-10 seconds in analytical grade methanol, and finally rinsing a further time in 18.2 MΩ DI water. Samples were analyzed at Cardiff University on a ThermoFinnigan MAT253 with online sample preparation using an automated Kiel IV carbonate device. Results are reported relative to Vienna Pee Dee Belemnite, and long−term uncertainty based on repeat analysis of NBS−19 is ±0.08 ‰ (n=469, 2 standard deviations) and on repeat analysis of BCT63 is ±0.07 ‰ (n=310, 2 standard deviations). Data is available in Supplementary Table S2.

2.3 Solution ICP-MS trace metal analysis

Between 10 and 15 individuals of the planktic foraminifer *Dentoglobigerina altispira* from the 250 – 355 μm size fraction were picked and weighed on a six-decimal-place balance to determine average test weight. Individual tests were then crushed between two glass plates ensuring all chambers were opened. Due to the low foraminiferal abundance it was not possible to analyze the same species for stable isotope and trace metal composition. Any visible infill was removed using a fine paintbrush under a binocular microscope. Fragments were cleaned to remove clays and organic matter following the standard protocol (*Barker et al.*, 2003; *Boyle and Keigwin*, 1985). Due to the clay-rich nature of the sediment the clay removal procedure was conducted twice. To test for the possible presence of metal oxides half of the samples were reductively cleaned between the clay removal and oxidative cleaning steps. Samples were dissolved in trace metal pure 0.065 M HNO_3 and diluted with trace metal pure 0.5M HNO_3 to a final volume of 350 µl. Samples were analyzed at Cardiff University on a Thermo Element XR ICP−MS using standards with matched calcium concentrations to reduce matrix effects (*Lear et al.*, 2010; *Lear et al.*, 2002). Together with Mg/Ca, several other ratios (Al/Ca, Mn/Ca, and U/Ca) were analyzed to screen for potential contaminant phases. Data are available in Supplementary Table S3. Long-term analytical precision for Mg/Ca throughout the study is better than 2%.

2.4 Laser ablation-ICP-MS analysis

Direct sampling of solid phase material via laser ablation (LA-) allows for geochemical analyses through individual foraminiferal tests at the sub-micron scale when coupled to an inductively-coupled-plasma mass spectrometer (ICP-MS) (*Detlef et al.*, 2019; *Eggins et al.*, 2004; *Evans et al.*, 2015a; *Fehrenbacher et al.*, 2015; *Hines et al.*, 2017; *Petersen et al.*, 2018; *Reichart et al.*, 2003). A key advantage of analyzing the trace element composition of foraminifera using LA-ICP-MS over the more traditional solution-based ICP-MS is the ability to recognize the diagenetically altered portions of the tests, allowing identification of the primary calcite (*Creech et al.*, 2010; *Hasenfratz et al.*, 2016; *Pena et al.*, 2005). The elemental composition of this primary calcite can provide important information about palaeotemperature (*Nooijer et al.*, 2017; *Eggins et al.*, 2003; *Pena et al.*, 2005) and other paleo-environmental conditions such as pH (*Mayk et al.*, 2020; *Thil et al.*, 2016) and oxygenation (*Koho et al.*, 2015; *Petersen et al.*, 2018).

Up to six specimens of *D. altispira* per sample were selected from 44 depth intervals through the Sunbird-1 core for LA-ICP-MS analysis. Foraminiferal sample preparation included the removal of fine clays and other detrital material on the outer surface of the test using DI water and methanol, but the more aggressive oxidative and reductive steps (*Barker et al.*, 2003; *Boyle and Keigwin*, 1985), were not required for laser ablation analysis (*Vetter et al.*, 2013). The cleaned tests were mounted onto glass slides using double sided carbon tape and were allowed to dry before being mounted into the sample cell (*Evans et al.*, 2015b; *Fehrenbacher et al.*, 2015; *Hines et al.*, 2017).

Analyses were performed using an ArF excimer (193nm) LA- system with dual-volume laser-ablation cell (RESOlution S-155, Australian Scientific Instruments) coupled to a Thermo Element XR ICP-MS. Optimized ablation parameters and analytical settings determined for analyzing foraminifera in the Cardiff University CELTIC laboratory (Supplementary Table S4; (*Detlef et al.*, 2019; *Nairn*, 2018)) were used for this study. Three cleaning pulses to remove any contaminant on the outer ~0.5 µm of the test surface were included prior to analysis. We analyzed ^{25}Mg, ^{27}Al, ^{43}Ca, ^{55}Mn and ^{88}Sr, each isotope having a constant 50 ms dwell time. Typically, intervals with elevated Mn and Al in concert with elevated Mg are interpreted as being contaminant phases (e.g., Fe-Mn oxides-hydroxides or clays), and are commonly found on the inner and outer test surface (*Barker et al.*, 2003; *de Nooijer et al.*, 2014; *Hasenfratz et al.*, 2016; *Koho et al.*, 2015; *Pena et al.*, 2005).

Where possible, three laser spot depth profiles were collected on each of the penultimate (f-1) and previous (f-2) chambers by ablating with 100 consecutive laser pulses in one position on the test. Assuming that each laser pulse only ablates a ~0.1 μm layer of calcite (*Eggins et al.*, 2003), we estimate the profile to represent a transect through the test wall approximately 15 μm long. However, in some cases older chambers were required to ensure six laser profiles per specimen were analyzed (*Nairn*, 2018). NIST SRM 610 glass standard was measured between every six laser profiles, and NIST SRM 612 at the beginning and end of analyses from each sample depth. The reference values for elemental concentrations in both silicate glass standards are taken from the GEOREM website (http://georem.mpch-mainz.gwdg.de/sample_query_pref.asp), updated from *Jochum et al.* (2011a). NIST SRM 612 was used to determine long term external reproducibility using NIST SRM 610. For Mg/Ca, NIST 612 (n=90) had an accuracy of 12.0% and a precision of 3.7% relative to the reported value. A similar ~12% negative offset relative to the reported value of NIST 610-calibrated NIST 612 has been observed over a much longer period of data collection (*Evans and Müller*, 2018). To supplement this assessment, we also conducted accuracy tests using the GOR-132 and KL-2 MPI-DING glasses (*Jochum et al.*, 2011b). For this, GOR-132 and KL2 were treated as unknowns, with both NIST 610 and NIST 612 as calibration standards. For Mg/Ca, GOR-132 (n=25) had an accuracy of 1.1% and a precision of 3.2% relative to the reported value, and KL-2 (n=25) had an accuracy of 0.6% and a precision of 2.6% relative to the reported value when calibrated using NIST 610. These values increased to 10.9% and 9.4% for GOR-132, and 8.2% and 5.4% for KL-2 when calibrated using NIST 612. The NIST 610-calibrated data presented here supports the determination of *Evans et al.,* (2015a) that the Mg values for NIST 612 requires reassessment.

An important issue related to accuracy is that because a well-characterized, homogenous calcite reference material is not currently available for laser ablation use, the glass standards we used have a different matrix to the calcite foraminifera tests (*Evans et al.*, 2015a; *Evans and Müller*, 2018; *Fehrenbacher et al.*, 2015). Therefore, while we have high confidence in the accuracy of the intra-and inter-specimen geochemical variability described in Section 2.6, we must consider the possibility of an analytical bias in the absolute geochemical composition of foraminiferal tests determined by laser ablation ICP-MS. One way to assess the magnitude of such potential bias is to analyse foraminiferal samples by both solution and laser ablation ICP-MS. However, it is important to note that the corrosive cleaning protocol for solution analysis tends to slightly lower primary test calcite Mg/Ca, an issue that is routinely circumvented by employing the same cleaning on calibration samples for paleotemperature reconstructions (*Barker et al.,* 2003). For the purpose of this study, it is therefore important that our LA-ICP-MS technique gives values that are consistent with our samples analysed by solution ICP-MS. We are able to make a direct comparison of our youngest samples in this way, because these do not have significant authigenic coatings biasing the solution analyses. For these samples, our solution and laser ablation results are in excellent agreement, which gives us confidence in the

LA-ICP-MS values for the older samples, where we know the solution ICP-MS results are compromised by authigenic coatings (Supplementary Figure S2). Furthermore, we note that if future work indicates a consistent offset between laser ablation Mg/Ca analyses of carbonates and silicate glasses, owing to their differing matrices, our standard values reported above will allow our data to be corrected to obtain an accurate composition of the uncleaned foraminiferal calcite.

2.5 LA-ICP-MS data processing and screening

Each individual laser ablation profile was carefully inspected and processed using the SILLS data reduction software package (*Guillong et al.*, 2008) following the established protocol outlined in *Longerich et al.* (1996). Profiles generally followed one of two patterns: (i) a rise from background values to a transient peak, followed by a somewhat lower plateau, or (ii) a rise from background values to a general plateau (Figure 2). There are two likely explanations for the initial transient peak in some isotope profiles: ablation of authigenic coatings enriched in some trace metals, or laser ablation induced isotope fractionation (so-called “pit effects”). We favor the first explanation because we used the same operating parameters on every profile, and would therefore expect any “pit effects” to be consistent among the profiles. Furthermore, profiles containing the transient peaks were more prevalent in the older part of the record, where our solution Mn/Ca analyses demonstrate the presence of authigenic coatings. Therefore, we assume the transient peaks represent contaminated portions of the test and exclude those regions. The integration interval for the profile was selected based upon the following three criteria: (i) stable ^{43}Ca counts, indicating ablation of calcite, (ii) stable Mg/Ca signal, indicating a consistent primary calcite phase, (iii) flat Mn/Ca and Al/Ca signals, avoiding any peaks indicating intervals of contamination (Figure 2).

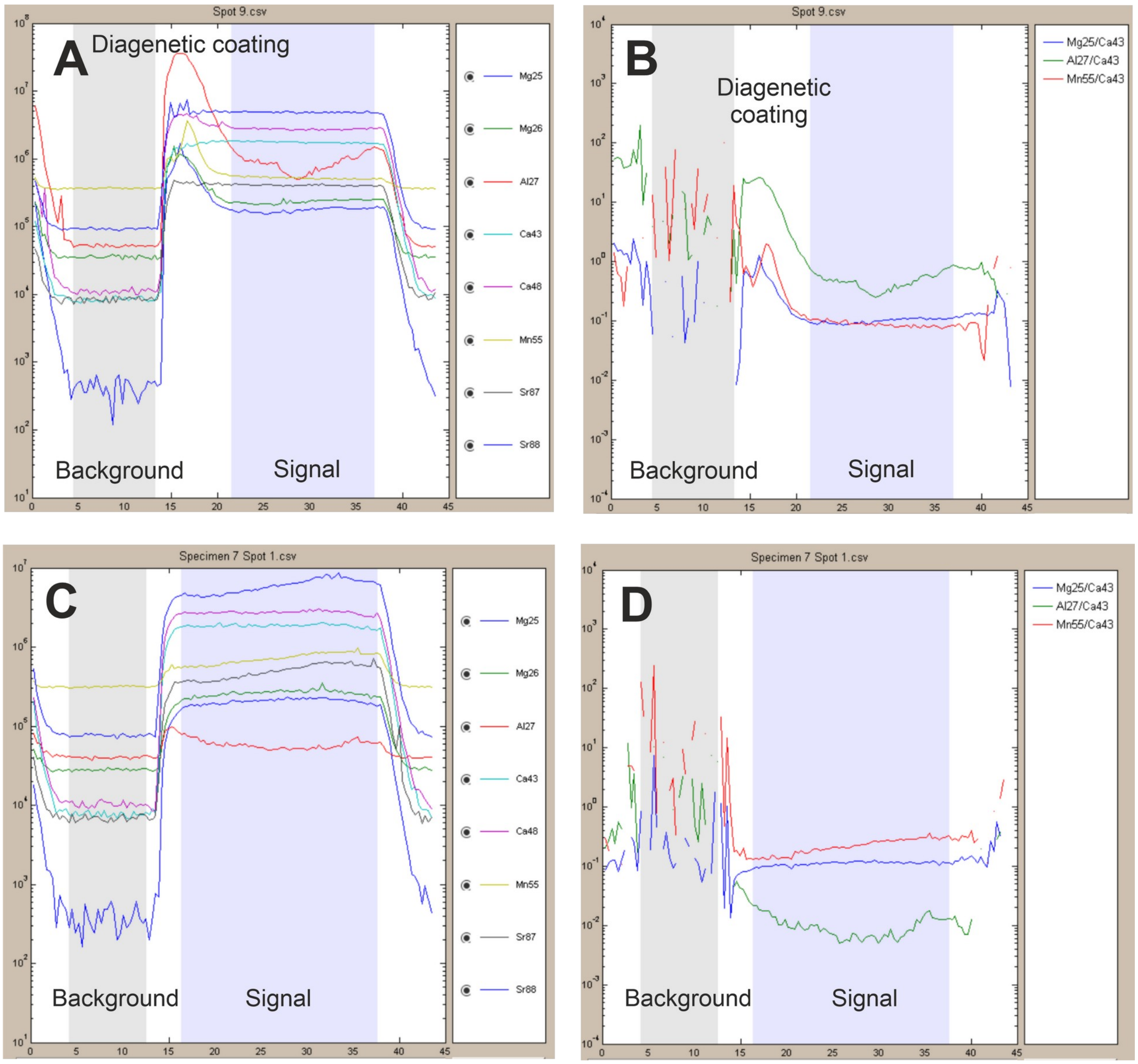

Figure 2: Representative LA-ICP-MS Mg, Al, and Mn profiles demonstrating the selection of background (grey panel) and sample (blue panel) signals for a profile with an authigenic coating (A, B) and for a profile without an authigenic coating (C, D). Both examples are shown in raw isotopic counts (A, C), and ratios mode (B, D) where the isotopes of interest are relative to ^{43}Ca, the internal standard. In both examples the x axis is analysis time (seconds), and the y axis is the raw intensity of the isotopes or ratios on a log scale. The sample interval is selected to avoid the elevated Mg/Ca, Mn/Ca, and Al/Ca at the outer surface of the test.

Individual depth profiles were corrected by first subtracting the mean background signal (determined from ~15 seconds of data acquired when the laser was turned off prior to ablation). The repeated analysis of the NIST 610 standard reference material was used to linearly correct for any instrumental drift. Typically, this is small, <2%, because of the good counting statistics and stable data acquisition during ablation. The ablation profiles were normalized to ^{43}Ca as the internal standard and elemental concentrations (TM/Ca) were calculated, assuming 40 wt % for $CaCO_3$.

Following data processing, rigorous screening of the Mg/Ca ratios for the influence of intratest contamination was conducted. It is important to recognise that Mn/Mg and Al/Mg of contaminant phases vary greatly, such that there is no single universal threshold for these elements that can be applied in every situation (*Lear et al*., 2015). For the Sunbird-1 samples we examined co-variation of Mg/Ca and Mn/Ca and chose to exclude all samples above a Mn/Ca threshold of 200 μmol/mol (Supplementary Figure S3). Consideration of Al/Ca was more complex, as some samples with extremely high Al/Ca (>1000 μmol/mol) was not associated with markedly elevated Mg/Ca. This result demonstrates that aluminum is sporadically present in foraminiferal tests in variable phases (with differing Al/Mg). We therefore used a dual-pronged approach, considering both Al/Ca and intra-sample heterogeneity. We excluded profiles where two conditions were met: (i) Al/Ca was >100 μmol/mol, and (ii) the associated Mg/Ca was substantially elevated relative to the other depth profiles from the same sample.

2.6 Determination of mean foraminiferal test Mg/Ca by laser ablation

Geochemical heterogeneity exists both within an individual foraminiferal test and between foraminiferal tests from the same sample (*Eggins et al.*, 2004; *Fehrenbacher and Martin*, 2014; *Sadekov et al.*, 2008; *Sadekov et al.*, 2005). Therefore, several laser ablation profiles are required to produce a consistent Mg/Ca ratio for temperature reconstructions. Here we analyzed ten depth profiles through each of ten individual *D. altispira* tests from the 1551-1554 m (11.74 Ma) sample to determine representative inter-specimen variability for these samples (Figure 3). Approximately one third (n=28) of the 100 depth profiles were excluded during screening for elevated Al/Ca and Mn/Ca indicative of diagenetic contamination. The Mg/Ca value of individual depth profiles in *D. altispira* from the 1551-1554 m sample ranges from 2.67 mmol/mol to 5.23 mmol/mol, with a mean of 3.63 ± 0.14 mmol/mol (n=72) (Figure 3a; Supplementary Table S5). The mean Mg/Ca value from four specimens, a total of 28 profiles, is 3.41 ± 0.18 mmol/mol (Figure 3a). Averaging profiles from ten individual tests did therefore not produce significantly better accuracy or precision than averaging profiles from four individual tests (Figure 3b). Therefore, for a Mg/Ca ratio to be considered representative it must represent an average of at least 28 laser ablation profiles, from at least four specimens, with the analytical uncertainty (2 SE) indicating the intra- and inter-specimen variability this incorporates. To account for depth profiles excluded due to contamination, where possible the number of measurements per sample was increased to 36, six depth profiles per specimen and six specimens per sample. This result is in line with other LA-ICP-MS studies (*Rathmann et al.*, 2004; *Sadekov et al.*, 2008). Future studies are advised to conduct similar testing to determine the number of measurements required for a mean sample Mg/Ca to be representative, as this will likely be site dependent.

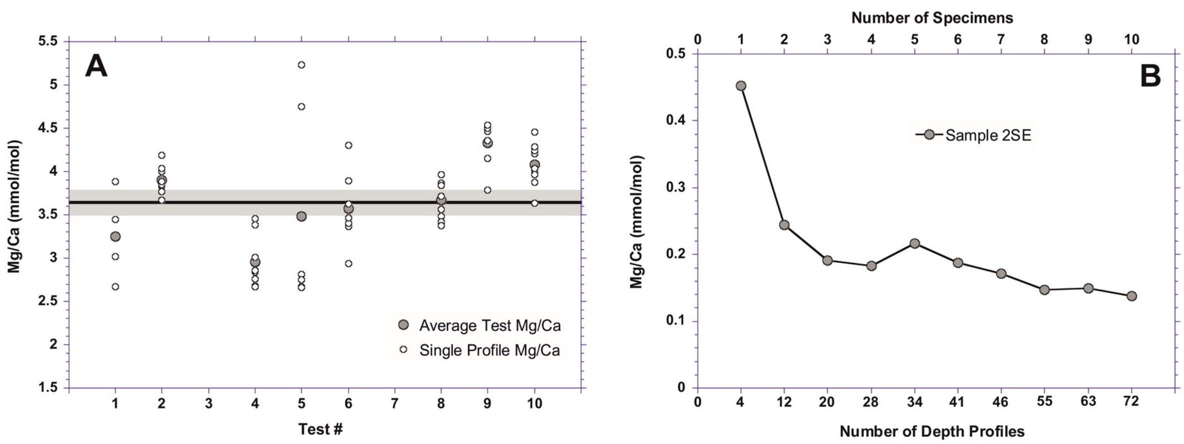

Figure 3: Distribution of *D. altispira* Mg/Ca values from LA-ICP-MS profiles of the 1551-1554 m sample. (A) A summary of all Mg/Ca values, where open circles denote individual measurements, and filled circles denote mean Mg/Ca values for each specimen. The horizontal black line is the mean of all depth profiles from the sample, and the gray bar the ±2 SE sample uncertainty. (B) The evolution of the sample 2 SE with increasing specimens. Only profiles that passed data screening are included (n=72). Data is provided in Supplementary Table S5.

2.7 Mg/Ca paleo-sea surface temperature calculations

The influence of calcification temperature (T) on the Mg/Ca ratio of foraminiferal calcite can be explained by an exponential curve of general form Mg/Ca = B$\exp^{AT}$ where the pre-exponential constant (B) and exponential constant (A) are species specific (*Anand et al.*, 2003; *Lear et al.*, 2002; *Nürnberg et al.*, 1996; *Rosenthal et al.*, 1997). To convert raw Mg/Ca ratios to absolute temperatures, several secondary controls on Mg/Ca must be considered, and accounted for (*Gray et al.*, 2018; *Hollis et al.*, 2019; *Holland et al.,* 2020).

In this study we use Mg/Ca values from *D. altispira*, a near surface dweller present from the Oligocene to the Pliocene. Since this is not an extant species, we consider two approaches to calculating SST: (i) using the multi-species calibration equation from *Anand et al.* (2003) and (ii) using the *Globigerinoides ruber* Mg/Ca-SST equation and pH correction from *Evans et al.* 2016.

In scenario (i), we apply a compilation of nine modern planktic foraminifera (*Anand et al.,* 2003). This calibration is commonly applied to extinct planktic foraminiferal species such as *D. altispira* and applies a power law relationship, where H is a constant that describes the sensitivity of $Mg/Ca_{CALCITE}$ to seawater Mg/Ca (Mg/Ca_{SW}) (*Hasiuk and Lohmann,* 2010; *Cramer et al.,* 2011; *Evans and Müller*, 2012) (Equation 1).

$$Equation\,1: Mg/Ca = \frac{B}{Mg/Ca_{SW}^{t=0^H}}\, x\, Mg/Ca_{SW}^{t=t^H}\, ex\, p^{AT}$$

Fluxes of Mg^{2+} and Ca^{2+} into and out of the oceans leads to secular variation in Mg/Ca_{sw}. This variability must be accounted for when determining absolute sea surface temperatures on Cenozoic timescales (*Hollis et al.*, 2019). Reconstructions of Mg/Ca_{sw} based on large benthic foraminifera (*Evans et al.*, 2018), calcite veins (*Coggon et al.*, 2010), fluid inclusions (*Horita et al.*, 2002), and echinoderms (*Dickson*, 2002) have constrained this variability through the Cenozoic (Supplementary Figure S4). The Eocene-Oligocene demonstrates relatively stable values of 2.0-2.5 mol/mol (*Coggon et al.*, 2010; *Evans et al.*, 2018). However, only one data point exists from the Miocene, through which Mg/Ca_{sw} more than doubles from ~2.2 mol/mol in the late Oligocene (*Coggon et al.*, 2010) to the well constrained value of 5.2 mol/mol in the modern ocean (*Broecker et al.*, 1982; *Dickson*, 2002; *Horita et al.*, 2002; *Kısakürek et al.*, 2008). Therefore, the method of *Lear et al.* (2015) is followed by fitting the fourth-order polynomial curve fit through the compiled Mg/Ca_{sw} proxy records (Supplementary Figure S4). We use a ±0.5 mol/mol uncertainty window in the following temperature calculations, this error envelope incorporating the majority of the spread in the proxy data.

The power law function negates the assumption that the temperature sensitivity remains constant, independent of changing Mg/Ca_{SW} through the Cenozoic era. We apply a power law constant of H=0.41, similar to the value applied for *T. trilobus*, a symbiont-bearing, mixed layer dweller (*Delaney et al.,* 1985; *Evans and Müller*, 2012). Adapting Equation 1 to include our H value, a modern-day Mg/Ca_{sw} value of 5.2 mol/mol, and the calibration constants of *Anand et al.,* (2003) derives Equation (2).

$$Equation\,2:$$
$$\frac{Mg}{Ca} = \frac{0.38 \pm 0.02}{5.2^{0.41}}\, x\, Mg/Ca_{sw}{}^{0.41}\, ex\, p^{(0.090 \pm 0.003\, x\, SST)}$$

This first calibration approach assumes that foraminiferal Mg/Ca is not influenced by changes in the carbonate system. However, studies have shown that planktic foraminiferal Mg/Ca is influenced by changes in the carbonate system, the ratio increasing with decreased pH and/or $\Delta[CO_3^{2-}]$ (*Evans et al.*, 2016; *Gray and Evans*, 2019; *Gray et al.*, 2018; *Russell et al.*, 2004; *Yu and Elderfield*, 2008). However, the ultimate driver of this effect is not certain and some species are insensitive to changes in the carbonate system. Further, it has been shown that for *Orbulina universa* dissolved inorganic carbon (DIC) plays a role in test Mg/Ca variability (*Holland et al.*, 2020). We follow recent results which interpret pH, as opposed to $\Delta[CO_3^{2-}]$ or DIC, as the parameter which controls the carbonate system's influence on Mg/Ca (*Evans et al.*, 2016; *Gray et al.*, 2018). Furthermore, unlike with either DIC or $\Delta[CO_3^{2-}]$, it is possible to reconstruct pH through the Neogene using boron isotopes in foraminifera (*Foster and Rae*, 2015; *Greenop et al.*, 2014; *Henehan et al.*, 2013; *Sosdian et al.*, 2018). For these reasons we use the recent Neogene boron isotope compilation of *Sosdian et al.* (2018), which provides well constrained estimates of pH across this time interval (Supplementary Figure S5; Supplementary Table S9). Linear interpolation between these pH values allows us to estimate a mean pH value, and associated uncertainty envelope, for each Sunbird-1 sample, where the uncertainty envelope is maximum and minimum pH at the 17% and 83% confidence interval (~± 0.06 pH units).

Therefore, in addition to scenario (i) we also consider the approach from *Evans et al.* (2016) which corrects for pH changes using the interpolated Neogene pH record of *Sosdian et al.* (2018) (Supplementary Figure S5). Measured planktic foraminiferal Mg/Ca values are corrected for this influence of pH using the equation of *Evans et al.* (2016) (Equation 3).

$$Equation\,3: Mg/Ca_{CORRECTED} = \frac{Mg/Ca_{MEASURED}}{\frac{0.66}{1+\exp\left(6.9\left(pH-8.0\right)\right)}+0.76}$$

The preferred equation of *Evans et al.* (2016) is used to account for the influence of changing Mg/Ca_{sw} when estimating SST. These authors determined that the best fit to culture-derived calibration lines is when both the pre-exponential (B) and exponential (A) coefficients vary quadratically with Mg/Ca_{sw} (Equation 4 and 5).

Equation 4: $B = (0.019 \times Mg/Ca_{sw}^{2}) - (0.16 \times Mg/Ca_{sw}) + 0.804$

Equation 5: $A = (-0.0029 \times Mg/Ca_{sw}^{2}) + (0.032 \times Mg/Ca_{sw})$

We substitute these equations into the general exponential calibration, $Mg/Ca = B\exp^{AT}$, to account for changing Mg/Ca_{sw}. Although the *Evans et al.* (2016) equation is specific to *G. ruber*, this species inhabits a shallow water depth of 0-50m (*Schiebel and Hemleben*, 2017) similar to the inferred mixed-layer habitat depth *D. altispira* (*Aze et al.*, 2011). Furthermore, as with *G. ruber*, *D. altispira* was a tropical/subtropical species, with symbionts (*Aze et al.*, 2011).

Salinity can exert a secondary effect on foraminiferal Mg/Ca, sensitivity measurements from culture and core-top studies show this to be ~3-5% per practical salinity unit (psu) (*Gray et al.*, 2018; *Hollis et al.*, 2019; *Hönisch et al.*, 2013; *Kısakürek et al.*, 2008). In the absence of a robust, independent salinity proxy (although we do note the promise of Na/Ca (*Bertlich et al.*, 2018; *Geerken et al.*, 2018)) and the relatively minor effect of salinity on foraminiferal Mg/Ca, this potential secondary control is not empirically accounted for. Sunbird-1 was located in a coastal setting and likely experienced a highly variable hydrological cycle due to changes in the position of the ITCZ making it susceptible to changes in salinity. Therefore, an error of ± 0.5^{0}C is incorporated into the final sea surface temperature estimates, equivalent to an assumed salinity variability of ~± 1 PSU.

Mg/Ca-derived sea surface temperature estimates calculated using both approaches (i) and (ii) yield extremely similar trends (Supplementary Figure S6). Across the time interval of the Sunbird-1 dataset (~13.5 Ma – 9.5 Ma) pH changes by a small amount and thus the choice of approach has little influence on the Sunbird-1 absolute SST record. In our discussion below, we adopt approach (i); the multi-species calibration equation from *Anand et al.* (2003) without a pH correction. This approach avoids any potential species-specific effects from applying the *Evans et al.* (2016) calibration specific to *G. ruber* to the extinct *D. altispira* used in this study. Furthermore, *D. altispira* has been considered to be symbiont bearing, so may demonstrate a muted response to changes in pH and insensitivity to pH changes, similar to *Trilobatus trilobus* (*Gray and Evans*, 2019).

The uncertainties (± 2SE) associated with the conversion from Mg/Ca to absolute SST estimates incorporate the uncertainty on the Mg/Ca_{sw} record, and the potential uncertainty due to varying salinity. Additionally, scenario (i) incorporates the uncertainty in the calibration of *Anand et al.* (2003) (Equation 2), and scenario (ii) using the approach of *Evans et al. (*2016) incorporates the uncertainty in the pH correction. These combined are termed the calibration uncertainty and are considerably greater than the independent analytical uncertainty, which only incorporates the intra- and inter- specimen variability (±2 SE). Absolute sea surface temperature estimates, and associated uncertainties, calculated using approach (i) and (ii) are available in Table 1 and Supplementary Table S9 respectively

Age (Ma)	Minimum Age (Ma)	Maximum Age (Ma)	Temperature (°C)	Maximum Temperature (°C)	Minimum Temperature (°C)	Analytical Error Only Maximum Temperature (°C)	Analytical Error Only Minimum Temperature (°C)
9.53	9.43	9.62	27.73	31.08	24.64	28.30	27.12
9.86	9.86	9.86	28.15	31.86	24.68	29.06	27.17
10.19	10.05	10.33	29.54	33.49	25.81	30.62	28.34
10.43	10.43	10.43	26.82	30.55	23.32	27.78	25.77
10.48	10.48	10.48	28.13	31.58	24.94	28.77	27.44
10.57	10.57	10.57	27.81	31.47	24.41	28.66	26.90
10.62	10.62	10.62	24.88	28.12	21.90	25.43	24.30
10.78	10.73	10.89	29.48	33.14	26.09	30.27	28.64
10.92	10.92	10.92	28.95	32.78	25.36	29.92	27.89
11.13	10.98	11.28	28.42	32.47	24.58	29.61	27.09
11.40	11.40	11.40	28.18	31.50	25.15	28.67	27.68
11.50	11.46	11.55	29.36	32.85	26.15	29.98	28.71
11.61	11.10	11.61	26.78	30.39	23.44	27.59	25.91
11.63	11.63	11.63	26.65	30.34	23.21	27.55	25.68
11.64	11.64	11.64	29.57	33.29	26.11	30.40	28.68
11.67	11.67	11.67	25.44	29.02	22.12	26.26	24.55
11.72	11.69	11.74	28.19	31.84	24.81	28.99	27.33
11.77	11.77	11.77	26.89	30.09	23.96	27.30	26.46
11.82	11.82	11.82	26.39	29.69	23.37	26.92	25.85
11.87	11.87	11.87	28.84	32.47	25.47	29.60	28.02
12.03	12.03	12.03	28.10	31.66	24.82	28.81	27.35
12.71	12.57	12.85	29.14	32.80	25.77	29.90	28.34
13.23	13.13	13.33	28.85	32.54	25.43	29.64	28.00

Table 1. Sunbird-1 LA-ICP-MS Mg/Ca derived SST using the approach of *Anand et al.* (2003) without a pH correction. Minimum and maximum age refer to the age range of the pooled samples (Supplementary Table S7). Maximum and Minimum temperatures refer to the full range of absolute temperatures derived incorporating the analytical and calibration uncertainty, whereas Analytical Error Only Maximum and Minimum temperatures refer to the range of temperatures derived from the analytical uncertainty only.

2.8 $\delta^{18}O$ paleo-sea surface temperature calculations

Due to the limited sampling resolution of the trace metal data, SST is also calculated using foraminiferal $\delta^{18}O$. Foraminiferal $\delta^{18}O$ ($\delta^{18}O_{calcite}$) is converted to temperature (T) using the palaeotemperature equation of *Bemis et al.* (1998) (Equation 4), changes in global ice volume being corrected using the $\delta^{18}O_{sw}$ value from the nearest 0.1 Myr time interval in the compilation of *Cramer et al.* (2011).

$$Equation\,4: \left(\delta^{18}O_{calcite} - \delta^{18}O_{sw} + 0.27\right) = -0.21 \pm 0.003\,T + 3.10 \pm 0.07$$

The absence of a robust, independent salinity proxy makes any quantitative attribution of its influence on foraminiferal $\delta^{18}O$ challenging. Therefore, we incorporate potential $\delta^{18}O$ variability due to salinity into any temperature estimate uncertainty. Salinity of the upper water column in a 0.75° x 0.75° grid square around the modern-day study site varies between 34.9 and 35.4 PSU (*Boyer et al.*, 2013). Using the Indian Ocean $\delta^{18}O_{sw}$-salinity relationship of *LeGrande and Schmidt* (2006) (Equation 5) this equates to a maximum $\delta^{18}O_{sw}$ uncertainty of ±0.091‰. Using Equation 4 this equates to a 0.4 ^{0}C uncertainty in the calculated surface temperature.

$$Equation\,5: \delta^{18}O_{sw}\left(SMOW\right) = \left(0.16 \pm 0.004\,x\,Salinity\right) - 5.31 \pm 0.135$$

We acknowledge the likelihood of variability in sea surface salinity in this downcore record. We use the paleolatitude calculator of *van Hinsbergen et al.* (2015) to calculate a paleolatitude for Sunbird-1 at 10 Ma of approximately 5.5 °S. The latitudinal correction of *Zachos et al.* (1994) gives a $\delta^{18}O_{sw}$ of 0.1‰. The absence of a significant offset from SMOW (0‰) suggests that this will have a negligible influence on the isotopic SST reconstructions.

3 Results

3.1 Solution ICP-MS trace element chemistry

D. altispira Mg/Ca measured by solution ICP-MS ranges from 3.15 ± 0.1 to 40.2 ± 0.2 mmol/mol (Figure 4a), translating to unrealistically high reconstructed sea surface temperatures. The high Mg/Ca ratios strongly suggest the addition of magnesium from a secondary, post-depositional source, prior to 11.75 Ma. The elevated Mg/Ca ratios are associated with correspondingly high Mn/Ca, Al/Ca, and U/Ca (Figure 4b-d). Six of the sixteen Mn/Ca ratios are in excess of the proposed 200 µmol/mol threshold, from our LA-ICP-MS analysis, above which Mg/Ca ratios are excluded due to contamination (Supplementary Figure S3). Furthermore, every foraminiferal U/Ca ratio is considerably higher than typical U/Ca ratios of primary foraminiferal calcite, which range from ~3-23 nmol/mol (*Chen et al.*, 2017; *Raitzsch et al.*, 2011; *Russell et al.*, 2004). In addition, foraminiferal Al/Ca exceeds the commonly applied 100 µmol/mol threshold in all but the four youngest samples.

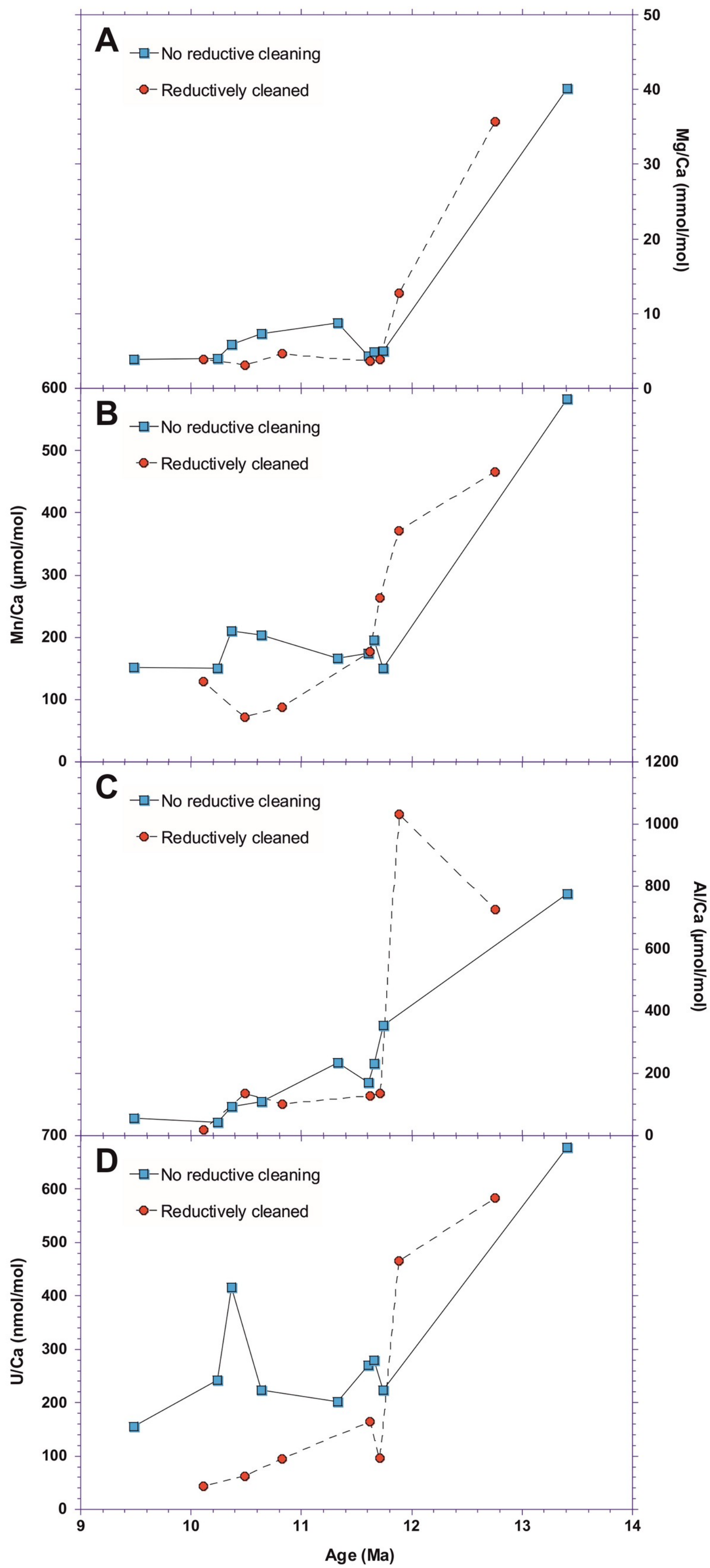
A
No reductive cleaning
Reductively cleaned
Mg/Ca (mmol/mol)
0
10
20
30
40
50
B
No reductive cleaning
Reductively cleaned
Mn/Ca (µmol/mol)
0
100
200
300
400
500
600
C
No reductive cleaning
Reductively cleaned
Al/Ca (µmol/mol)
0
200
400
600
800
1000
1200
D
No reductive cleaning
Reductively cleaned
U/Ca (nmol/mol)
0
100
200
300
400
500
600
700
9
10
11
12
13
14
Age (Ma)

515

Figure 4: Downcore solution ICP-MS (a) Mg/Ca, (b) Mn/Ca, (C) U/Ca, and (d) Al/Ca records for *D. altispira* in the Sunbird-1 core, distinguishing between sample that were reductively cleaned (red circles) and those that were not (blue squares).

The presence of elevated foraminiferal Mn/Ca, Al/Ca, and U/Ca ratios does not necessarily mean that the Mg/Ca ratios are contaminated. However, the downcore, point to point correlation (Figure 4) and covariance (Supplementary Figure S7) between Mg/Ca and contaminant indicators suggest a strong association. This downcore association between Mg/Ca and contaminant indicators, despite a rigorous chemical cleaning protocol, suggests one of two things; (i) the chemical cleaning protocol is not fully effective at removing contaminant coatings, and/or (ii) an Mg-rich contaminant phase is pervasive throughout the calcite test.

Including the reductive cleaning step lowers Mg/Ca, Mn/Ca, and U/Ca ratios in the post 11.8 Ma portion of the record, but has a negligible effect on Al/Ca. Neither cleaning protocol is effective at removing the authigenic coatings on the Sunbird-1 foraminifera in the pre 11.8 Ma portion of the record (Figure 4). For this reason, we also analyzed Sunbird-1 planktic foraminifera by laser ablation ICP-MS.

3.2 Downcore Laser Ablation ICP-MS Mg/Ca

Our laser ablation profiles clearly demonstrate that the metal-rich contaminant is present as an authigenic surface coating on the glassy foraminifera (e.g., Figure 2a-b). Because the alteration is not pervasive throughout the calcite test, laser ablation ICP-MS is an ideal approach to determine primary test Mg/Ca on these coated samples (section 2.6). *D. altispira* Mg/Ca determined by laser-ablation ICP-MS ranges from 3.03 to 5.07 mmol/mol, with an average value of 4.18 ± 0.40 mmol/mol, and errors (±2SE) range from 0.10 to 1.04 mmol/mol (Supplementary Table S6). However, due to elevated Al/Ca and Mn/Ca ratios, only 14 of the 44 samples are represented by at least 28 laser profiles. To alleviate this problem, adjacent samples have been combined into longer time slices to ensure that the absolute mean Mg/Ca measurements are robust (Supplementary Table S7). Samples comprising the mean of at least 28 laser profiles are termed “un-pooled samples”. Samples pooled to achieve a minimum of 28 laser profiles are termed “pooled samples”. It is acknowledged that combining adjacent samples, which span up to 420 kyr, could incorporate orbital scale climatic variability into these pooled samples. However, we do not infer climatic variability on orbital timescales because the coarse sampling resolution could incorporate aliasing of any precessional or obliquital periodicity into longer term eccentricity cycles (*Pisias and Mix*, 1988). Combining adjacent samples to generate a representative mean Mg/Ca for a longer time-slice could smooth orbital scale variability, could reduce uncertainty and assist the interpretation of longer-term climatic trends.

The mean Mg/Ca of representative samples after incorporating the nine pooled Mg/Ca samples with the 14 un-pooled samples ranges from 3.08 to 4.70 mmol/mol, with an average value of 4.04 ± 0.29 mmol/mol, and errors (±2SE) range from 0.14 to 0.48 mmol/mol (Supplementary Table S8). These values are in good agreement with the reductively cleaned solution ICP-MS data for the post-11.8 Ma portion of the record (Supplementary Figure S2), coinciding with the interval when contaminant indicators (Mn/Ca, Al/Ca, and U/Ca) are substantially lower (Figure 4b-d). This agreement between Mg/Ca values obtained by LA-ICP-MS and solution ICP-MS following effective reductive-cleaning supports the suitability of the LA-ICP-MS analyses. Because we can be more confident that the laser ablation data are not biased by authigenic coatings, the laser-ablation approach has the advantage that we can also determine original test Mg/Ca in the older part of the record.

There is no obvious long-term trend in Mg/Ca through the interval (Figure 5a). Between 11.8 Ma and 11.7 Ma there is a 0.7-0.8 mmol/mol decrease in Mg/Ca followed by a recovery to approximately previous values at 11.5-11.4 Ma. There is a Mg/Ca decrease of similar magnitude from between 10.7 Ma and 10.36 Ma, recovering by 9.85 Ma. We acknowledge that the coarse sampling frequency, and the combining of samples could be obscuring similar variability through the rest of the record.

3.3 *G. obliquus* $\delta^{18}O$

G. obliquus $\delta^{18}O$ ranges from -3.63‰ to -2.34‰ with a mean value of -2.92‰. The $\delta^{18}O$ record shows very little variability, values remaining stable at -3.4‰ prior to a positive 0.6‰ shift at ~12.5 Ma, and -2.7‰ after (Figure 5b). The low variability translates to a stable $\delta^{18}O$ SST record, temperatures ranging between 27°C and 31°C with the only distinctive trend being a ~3°C decrease between ~12.7 Ma and 12.0 Ma. The coeval positive 0.3‰ shift in seawater $\delta^{18}O$ (*Cramer et al.*, 2011) dampens the influence on the SST estimate of the positive 0.6‰ shift in *G. obliquus* $\delta^{18}O$ at ~12.5 Ma.

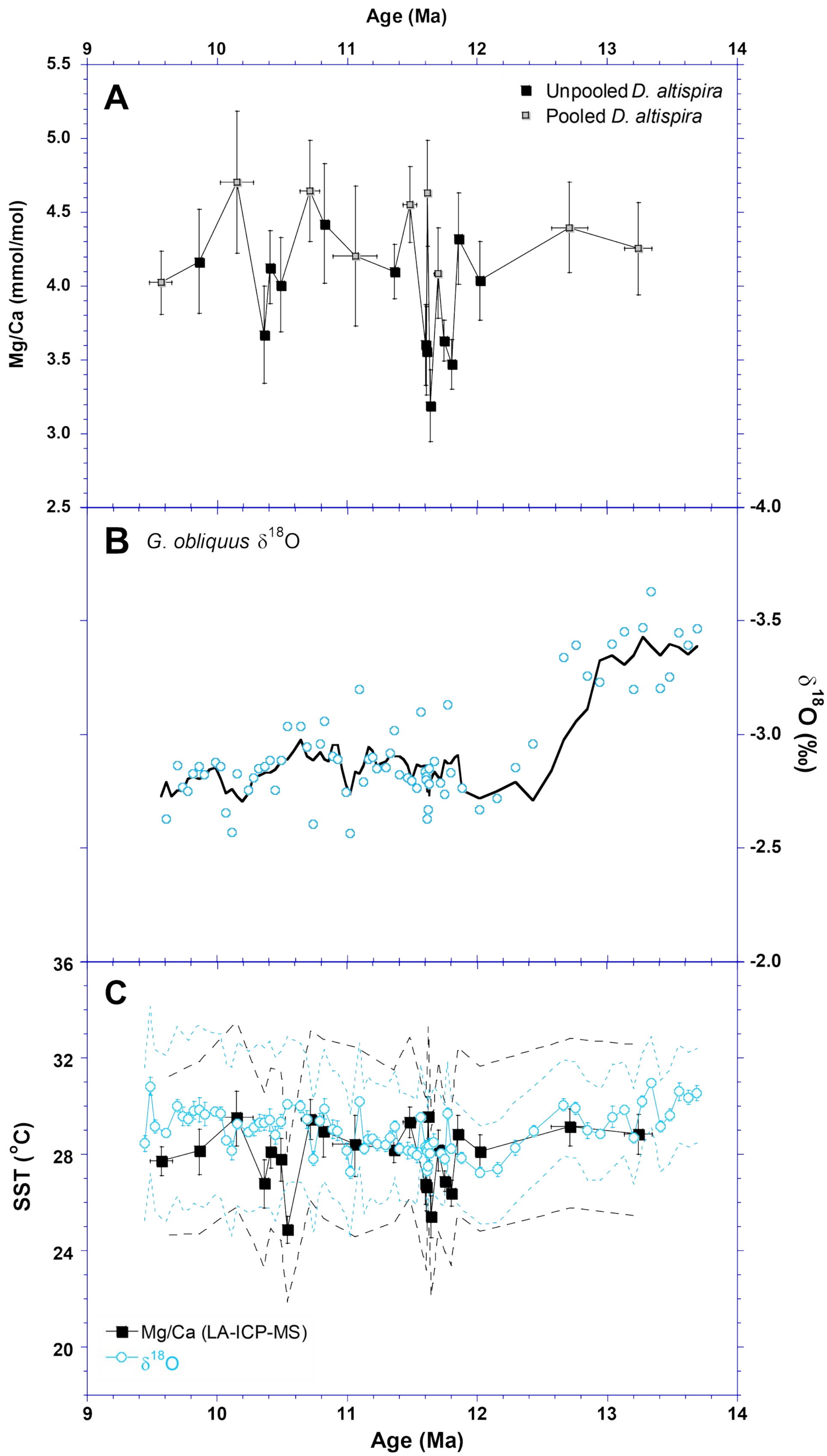
Age (Ma)
A
Unpooled D. altispira
Pooled D. altispira
Mg/Ca (mmol/mol)
B
G. obliquus δ18O
δ18O (‰)
C
SST (°C)
Mg/Ca (LA-ICP-MS)
δ18O
Age (Ma)

582

Figure 5: (a) Mean *D. altispira* LA-ICP-MS Mg/Ca ratios (mmol/mol) for unpooled (black squares) and pooled (grey squares) samples from Sunbird-1. Error bars denote the age range for pooled samples, and the ± 2SE of Mg/Ca from all depth profiles in the sample. (b) *G. obliquus* $\delta^{18}O$ from Sunbird-1. Solid line is a five-point moving average. (c) Sea surface temperature records at Sunbird-1 from planktic foraminiferal $\delta^{18}O$, and LA-ICP-MS Mg/Ca using our preferred approach that applies the calibration of *Anand et al.* (2003) without a pH correction. Symbols are the same as in (a) and (b). Error bars on the $\delta^{18}O$ record denote the analytical uncertainty (± 2SD), and error bars on the Mg/Ca record denote the sample uncertainty (± 2SE). As in (a), pooled Mg/Ca samples also have horizontal error bars denoting the sample age range. Dashed blue and black lines denote the full uncertainty on the temperature estimates, including that derived from the calibration uncertainty, for $\delta^{18}O$ and LA-ICP-MS Mg/Ca respectively. Supplementary Figure S8 provides LA-ICP-MS Mg/Ca sea surface temperatures using the alternative approach of *Evans et al.*, (2016).

4 Discussion

4.1 Reconstructing sea surface temperature from diagenetically altered foraminifera using laser ablation ICP-MS

Robust paleotemperature reconstructions using foraminiferal Mg/Ca ratios are reliant upon the Mg/Ca ratio recording a primary environmental signal, unaltered by diagenetic alteration. Despite employing a thorough cleaning protocol (*Barker et al.*, 2003; *Boyle and Keigwin*, 1985), our Mg/Ca ratios from solution-based ICP-MS analysis in the >11.8 Ma portion of the record are clearly influenced by a diagenetic contaminant phase containing elevated magnesium (Figure 4). This finding demonstrates that foraminifera with a glassy appearance under the light microscope are not necessarily free from the influence of all modes of diagenetic alteration. We therefore emphasize the importance of complementary trace metal ratios indicative of contamination (i.e. Al/Ca, Mn/Ca, U/Ca) to assess the reliability of foraminiferal Mg/Ca ratios (Figure 4). The application of LA-ICP-MS to collect high resolution elemental profiles through the foraminiferal tests, excluding regions displaying diagenetic contamination, has facilitated the identification of what we interpret to be primary paleotemperatures from diagenetically altered foraminifera (*Hines et al.*, 2017; *Hollis et al.*, 2015).

The Sunbird-1 $\delta^{18}O_{PF}$ SST record from *G. obliquus* reconstructs very similar absolute temperatures to the planktic foraminiferal Mg/Ca SST record (Figure 5c). Mean SST from the Sunbird-1 $\delta^{18}O_{PF}$ record (29^{0}C) is 2^{0}C higher than mean SST from the Mg/Ca record (27^{0}C), although with the exception of the two transient decreases in Mg/Ca reconstructed SST initiating at 11.8 Ma and 10.7 Ma the records are within error. The similarity of the absolute SSTs reconstructed by the two proxies strengthens the case for the LA-ICP-MS Mg/Ca SST record recording a primary temperature signal, and that these absolute sea surface temperatures at Sunbird-1 should be considered primary.

The majority of the uncertainty in the absolute temperature estimates is derived from the uncertainties incorporated from the relevant calibrations, in particular the seawater Mg/Ca and seawater $\delta^{18}O$ records (Figure 5c). This is true for both LA-ICP-MS Mg/Ca (Table 1 and Supplementary Table S9) and $\delta^{18}O$ (Supplementary Table S10). Therefore, despite being appreciable, the uncertainty resulting from the geochemical heterogeneity both within an individual foraminiferal test and between foraminiferal tests from the same sample (Figure 3) is not the primary contributor to the final absolute temperature uncertainty.

4.2 Mid-late Miocene sea surface temperatures in the equatorial Indian Ocean

The results from Sunbird-1 indicate that SST in the equatorial Indian Ocean remained stable at ~27^{0}C-29^{0}C through the 13.3 Ma to 9.5 Ma interval (Figure 5c). This finding suggests that tropical climate was relatively stable following the global cooling associated with the expansion of the East Antarctic Ice Sheet across the MMCT. These records from Sunbird-1 supports the robustness of contemporaneous alkenone based studies which exhibit similar absolute tropical SST estimates (*Herbert et al.*, 2016; *Huang et al.*, 2007; *Rousselle et al.*, 2013; *Seki et al.*, 2012; *Zhang et al.*, 2014) (Figure 6a). The U^{k}_{37} SST calibration fails to reconstruct SST>29^{0}C (*Müller et al.*, 1998) but these results using Mg/Ca paleo-thermometry suggest that outside the western Pacific warm pool this restriction does not apply to this time interval, unlike the preceding Miocene Climatic Optimum during which Mg/Ca temperature estimates are higher than those estimated with the U^{k}_{37} proxy (*Badger et al.*, 2013).

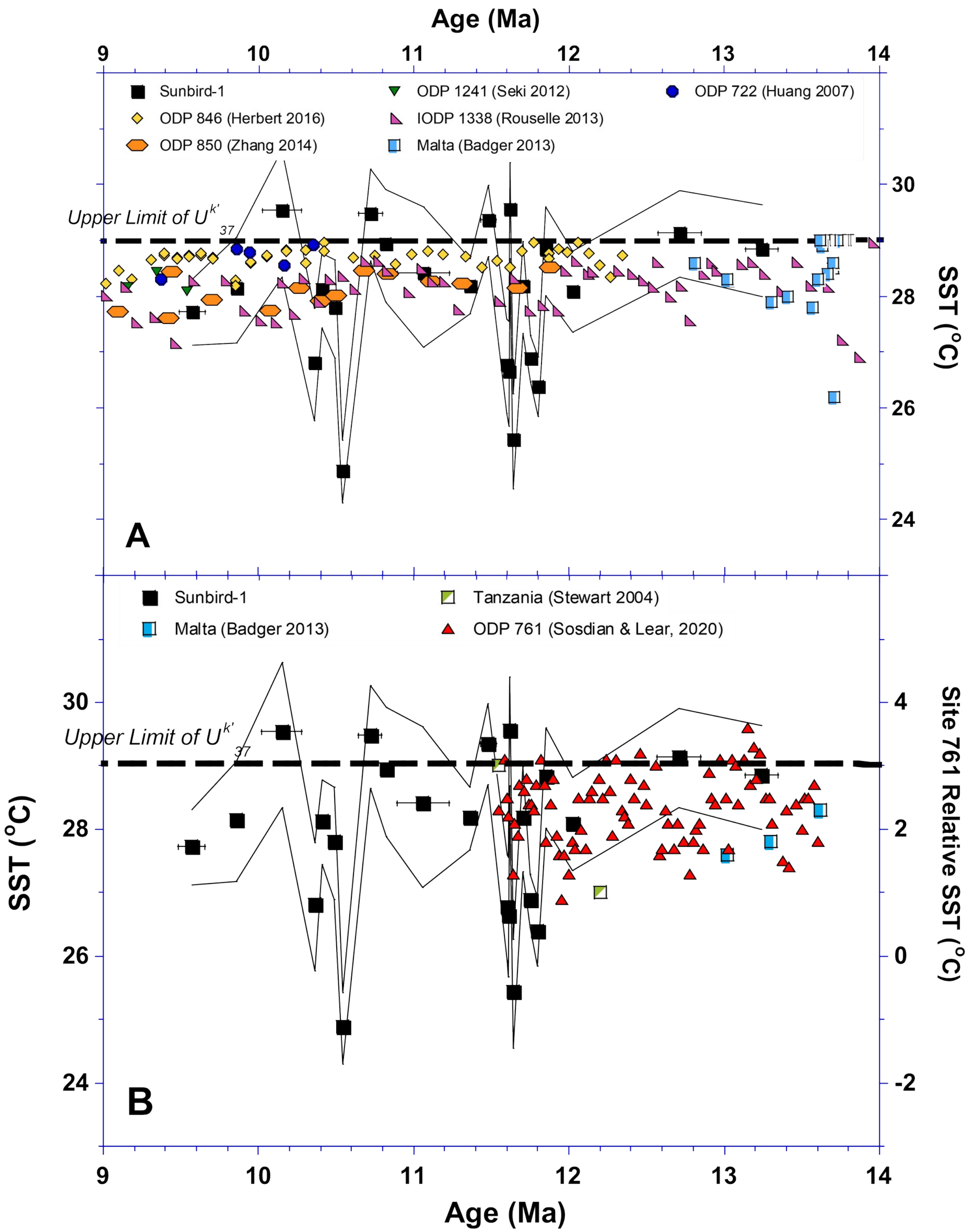
Age (Ma)
Sunbird-1
ODP 1241 (Seki 2012)
ODP 722 (Huang 2007)
ODP 846 (Herbert 2016)
IODP 1338 (Rouselle 2013)
ODP 850 (Zhang 2014)
Malta (Badger 2013)
Upper Limit of U^k'_37
SST (°C)
A
Sunbird-1
Tanzania (Stewart 2004)
Malta (Badger 2013)
ODP 761 (Sosdian & Lear, 2020)
Upper Limit of U^k'_37
SST (°C)
Site 761 Relative SST (°C)
B
Age (Ma)

645

Figure 6: Sunbird-1 LA-ICP-MS Mg/Ca derived SST using the approach of *Anand et al.* (2003) without a pH correction compared to and SST estimates at contemporaneous sites from (a) U^k_{37}, and (b) foraminiferal geochemistry. Estimates applying U^k_{37} are from ODP Site 722 (*Huang et al.,* 2007) in the Arabian Sea, ODP & IODP Sites 846 (*Herbert et al.,* 2016), 850 (*Zhang et al.,* 2014), 1241 (*Seki et al.,* 2012), and U1338 (*Rousselle et al.,* 2013) in the Eastern Equatorial Pacific, terrestrial outcrops in Malta (*Badger et al.,* 2013). Estimates applying the foraminiferal Mg/Ca proxy are from ODP Sites 761 (*Sosdian and Lear,* 2020) and terrestrial outcrops in Malta (*Badger et al.,* 2013). ODP Site 761 data is displayed on an alternative axis as SST anomalies relative to the baseline average from 16.0 – 15.5 Ma. Two temperature estimates using the $\delta^{18}O$ of exceptionally preserved foraminifera from Tanzania are also shown (*Stewart et al.,* 2004). The upper limit for the U^k_{37} proxy (29°C) is marked by the thick dashed black line. All previously published records used for comparison are kept on their original age models. Supplementary Figure S9 provides LA-ICP-MS Mg/Ca sea surface temperatures using the alternative approach of *Evans et al.*, (2016).

Although not a true tropical location, and consisting of only three data points, the *Badger et al.* (2013) Mg/Ca record from the Mediterranean estimates SST of ~27.5^{0}C between 13.5 and 13 Ma, within the Sunbird-1 SST uncertainty envelope (Figure 6b). Mg/Ca-SST records based on less well-preserved planktic foraminifera also suggest stable tropical SST between 13.8 and 11.4 Ma (*Sosdian and Lear,* 2020) (Figure 6b). Furthermore, well preserved planktic foraminifera from clay-rich sediments of coastal Tanzania yield Indian Ocean sea surface temperatures of 27^{0}C at 12.2 Ma and 29^{0}C at 11.55 Ma using the $\delta^{18}O$ paleo-thermometer (*Stewart et al.*, 2004), again in agreement with the Sunbird-1 temperature estimates (Figure 6b). It is worth noting that this study, as well as the tropical SST records of *Herbert et al.* (2016) and references therein, do not sample the warm pool of the Western Pacific. Sea surface temperature estimates for the western equatorial Pacific using the TEX_{86} paleothermometer suggest a slight, ~1°C, SST decrease between 12 Ma and 9 Ma, whilst those for the eastern equatorial Pacific are more or less constant across the same interval (*Zhang et al.,* 2014).

Although the estimates provided by the Sunbird-1 record suggest absolute tropical sea surface temperatures remained relatively stable through the mid-late Miocene, some temporal variability does persist. Between 11.8 Ma and 11.7 Ma SST drops sharply by ~3^{0}C. Excluding one value of 28.6^{0}C at 11.62 Ma, this decrease in SST to ~24-25^{0}C persists for ~300 kyr before recovering to pre excursion values by 11.5 Ma. However, no transient decrease in sea surface temperature is recorded from contemporaneous alkenone based estimates of tropical SST utilizing the U^k_{37} proxy from the Arabian Sea (*Huang et al.*, 2007), and the Eastern Equatorial Pacific (*Herbert et al.*, 2016; *Rousselle et al.*, 2013; *Seki et al.*, 2012; *Zhang et al.*, 2014) (Figure 6a). We therefore suggest that the observed transient ~3^{0}C SST decrease is not the result of a global driver, and supports a mechanism causing local ocean cooling of the surface waters at Sunbird-1. An alternative hypothesis is that an unaccounted increase in local salinity and/or pH, lowering foraminiferal Mg/Ca ratios, caused a bias to cooler temperatures between ~11.8 and 11.5 Ma. Assuming constant SST, the observed ~0.7 mmol/mol decrease in Mg/Ca would require a salinity increase on the order of 5.0 PSU (*Hönisch et al.*, 2013; *Gray et al.*, 2018). This salinity increase equates to a 0.8 ‰ change in $\delta^{18}O$ using the Indian Ocean $\delta^{18}O_{sw}$-salinity relationship of *LeGrande and Schmidt* (2006) (Equation 5). As well as being an extremely large change in salinity, the planktic foraminiferal $\delta^{18}O$ record does not support such a significant change in sea surface salinity between ~11.8 and 11.5 Ma (Figure 5b). However, we do acknowledge that a contribution from increased salinity control cannot be discounted. Despite incorporating varying pH from a globally distributed set of open ocean sites (*Sosdian et al.*, 2018), a localized increase in pH at Sunbird-1 cannot be ruled out. This possibility may be particularly relevant considering the land-proximal, tectonically active nature of the study site. A further possibility is that selective dissolution of foraminiferal chambers precipitated during warmer seasons occurred during post-burial diagenetic alteration, causing an apparent ~3°C lowering of SST between 11.8 Ma and 11.5 Ma. However, mean *D. altispira* test weights suggest that there was no increased dissolution of the foraminiferal tests through this interval of lower LA-ICP-MS Mg/Ca derived SST (Supplementary Table S11 and Supplementary Figure S10).

Therefore, our preferred interpretation is for a local cooling between ~11.8 and 11.5 Ma. The lack of a marked increase in the planktic $\delta^{18}O$ record at this time implies that the cooling was associated with a freshening of surface waters (Figure 5c). Interestingly, this interval corresponds to a period of very high sedimentation rates (Supplementary Figure S1), which might be consistent with enhanced precipitation and runoff, lowering regional surface salinity.

4.3 Implications for the global climate state during the mid-late Miocene

Previous studies utilizing the U^{k}_{37} proxy suggest a substantial cooling of sea surface temperature at mid-to-high latitudes in both hemispheres between 10 and 5.5 Ma, whilst tropical sea surface temperatures show limited cooling in the late Miocene prior to ~7 Ma (*Herbert et al.*, 2016; *LaRiviere et al.*, 2012). The absolute tropical SST record reported in this study supports the finding that the latitudinal temperature gradient steepened from ~10 Ma, as the climate system transitioned towards its modern-day state. Furthermore, support for the absolute temperatures reconstructed by the alkenone proxy suggests that the interval between 10 and 7.5 Ma was associated with enhanced polar amplification, significantly greater than that calculated for the greenhouse climate of the Eocene (*Cramwinckel et al.*, 2018). There is little evidence for a significant change in pCO_2 in this interval (*Sosdian et al.*, 2018; *Stoll et al.*, 2019) (Figure 7). We speculate that the marked regional cooling between 10 and 7.5 Ma perhaps reflects processes internal to the climate system, involving for example ocean-atmospheric heat transport, sea ice extent, or changes in regional cloud cover. A combined data-modelling approach would help constrain possible factors and explore potential relationships between this highly heterogenous cooling and the CO_2 drawdown that was associated with the subsequent global late Miocene Cooling starting ~7.5 Ma (Figure 7).

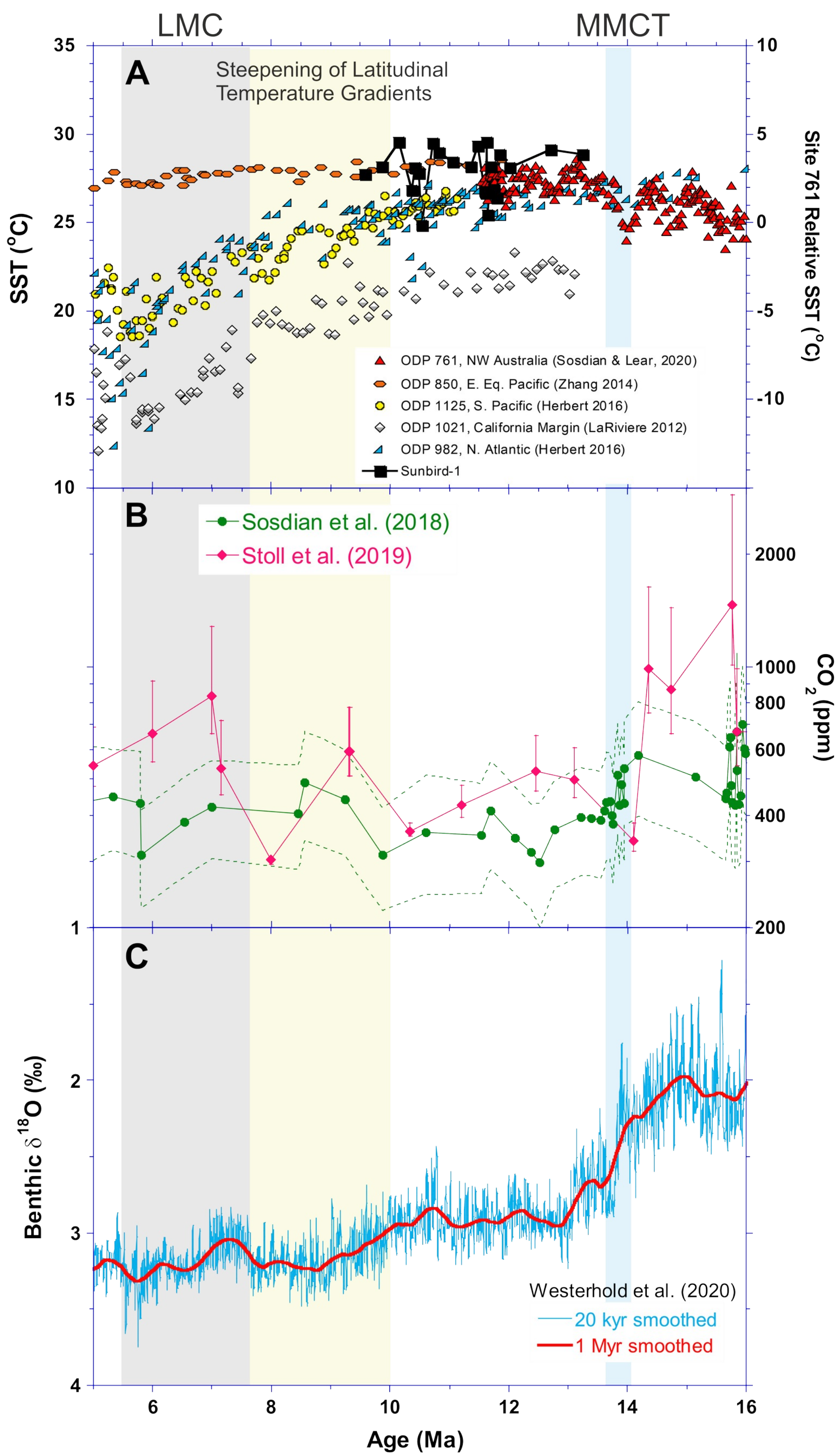
LMC
MMCT
A
Steepening of Latitudinal
Temperature Gradients
SST (°C)
Site 761 Relative SST (°C)
ODP 761, NW Australia (Sosdian & Lear, 2020)
ODP 850, E. Eq. Pacific (Zhang 2014)
ODP 1125, S. Pacific (Herbert 2016)
ODP 1021, California Margin (LaRiviere 2012)
ODP 982, N. Atlantic (Herbert 2016)
Sunbird-1
B
Sosdian et al. (2018)
Stoll et al. (2019)
CO2 (ppm)
C
Benthic δ18O (‰)
Westerhold et al. (2020)
20 kyr smoothed
1 Myr smoothed
Age (Ma)

727

Figure 7: Summary of global climate through the mid-to-late Miocene. (a) Sea surface temperature estimates from Sunbird-1, fellow low latitude ODP sites 850 (*Zhang et al.*, 2014) and 761 (*Sosdian and Lear,* 2020), mid latitude Northern Hemisphere ODP site 1021 (*LaRiviere et al.,* 2012), and mid-latitude Southern Hemisphere site 1125 (*Herbert et al.,* 2016), and high-latitude Northern Hemisphere ODP Site 982 (*Herbert et al.*, 2016). ODP Site 761 data is displayed on an alternative axis as SST anomalies relative to the baseline average from 16.0 – 15.5 Ma. (b) pCO_2 reconstructions, with Y axis on a log scale, of *Sosdian et al.* (2018) applying the CCD reconstruction of *Pälike et al.* (2012) and the $\delta^{11}B_{SW}$ scenario of *Greenop et al.* (2017), and *Stoll et al.* (2019) applying temperature estimates from *Bolton et al.* (2016) and *Zhang et al.* (2013). Confidence intervals (95%) are displayed as dashed lines and error bars respectively. (c) Composite benthic $\delta^{18}O$ record showing data that have been smoothed by a locally weighted function over 20 kyr (blue curve) and 1 Myr (red curve) (*Westerhold et al.*, 2020). Blue, yellow, and gray panels indicate intervals of ice sheet expansion across the Mid Miocene Climate Transition (MMCT) associated with CO_2 decline, the steepening of latitudinal temperature gradeints in the absence of a CO_2 trend, and the Late Miocene Cooling (LMC).

5 Conclusions

Our Sunbird-1 sea surface temperature estimates from LA-ICP-MS Mg/Ca analyses are in good agreement with those using the $\delta^{18}O$ paleo-thermometer on glassy foraminifera, supporting the use of LA-ICP-MS micro-analysis across multiple specimens for reconstructing paleotemperatures. This analytical technique has allowed the reconstruction of reliable Mg/Ca derived paleotemperatures using foraminifera whose bulk trace element ratios demonstrate diagenetic contamination by authigenic coatings. This finding opens the potential for Mg/Ca paleothermometry on other challenging time intervals, and locations, where contaminant coatings have previously inhibited the geochemical analysis of primary foraminiferal calcite. We present new sea surface temperature records from planktic foraminiferal Mg/Ca for the south west Indian Ocean between 13.5 Ma and 9.5 Ma. Absolute estimates of 24-31^{o}C suggest that sea surface temperature was relatively constant through the interval, although our record also suggests two intervals of regional cooling and freshening of surface waters at 11.8 and 10.7 Ma. The late Miocene represented a key interval in the transition of Earth's climate to its modern state, including the development of stronger latitudinal temperature gradients. Our new temperature record suggests that different mechanisms may have been responsible for this cooling. The initial cooling from ~10 Ma at mid to high latitudes in both hemispheres was not associated with significant cooling at low latitudes. On the other hand, the late Miocene cooling between ~7.5 and 5.5 Ma was global in nature and associated with a drawdown in pCO_2. Further work should therefore explore the mechanisms responsible for the enhanced polar amplification between 10 and 7.5 Ma, and the possibility of carbon cycle feedbacks contributing to the subsequent late Miocene Cooling.

Acknowledgments, Samples, and Data

This study uses samples from the Sunbird-1 core provided by BG-Group. All data from this study can be found in Table 1 and Supplementary Tables S1 to S11,and aredeposited in the Zenodo online data repository http://doi.org/10.5281/zenodo.4472994. We thank Alexandra Nederbragt and Anabel Morte-Rodeñas for laboratory assistance. We thank the reviewers and editor for their insightful comments that improved the manuscript. This research was supported by NERC iCASE studentship BW/22003105 (M.G.N.), and NE/L009633/1 grant to C.H.L.

References

Anand, P., Elderfield, H., & Conte, M. H. (2003). Calibration of Mg/Ca thermometry in planktonic foraminifera from a sediment trap time series. *Paleoceanography, 18*(2). https://doi.org/10.1029/2002PA000846

Aze, T., Ezard, T. H., Purvis, A., Coxall, H. K., Stewart, D. R., Wade, B. S., & Pearson, P. N. (2011). A phylogeny of Cenozoic macroperforate planktonic foraminifera from fossil data. *Biological Reviews, 86*(4), 900-927. https://doi.org/10.1111/j.1469-185X.2011.00178.x

Backman, J., Raffi, I., Rio, D., Fornaciari, E., & Pälike, H. (2012). Biozonation and biochronology of Miocene through Pleistocene calcareous nannofossils from low and middle latitudes. *Newsletters on Stratigraphy, 45*(3), 221-244. 10.1127/0078-0421/2012/0022

Badger, M. P., Lear, C. H., Pancost, R. D., Foster, G. L., Bailey, T. R., Leng, M. J., & Abels, H. A. (2013). CO2 drawdown following the middle Miocene expansion of the Antarctic Ice Sheet. *Paleoceanography, 28*(1), 42-53. https://doi.org/10.1002/palo.20015

Barker, S., Greaves, M., & Elderfield, H. (2003). A study of cleaning procedures used for foraminiferal Mg/Ca paleothermometry. *Geochemistry, Geophysics, Geosystems, 4*(9). https://doi.org/10.1029/2003GC000559

Bemis, B. E., Spero, H. J., Bijma, J., & Lea, D. W. (1998). Reevaluation of the oxygen isotopic composition of planktonic foraminifera: Experimental results and revised paleotemperature equations. *Paleoceanography, 13*(2), 150-160. https://doi.org/10.1029/98PA00070

Bertlich, J., Nürnberg, D., Hathorne, E. C., De Nooijer, L. J., Mezger, E. M., Kienast, M., et al. (2018). Salinity control on Na incorporation into calcite tests of the planktonic foraminifera Trilobatus sacculifer–evidence from culture experiments and surface sediments. *Biogeosciences (BG), 15*(20), 5991-6018. http://dx.doi.org/10.5194/bg-2018-164

Boyer, T. P., Antonov, J. I., Baranova, O. K., Coleman, C., Garcia, H. E., Grodsky, A., et al. (2013). World Ocean Database 2013.

Boyle, E., & Keigwin, L. (1985). Comparison of Atlantic and Pacific paleochemical records for the last 215,000 years: Changes in deep ocean circulation and chemical inventories. *Earth and Planetary Science Letters, 76*(1), 135-150. http://doi.org/0012-821x/85/$03.30

Boyle, E. A. (1983). Manganese carbonate overgrowths on foraminifera tests. *Geochimica et Cosmochimica Acta, 47*(10), 1815-1819. https://doi.org/10.1016/0016-7037(83)90029-7

Broecker, W. S., Peng, T.-H., & Beng, Z. (1982). *Tracers in the Sea*: Lamont-Doherty Geological Observatory, Columbia University.

Chen, P., Yu, J., & Jin, Z. (2017). An evaluation of benthic foraminiferal U/Ca and U/Mn proxies for deep ocean carbonate chemistry and redox conditions. *Geochemistry, Geophysics, Geosystems*. Article in Press. http://doi.org/10.1002/2016GC006730

Coggon, R. M., Teagle, D. A., Smith-Duque, C. E., Alt, J. C., & Cooper, M. J. (2010). Reconstructing past seawater Mg/Ca and Sr/Ca from mid-ocean ridge flank calcium carbonate veins. *Science, 327*(5969), 1114-1117. http://doi.org/10.1126/science.1182252

Cramer, B., Miller, K., Barrett, P., & Wright, J. (2011). Late Cretaceous–Neogene trends in deep ocean temperature and continental ice volume: reconciling records of benthic foraminiferal geochemistry (δ18O and Mg/Ca) with sea level history. *Journal of Geophysical Research: Oceans (1978–2012), 116*(C12). https://doi.org/10.1029/2011JC007255

Cramwinckel, M. J., Huber, M., Kocken, I. J., Agnini, C., Bijl, P. K., Bohaty, S. M., et al. (2018). Synchronous tropical and polar temperature evolution in the Eocene. *Nature, 559*(7714), 382-386. http://doi.org/10.1038/s41586-018-0272-2

Creech, J. B., Baker, J. A., Hollis, C. J., Morgans, H. E. G., & Smith, E. G. C. (2010). Eocene sea temperatures for the mid-latitude southwest Pacific from Mg/Ca ratios in planktonic and benthic foraminifera. *Earth and Planetary Science Letters, 299*(3–4), 483-495. http://dx.doi.org/10.1016/j.epsl.2010.09.039

de Nooijer, L. J., Hathorne, E. C., Reichart, G.-J., Langer, G., & Bijma, J. (2014). Variability in calcitic Mg/Ca and Sr/Ca ratios in clones of the benthic foraminifer Ammonia tepida. *Marine Micropaleontology, 107*, 32-43. https://doi.org/10.1016/j.marmicro.2014.02.002

de Nooijer, L. J., van Dijk, I., Toyofuku, T., & Reichart, G. J. (2017). The Impacts of Seawater Mg/Ca and Temperature on Element Incorporation in Benthic Foraminiferal Calcite. *Geochemistry, Geophysics, Geosystems, 18*(10), 3617-3630. http://doi.org/10.1002/2017GC007183Delaney, M. L., Be, A. W. H., & Boyle, E. A. (1985). Li, Sr, Mg, and Na in foraminiferal calcite shelss from laboratory culture sediment traps, and sediment cores. *Geochim. Cosmochim. Acta, 49*(6), 1327-1341. https://doi.org/10.1016/0016-7037(85)90284-4

Detlef, H., Sosdian, S. M., Kender, S., Lear, C. H., & Hall, I. R. (2019). Multi-elemental composition of authigenic carbonates in benthic foraminifera from the eastern Bering Sea continental margin (International Ocean Discovery Program Site U1343). *Geochimica et Cosmochimica Acta*. https://doi.org/10.1016/j.gca.2019.09.025

Dickson, J. A. D. (2002). Fossil Echinoderms As Monitor of the Mg/Ca Ratio of Phanerozoic Oceans. *Science, 298*(5596), 1222-1224. http://doi.org/10.1126/science.1075882

Eggins, S., De Deckker, P., & Marshall, J. (2003). Mg/Ca variation in planktonic foraminifera tests: implications for reconstructing palaeo-seawater temperature and habitat migration. *Earth and Planetary Science Letters, 212*(3), 291-306. https://doi.org/10.1016/S0012-821X(03)00283-8

Eggins, S. M., Sadekov, A., & De Deckker, P. (2004). Modulation and daily banding of Mg/Ca in Orbulina universa tests by symbiont photosynthesis and respiration: a complication for seawater thermometry? *Earth and Planetary Science Letters, 225*(3), 411-419. https://doi.org/10.1016/j.epsl.2004.06.019

Evans, D. and Müller, W. (2012). Deep time foraminifera Mg/Ca paleothermometry: Nonlinear correction for secular change in seawater Mg/Ca. *Paleoceanography, 27(4).* https://doi.org/10.1029/2012PA002315

Evans, D., Erez, J., Oron, S. and Müller, W., (2015a). Mg/Ca-temperature and seawater-test chemistry relationships in the shallow-dwelling large benthic foraminifera Operculina ammonoides. Geochimica et Cosmochimica Acta, 148, pp.325-342. https://doi.org/10.1016/j.gca.2014.09.039

Evans, D., Bhatia, R., Stoll, H., & Müller, W. (2015b). LA−ICPMS Ba/Ca analyses of planktic foraminifera from the Bay of Bengal: Implications for late Pleistocene orbital control on monsoon freshwater flux. *Geochemistry, Geophysics, Geosystems, 16*(8), 2598-2618. https://doi.org/10.1002/2015GC005822

Evans, D., Brierley, C., Raymo, M. E., Erez, J., & Müller, W. (2016). Planktic foraminifera shell chemistry response to seawater chemistry: Pliocene-Pleistocene seawater Mg/Ca, temperature and sea level change. *Earth and Planetary Science Letters*. Article in Press. http://doi.org/10.1016/j.epsl.2016.01.013

Evans, D., & Müller, W. (2018). Automated Extraction of a Five−Year LA−ICP−MS Trace Element Dataset of Ten Common Glass and Carbonate Reference Materials: Long−Term Data Quality, Optimisation and Laser Cell Homogeneity. *Geostandards and Geoanalytical Research*. https://doi.org/10.1111/ggr.12204

Evans, D., Sagoo, N., Renema, W., Cotton, L. J., Müller, W., Todd, J. A., et al. (2018). Eocene greenhouse climate revealed by coupled clumped isotope-Mg/Ca thermometry. *Proceedings of the National Academy of Sciences of the United States of America, 115*(6), 1174-1179. Article. http://doi.org/10.1073/pnas.1714744115

Evans, D., Wade, B. S., Henehan, M., Erez, J., & Müller, W. (2016). Revisiting carbonate chemistry controls on planktic foraminifera Mg / Ca: Implications for sea surface temperature and hydrology shifts over the Paleocene-Eocene Thermal Maximum and Eocene-Oligocene transition. *Climate of the Past, 12*(4), 819-835. Article. http://doi.org/10.5194/cp-12-819-2016

Farrell, J. W., Raffi, I., Janecek, T. R., Murray, D. W., Levitan, M., Dadey, K. A., et al. (1995). 35. LATE NEOGENE SEDIMENTATION PATTERNS IN THE EASTERN EQUATORIAL PACIFIC OCEAN1.

Fehrenbacher, J. S., & Martin, P. A. (2014). Exploring the dissolution effect on the intrashell Mg/Ca variability of the planktic foraminifer Globigerinoides ruber. *Paleoceanography, 29*(9), 854-868. https://doi.org/10.1002/2013PA002571

Fehrenbacher, J. S., Spero, H. J., Russell, A. D., Vetter, L., & Eggins, S. (2015). Optimizing LA-ICP-MS analytical procedures for elemental depth profiling of foraminifera shells. *Chemical Geology, 407-408*, 2-9. http://doi.org/10.1016/j.chemgeo.2015.04.007

Foster, G. L., Lear, C. H., & Rae, J. W. B. (2012). The evolution of pCO2, ice volume and climate during the middle Miocene. *Earth and Planetary Science Letters, 341–344*(0), 243-254. http://dx.doi.org/10.1016/j.epsl.2012.06.007

Foster, G. L., & Rae, J. W. (2015). Reconstructing Ocean pH with Boron Isotopes in Foraminifera. *Annual Review of Earth and Planetary Sciences*(0). https://www.annualreviews.org/doi/full/10.1146/annurev-earth-060115-012226#_i63

Geerken, E., De Nooijer, L. J., Van DIjk, I., & Reichart, G.-J. (2018). Impact of salinity on element incorporation in two benthic foraminiferal species with contrasting magnesium contents. *Biogeosciences, 15*(7), 2205-2218. https://doi.org/10.5194/bg-15-2205-2018

Gray, W. R., & Evans, D. (2019). Nonthermal influences on Mg/Ca in planktonic foraminifera: a review of culture studies and application to the Last Glacial Maximum. *Paleoceanography and Paleoclimatology, 34*(3), 306-315. https://doi.org/10.1029/2018PA003517

Gray, W. R., Weldeab, S., Lea, D. W., Rosenthal, Y., Gruber, N., Donner, B., & Fischer, G. (2018). The effects of temperature, salinity, and the carbonate system on Mg/Ca in Globigerinoides ruber (white): A global sediment trap calibration. *Earth and Planetary Science Letters, 482*, 607-620. Article. http://doi.org/10.1016/j.epsl.2017.11.026

Greenop, R., Foster, G. L., Wilson, P. A., & Lear, C. H. (2014). Middle Miocene climate instability associated with high−amplitude CO2 variability. *Paleoceanography, 29*(9), 845-853. https://doi.org/10.1002/2014PA002653

Greenop, R., Hain, M. P., Sosdian, S. M., Oliver, K. I. C., Goodwin, P., Chalk, T. B., et al. (2017). A record of Neogene seawater δ11B reconstructed from paired δ11B analyses on benthic and planktic foraminifera. *Climate of the Past, 13*(2), 149-170. Article. https://doi.org/10.5194/cp-13-149-2017

Guillong, M., L. Meier, D., Allan, M., A. Heinrich, C., & Yardley, B. (2008). *SILLS: A MATLAB-based program for the reduction of laser ablation ICP-MS data of homogeneous materials and inclusions* (Vol. 40).

Hasenfratz, A. P., Martínez-García, A., Jaccard, S. L., Vance, D., Wälle, M., Greaves, M., & Haug, G. H. (2016). Determination of the Mg/Mn ratio in foraminiferal coatings: An approach to correct Mg/Ca temperatures for Mn-rich contaminant phases. *Earth and Planetary Science Letters*. http://dx.doi.org/10.1016/j.epsl.2016.10.004

Hasiuk, F.J. and Lohmann, K.C., 2010. Application of calcite Mg partitioning functions to the reconstruction of paleocean Mg/Ca. Geochimica et Cosmochimica Acta, 74(23), pp.6751-6763. https://doi.org/10.1016/j.gca.2010.07.030

Henehan, M. J., Rae, J. W. B., Foster, G. L., Erez, J., Prentice, K. C., Kucera, M., et al. (2013). Calibration of the boron isotope proxy in the planktonic foraminifera Globigerinoides ruber for use in palaeo-CO2 reconstruction. *Earth and Planetary Science Letters, 364*, 111-122. https://doi.org/10.1016/j.epsl.2012.12.029

Herbert, T. D., Lawrence, K. T., Tzanova, A., Peterson, L. C., Caballero-Gill, R., & Kelly, C. S. (2016). Late Miocene global cooling and the rise of modern ecosystems. *Nature Geoscience*. https://doi.org/10.1038/ngeo2813

Hines, B. R., Hollis, C. J., Atkins, C. B., Baker, J. A., Morgans, H. E. G., & Strong, P. C. (2017). Reduction of oceanic temperature gradients in the early Eocene Southwest Pacific Ocean. *Palaeogeography, Palaeoclimatology, Palaeoecology, 475*, 41-54. https://doi.org/10.1016/j.palaeo.2017.02.037

Holland, K., Branson, O., Haynes, L. L., Hönisch, B., Allen, K. A., Russell, A. D., et al. (2020). Constraining multiple controls on planktic foraminifera Mg/Ca. *Geochimica et Cosmochimica Acta, 273*, 116-136. Article. https://doi.org/10.1016/j.gca.2020.01.015

Hollis, C., Dunkley Jones, T., Anagnostou, E., Bijl, P., Cramwinckel, M., Cui, Y., et al. (2019). The DeepMIP contribution to PMIP4: methodologies for selection, compilation and analysis of latest Paleocene and early Eocene climate proxy data, incorporating version 0.1 of the DeepMIP database. *Geoscientific Model Development Discussions, 2019*, 1-98. http://dx.doi.org/10.5194/gmd-12-3149-2019

Hollis, C., Hines, B., Littler, K., Villasante-Marcos, V., Kulhanek, D., Strong, C., et al. (2015). The Paleocene–Eocene Thermal Maximum at DSDP Site 277, Campbell Plateau, southern Pacific Ocean. https://doi.org/10.5194/cp-11-1009-2015

Hönisch, B., Allen, K. A., Lea, D. W., Spero, H. J., Eggins, S. M., Arbuszewski, J., et al. (2013). The influence of salinity on Mg/Ca in planktic foraminifers–Evidence from cultures, core-top sediments and complementary δ18O. *Geochimica et Cosmochimica Acta, 121*, 196-213. https://doi.org/10.1016/j.gca.2013.07.028

Horita, J., Zimmermann, H., & Holland, H. D. (2002). Chemical evolution of seawater during the Phanerozoic: Implications from the record of marine evaporites. *Geochimica et Cosmochimica Acta, 66*(21), 3733-3756. https://doi.org/10.1016/S0016-7037(01)00884-5

Huang, Y., Clemens, S. C., Liu, W., Wang, Y., & Prell, W. L. (2007). Large-scale hydrological change drove the late Miocene C4 plant expansion in the Himalayan foreland and Arabian Peninsula. *Geology, 35*(6), 531-534. https://doi.org/10.1130/G23666A.1

Hut, G. (1987). Consultants' group meeting on stable isotope reference samples for geochemical and hydrological investigations.

Jiang, S., Wise, S., & Wang, Y. (2007). *Cause of the middle/late Miocene carbonate crash: dissolution or low productivity.* Paper presented at the Proceedings of the Ocean Drilling Program. Scientific Results.

Jochum, K. P., Weis, U., Stoll, B., Kuzmin, D., Yang, Q., Raczek, I., et al. (2011a). Determination of reference values for NIST SRM 610–617 glasses following ISO guidelines. *Geostandards and Geoanalytical Research, 35*(4), 397-429. https://doi.org/10.1111/j.1751-908X.2011.00120.x

Jochum, K.P., Wilson, S.A., Abouchami, W., Amini, M., Chmeleff, J., Eisenhauer, A., Hegner, E., Iaccheri, L.M., Kieffer, B., Krause, J. and McDonough, W.F., (2011b). GSD−1G and

MPI−DING reference glasses for in situ and bulk isotopic determination. Geostandards and Geoanalytical Research, 35(2), pp.193-226. https://doi.org/10.1111/j.1751-908X.2010.00114.x

Keller, G. (1985). Depth stratification of planktonic foraminifers in the Miocene ocean. *The Miocene ocean: paleoceanography and biogeography, 163*, 177-196.

Keller, G., & Barron, J. A. (1987). Paleodepth distribution of Neocene deep−sea hiatuses. *Paleoceanography, 2*(6), 697-713. https://doi.org/10.1029/PA002i006p00697

Kısakürek, B., Eisenhauer, A., Böhm, F., Garbe-Schönberg, D., & Erez, J. (2008). Controls on shell Mg/Ca and Sr/Ca in cultured planktonic foraminiferan, Globigerinoides ruber (white). *Earth and Planetary Science Letters, 273*(3-4), 260-269. https://doi.org/10.1016/j.epsl.2008.06.026

Knorr, G., Butzin, M., Micheels, A., & Lohmann, G. (2011). A warm Miocene climate at low atmospheric CO2 levels. *Geophysical Research Letters, 38*(20). https://doi.org/10.1029/2011GL048873

Koho, K., de Nooijer, L., & Reichart, G. (2015). Combining benthic foraminiferal ecology and shell Mn/Ca to deconvolve past bottom water oxygenation and paleoproductivity. *Geochimica et Cosmochimica Acta, 165*, 294-306. https://doi.org/10.1016/j.gca.2015.06.003

LaRiviere, J. P., Ravelo, A. C., Crimmins, A., Dekens, P. S., Ford, H. L., Lyle, M., & Wara, M. W. (2012). Late Miocene decoupling of oceanic warmth and atmospheric carbon dioxide forcing. *Nature, 486*(7401), 97. https://doi.org/10.1038/nature11200

Lear, C. H., Coxall, H. K., Foster, G. L., Lunt, D. J., Mawbey, E. M., Rosenthal, Y., et al. (2015). Neogene ice volume and ocean temperatures: Insights from infaunal foraminiferal Mg/Ca paleothermometry. *Paleoceanography*. https://doi.org/10.1002/2015PA002833

Lear, C. H., Mawbey, E. M., & Rosenthal, Y. (2010). Cenozoic benthic foraminiferal Mg/Ca and Li/Ca records: Toward unlocking temperatures and saturation states. *Paleoceanography, 25*(4). https://doi.org/10.1029/2009pa001880

Lear, C. H., Rosenthal, Y., & Slowey, N. (2002). Benthic foraminiferal Mg/Ca-paleothermometry: A revised core-top calibration. *Geochimica et Cosmochimica Acta, 66*(19), 3375-3387. https://doi.org/10.1016/S0016-7037(02)00941-9

LeGrande, A. N., & Schmidt, G. A. (2006). Global gridded data set of the oxygen isotopic composition in seawater. *Geophysical Research Letters, 33*(12). https://doi.org/10.1029/2006GL026011

Lemarchand, D., Gaillardet, J., Lewin, E., & Allegre, C. (2002). Boron isotope systematics in large rivers: implications for the marine boron budget and paleo-pH reconstruction over the Cenozoic. *Chemical Geology, 190*(1), 123-140. https://doi.org/10.1016/S0009-2541(02)00114-6

Longerich, H. P., Jackson, S. E., & Günther, D. (1996). Inter-laboratory note. Laser ablation inductively coupled plasma mass spectrometric transient signal data acquisition and analyte concentration calculation. *Journal of analytical atomic spectrometry, 11*(9), 899-904. https://doi.org/10.1039/JA9961100899

Lübbers, J., Kuhnt, W., Holbourn, A. E., Bolton, C. T., Gray, E., Usui, Y., et al. (2019). The middle to late Miocene “Carbonate Crash” in the equatorial Indian Ocean. *Paleoceanography and Paleoclimatology, 34*(5), 813-832. https://doi.org/10.1029/2018PA003482

Lunt, D. J., Flecker, R., Valdes, P. J., Salzmann, U., Gladstone, R., & Haywood, A. M. (2008). A methodology for targeting palaeo proxy data acquisition: A case study for the terrestrial late Miocene. *Earth and Planetary Science Letters, 271*(1), 53-62. https://doi.org/10.1016/j.epsl.2008.03.035

Lyle, M., Dadey, K. A., & Farrell, J. W. (1995). 42. The Late Miocene (11–8 Ma) Eastern Pacific Carbonate Crash: evidence for reorganization of deep-water Circulation by the closure of the Panama Gateway. *1995 Proceedings of the Ocean Drilling Program, Scientific Results, 138*.

Mayk, D., Fietzke, J., Anagnostou, E., & Paytan, A. (2020). LA-MC-ICP-MS study of boron isotopes in individual planktonic foraminifera: A novel approach to obtain seasonal variability patterns. *Chemical Geology, 531*. Article. https://doi.org/10.1016/j.chemgeo.2019.119351

Müller, P. J., Kirst, G., Ruhland, G., Von Storch, I., & Rosell-Melé, A. (1998). Calibration of the alkenone paleotemperature index U 37 K′ based on core-tops from the eastern South Atlantic and the global ocean (60 N-60 S). *Geochimica et Cosmochimica Acta, 62*(10), 1757-1772. https://doi.org/10.1016/S0016-7037(98)00097-0

Nairn, M. (2018). *Mid-Late Miocene climate constrained by a new Laser Ablation ICP-MS set up.* Cardiff University,

Nürnberg, D., Bijma, J., & Hemleben, C. (1996). Assessing the reliability of magnesium in foraminiferal calcite as a proxy for water mass temperatures. *Geochimica et Cosmochimica Acta, 60*(5), 803-814.

Pagani, M., Freeman, K. H., & Arthur, M. A. (1999). Late Miocene Atmospheric CO₂ Concentrations and the Expansion of C₄ Grasses. *Science, 285*(5429), 876-879. https://doi.org/10.1126/science.285.5429.876

Pearson, P. N., & Burgess, C. E. (2008). Foraminifer test preservation and diagenesis: comparison of high latitude Eocene sites. *Geological Society, London, Special Publications, 303*(1), 59-72. https://doi.org/10.1144/SP303.5

Pearson, P. N., Ditchfield, P. W., Singano, J., Harcourt-Brown, K. G., Nicholas, C. J., Olsson, R. K., et al. (2001). Warm tropical sea surface temperatures in the Late Cretaceous and Eocene epochs. *Nature, 413*(6855), 481-487. https://doi.org/10.1038/35097000

Pena, L., Calvo, E., Cacho, I., Eggins, S., & Pelejero, C. (2005). Identification and removal of Mn−Mg−rich contaminant phases on foraminiferal tests: Implications for Mg/Ca past temperature reconstructions. *Geochemistry, Geophysics, Geosystems, 6*(9). https://doi.org/10.1029/2005GC000930

Petersen, J., Barras, C., Bézos, A., La, C., De Nooijer, L. J., Meysman, F. J. R., et al. (2018). Mn/Ca intra- and inter-test variability in the benthic foraminifer Ammonia tepida. *Biogeosciences, 15*(1), 331-348. Article. https://doi.org/10.5194/bg-15-331-2018

Pisias, N., & Mix, A. (1988). *Aliasing of the geologic record and the search for long-period Milankovitch cycles* (Vol. 3).

Pound, M. J., Haywood, A. M., Salzmann, U., Riding, J. B., Lunt, D. J., & Hunter, S. J. (2011). A Tortonian (Late Miocene, 11.61–7.25Ma) global vegetation reconstruction. *Palaeogeography, Palaeoclimatology, Palaeoecology, 300*(1), 29-45. https://doi.org/10.1016/j.palaeo.2010.11.029

Raffi, I., Wade, B.S., Pälike, H., Beu, A.G., Cooper, R., Crundwell, M.P., Krijgsman, W., Moore, T., Raine, I., Sardella, R. and Vernyhorova, Y.V. (2020). The Neogene Period. In Geologic Time Scale 2020, (pp. 1141-1215). *Elsevier.* https://doi.org/10.1016/B978-0-12-824360-2.00029-2.

Raitzsch, M., & Hönisch, B. (2013). Cenozoic boron isotope variations in benthic foraminifers. *Geology, 41*(5), 591-594. https://doi.org/10.1130/g34031.1

Raitzsch, M., Kuhnert, H., Hathorne, E. C., Groeneveld, J., & Bickert, T. (2011). U/Ca in benthic foraminifers: A proxy for the deep−sea carbonate saturation. *Geochemistry, Geophysics, Geosystems, 12*(6). https://doi.org/10.1029/2010GC003344

Rathmann, S., Hess, S., Kuhnert, H., & Mulitza, S. (2004). Mg/Ca ratios of the benthic foraminifera Oridorsalis umbonatus obtained by laser ablation from core top sediments: Relationship to bottom water temperature. *Geochemistry, Geophysics, Geosystems, 5*(12). https://doi.org/10.1029/2004gc000808

Reichart, G.-J., Jorissen, F., Anschutz, P., & Mason, P. R. (2003). Single foraminiferal test chemistry records the marine environment. *Geology, 31*(4), 355-358. https://doi.org/10.1130/0091-7613(2003)031<0355:SFTCRT>2.0.CO;2

Rosenthal, Y., Boyle, E. A., & Slowey, N. (1997). Temperature control on the incorporation of magnesium, strontium, fluorine, and cadmium into benthic foraminiferal shells from Little Bahama Bank: Prospects for thermocline paleoceanography. *Geochimica et Cosmochimica Acta, 61*(17), 3633-3643.

Rousselle, G., Beltran, C., Sicre, M.-A., Raffi, I., & De Rafélis, M. (2013). Changes in sea-surface conditions in the Equatorial Pacific during the middle Miocene–Pliocene as inferred from coccolith geochemistry. *Earth and Planetary Science Letters, 361*, 412-421. http://dx.doi.org/10.1016/j.epsl.2012.11.003

Russell, A. D., Hönisch, B., Spero, H. J., & Lea, D. W. (2004). Effects of seawater carbonate ion concentration and temperature on shell U, Mg, and Sr in cultured planktonic foraminifera. *Geochimica et Cosmochimica Acta, 68*(21), 4347-4361. https://doi.org/10.1016/j.gca.2004.03.013

Sadekov, A., Eggins, S. M., De Deckker, P., & Kroon, D. (2008). Uncertainties in seawater thermometry deriving from intratest and intertest Mg/Ca variability in Globigerinoides ruber. *Paleoceanography, 23*(1). https://doi.org/10.1029/2007pa001452

Sadekov, A. Y., Eggins, S. M., & De Deckker, P. (2005). Characterization of Mg/Ca distributions in planktonic foraminifera species by electron microprobe mapping. *Geochemistry, Geophysics, Geosystems, 6*(12). https://doi.org/10.1029/2005GC000973

Schiebel, R., & Hemleben, C. (2017). *Planktic Foraminifers in the Modern Ocean*.

Schlitzer, R., Ocean Data View, odv.awi.de, (2018).

Seki, O., Schmidt, D., Schouten, S., C. Hopmans, E., Sinninghe-Damste, J., & D. Pancost, R. (2012). *Paleoceanographic changes in the Eastern Equatorial Pacific over the last 10 Myr* (Vol. 27).

Sexton, P. F., Wilson, P. A., & Pearson, P. N. (2006). Microstructural and geochemical perspectives on planktic foraminiferal preservation:"Glassy" versus "Frosty". *Geochemistry, Geophysics, Geosystems, 7*(12). https://doi.org/10.1029/2006GC001291

Sosdian, S. M., Greenop, R., Hain, M. P., Foster, G. L., Pearson, P. N., & Lear, C. H. (2018). Constraining the evolution of Neogene ocean carbonate chemistry using the boron isotope pH proxy. *Earth and Planetary Science Letters, 498*, 362-376. https://doi.org/10.1016/j.epsl.2018.06.017

Sosdian, S.M. and Lear, C.H. (2020). Initiation of the Western Pacific Warm Pool at the Middle Miocene Climate Transition? *Paleoceanography and Paleoclimatology, 35(12)*, e2020PA003920. https://doi.org/10.1029/2020PA003920

Stewart, D. R. M., Pearson, P. N., Ditchfield, P. W., & Singano, J. M. (2004). Miocene tropical Indian Ocean temperatures: evidence from three exceptionally preserved foraminiferal assemblages from Tanzania. *Journal of African Earth Sciences, 40*(3), 173-189. https://doi.org/10.1016/j.jafrearsci.2004.09.001

Stoll, H. M., Guitian, J., Hernandez-Almeida, I., Mejia, L. M., Phelps, S., Polissar, P., et al. (2019). Upregulation of phytoplankton carbon concentrating mechanisms during low CO2 glacial periods and implications for the phytoplankton pCO2 proxy. *Quaternary Science Reviews, 208*, 1-20. https://doi.org/10.1016/j.quascirev.2019.01.012

Super, J. R., Thomas, E., Pagani, M., Huber, M., O'Brien, C., & Hull, P. M. (2018). North Atlantic temperature and p CO2 coupling in the early-middle Miocene. *Geology, 46*(6), 519-522. https://doi.org/10.1130/G40228.1

Thil, F., Blamart, D., Assailly, C., Lazareth, C. E., Leblanc, T., Butsher, J., & Douville, E. (2016). Development of laser ablation multi-collector inductively coupled plasma mass spectrometry for boron isotopic measurement in marine biocarbonates: New improvements and application to a modern Porites coral. *Rapid Communications in Mass Spectrometry, 30*(3), 359-371. Article. https://doi.org/10.1002/rcm.7448

van Hinsbergen, D. J., de Groot, L. V., van Schaik, S. J., Spakman, W., Bijl, P. K., Sluijs, A., et al. (2015). A paleolatitude calculator for paleoclimate studies. *PloS one, 10*(6). https://doi.org/DOI:10.1371/journal.pone.0126946

Vetter, L., Kozdon, R., Mora, C. I., Eggins, S. M., Valley, J. W., Hönisch, B., & Spero, H. J. (2013). Micron-scale intrashell oxygen isotope variation in cultured planktic foraminifers. *Geochimica et Cosmochimica Acta, 107*, 267-278. https://doi.org/10.1016/j.gca.2012.12.046

von der Heydt, A., & Dijkstra, H. A. (2006). Effect of ocean gateways on the global ocean circulation in the late Oligocene and early Miocene. *Paleoceanography, 21*(1). https://doi.org/10.1029/2005pa001149

Wade, B. S., Pearson, P. N., Berggren, W. A., & Pälike, H. (2011). Review and revision of Cenozoic tropical planktonic foraminiferal biostratigraphy and calibration to the geomagnetic polarity and astronomical time scale. *Earth-Science Reviews, 104*(1), 111-142. https://doi.org/10.1016/j.earscirev.2010.09.003

Yu, J., & Elderfield, H. (2008). Mg/Ca in the benthic foraminifera< i> Cibicidoides wuellerstorfi</i> and< i> Cibicidoides mundulus</i>: Temperature versus carbonate ion saturation. *Earth and Planetary Science Letters, 276*(1), 129-139. https://doi.org/10.1016/j.epsl.2008.09.015

Zachos, J. C., Stott, L. D., & Lohmann, K. C. (1994). Evolution of early Cenozoic marine temperatures. *Paleoceanography, 9*(2), 353-387. https://doi.org/10.1029/93PA03266

Zhang, Y. G., Pagani, M., & Liu, Z. (2014). A 12-Million-Year Temperature History of the Tropical Pacific Ocean. *Science, 344*(6179), 84-87. https://doi.org/10.1126/science.1246172

[Paleoceanography and Paleoclimatology]

Supporting Information for

Tropical Sea Surface Temperatures following the Middle Miocene Climate Transition from Laser-Ablation ICP-MS analysis of glassy foraminifera

Michael G. Nairn[1], Caroline H. Lear[1], Sindia M. Sosdian[1], Trevor R Bailey[2], and Simon Beavington-Penney[3]

[1]School of Earth and Environmental Sciences, Cardiff University, Cardiff, UK, [2]Department of Natural Sciences, Amgueddfa Cymru, National Museum Wales, Cathays Park, Cardiff, [3] BG Group, 100 Thames Valley Park Drive, Reading, RG6 1PT, UK*

*Current address: Department of Earth and Environmental Sciences, The University of Manchester, Williamson Building, Oxford Road, Manchester, M13 9PL, UK.

Contents of this file

Introduction
Figures S1 to S10
Table S4

Additional Supporting Information (Files uploaded separately)

Tables S1 to S3, and S5 to S11.

Introduction

This supporting information contains the age-depth model for the Sunbird-1 well used in this study, a figure comparing Mg/Ca ratios from solution-based and laser-ablation ICP-MS, a figure showing the relationship between Mg/Ca ratios and those of Al/Ca and Mn/Ca from a LA-ICP-MS sample, a figure showing the seawater Mg/Ca curve used to correct Mg/Ca for changes in seawater Mg/Ca, a figure showing the surface pH record used to correct Mg/Ca for changes in the carbonate system, a figure comparing SST estimates using both the *Anand et al.* (2003) and the *Evans et al.* (2016) approaches, a figure showing the covariance between solution-based

Mg/Ca ratios and those of Mn/Ca, Al/Ca, and U/Ca at Sunbird-1, a version of Figure 5 using the alternative approach of *Evans et al.* (2016) to calculate SST, a version of Figure 6 using the alternative approach of *Evans et al.* (2016) to calculate SST, and a figure showing *D. altispira* mean test weights.

There are 11 data tables, with all but Table S4 uploaded separately. Tables S1 to S3 show downcore % coarse fraction, $\delta^{18}O$, and solution-based ICP-MS data from Sunbird-1. Table S4 shows the LA-ICP-MS parameters used. There are further tables of the LA-ICP-MS trace metal data for all profiles from the 1551-1554m sample, the downcore LA-ICP-MS Mg/Ca ratios for all samples, a data table indicating the age range of pooled samples, and the downcore LA-ICP-MS Mg/Ca ratios distinguishing between pooled and unpooled samples. There are then data tables for the alternative sea surface temperature downcore record from LA-ICP-MS Mg/Ca data, and from the $\delta^{18}O$ data. The final data table provides *D. altispira* mean test weights.

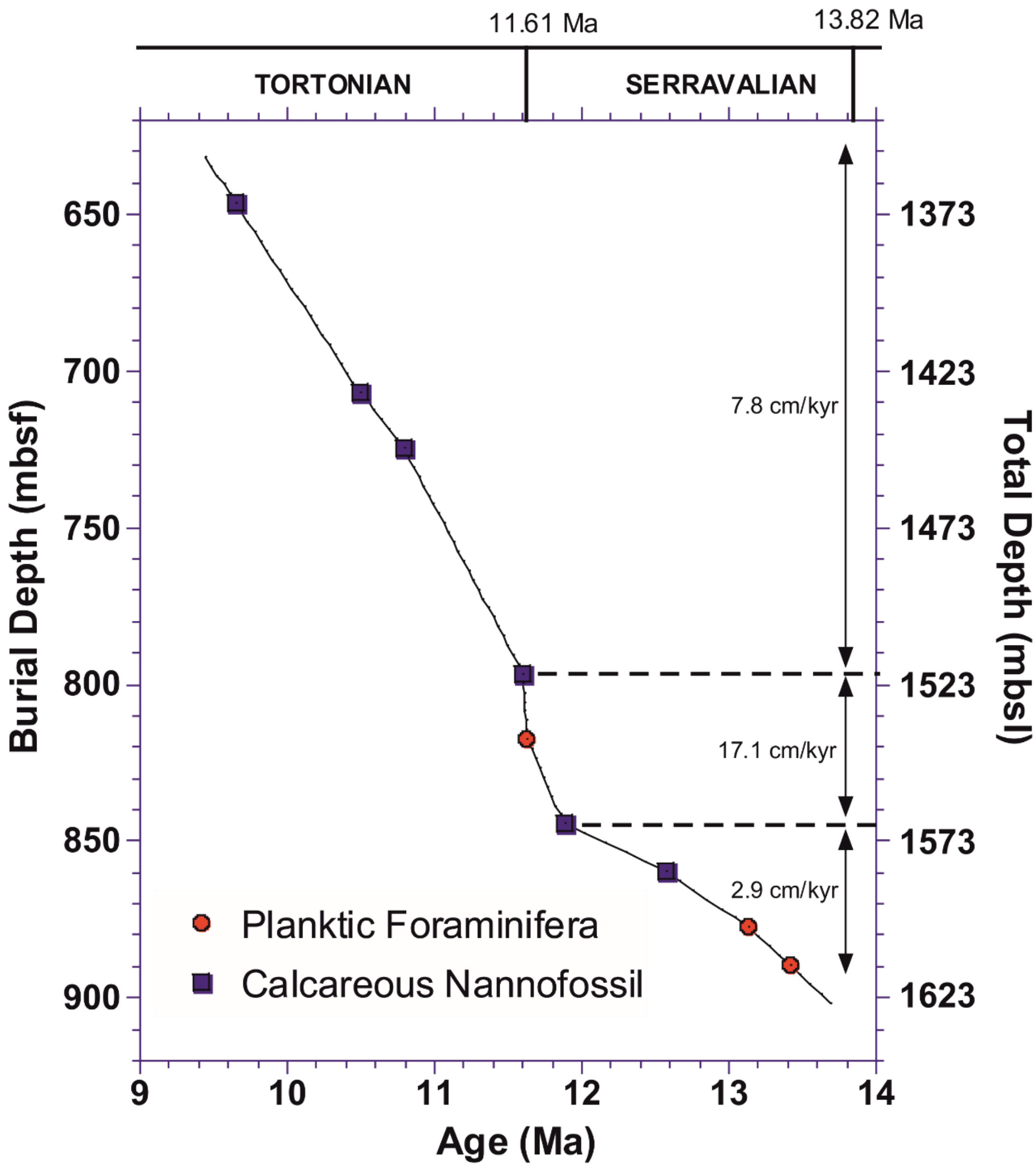

Figure S1. Age-depth model for Sunbird-1 using the biostratigraphic zonations of *Wade et al.* (2011) and *Backman et al.* (2012) updated in the astronomically tuned timescale of *Raffi et al.* (2020) using linear interpolation between reliable biostratigraphic datums. Burial depth in the sediment and the total depth below the sea surface are given (water depth =723m). Micropaleontological and calcareous nannoplankton assemblages for Sunbird-1 were analyzed by Haydon Bailey and Liam Gallagher of Network Stratigraphic Consulting.

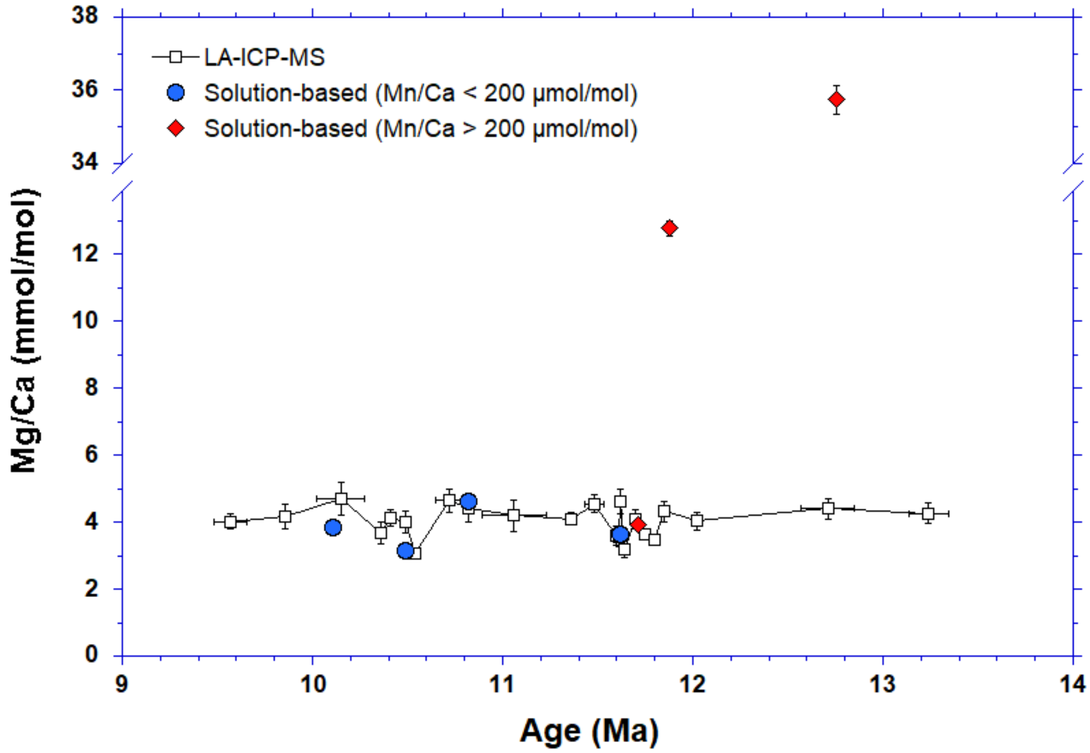

Figure S2. Comparison of Sunbird-1 *D. altispira* Mg/Ca results from LA-ICP-MS analysis (white squares) and reductively cleaned, solution-based analysis where blue circles represent values with Mn/Ca < 200 µmol/mol and red diamonds represent values with Mn/Ca > 200 µmol/mol. Error bars on the LA-ICP-MS data denote the age range for pooled samples and the ± 2SE of Mg/Ca from all depth profiles in the sample. Error bars on the solution-based data denote the ± 2SD from the analysis. Note the break between 13.9 mmol/mol and 34 mmol/mol.

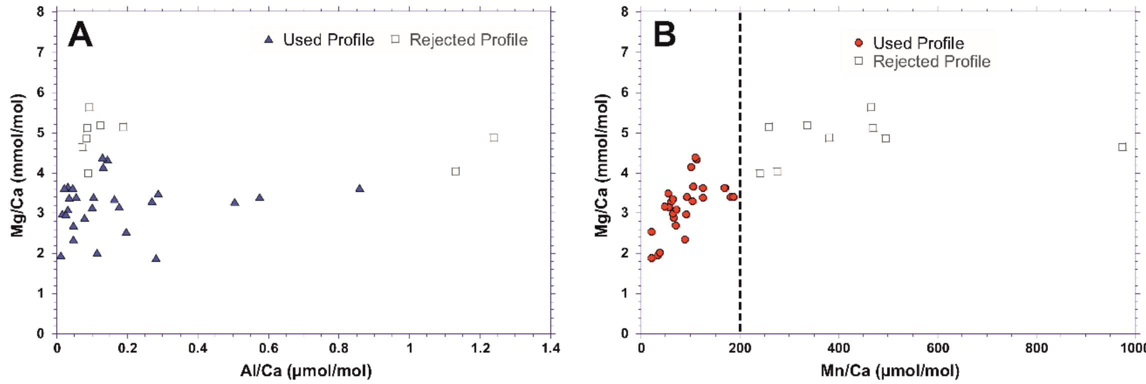

Figure S3. Covariance between *D. altispira* Mg/Ca and (a) Al/Ca, and (b) Mn/Ca from LA-ICP-MS profiles from the 1539-1542 m sample. Used profiles are filled blue triangles and red circles, respectively, whereas profiles excluded during screening are open squares.

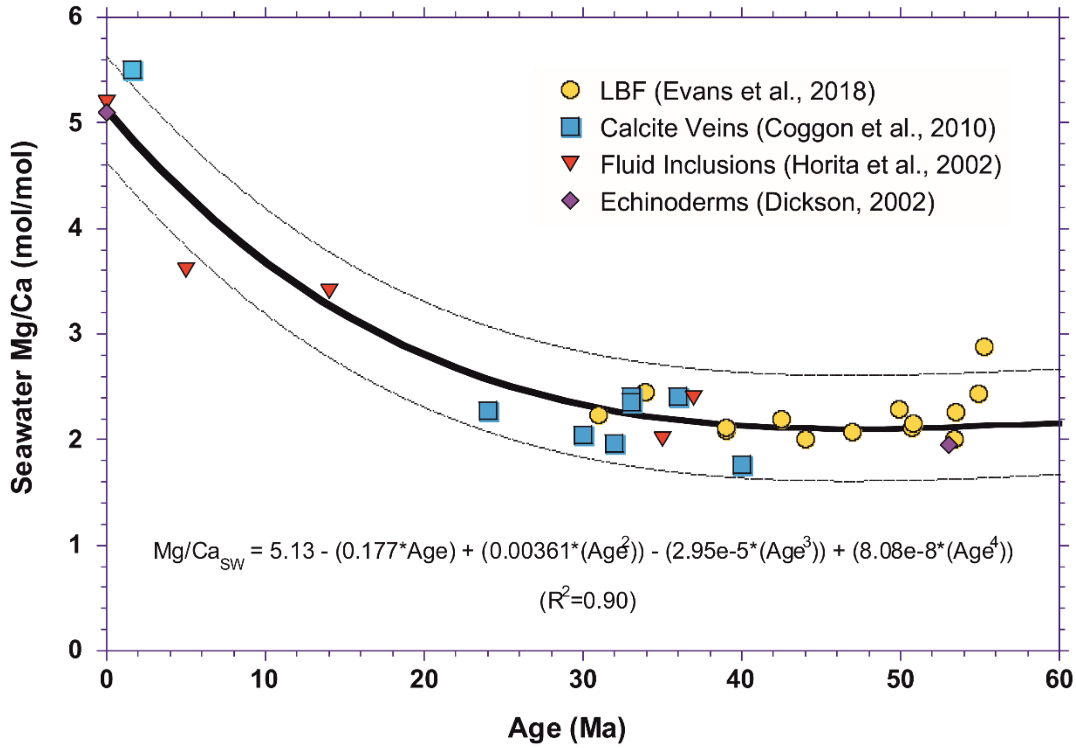

Figure S4. The evolution of seawater Mg/Ca (Mg/Ca$_{SW}$) through the Cenozoic from records of large benthic foraminifera (LBF) (*Evans et al.*, 2018) (yellow circles), calcite veins (*Coggon et al.*, 2010) (blue squares), fluid inclusions (*Horita et al.*, 2002) (red triangles), and echinoderms (Dickson, 2002) (purple diamonds). Fourth order polynomial fit (thick black line) through the compiled data. The thin lines represent a ±0.5 mol/mol uncertainty window used in the following temperature calculations.

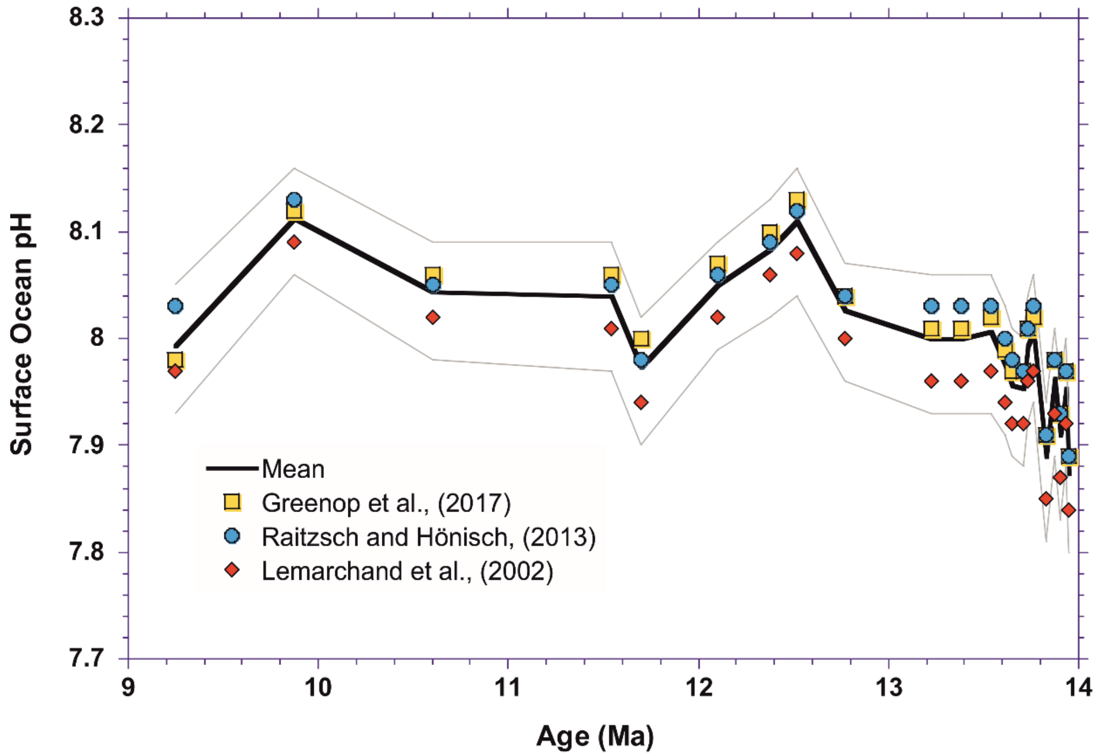

Figure S5. Surface ocean pH determined using $\delta^{11}B$ measurements on planktic foraminifera from a global distribution of open ocean sites (Sosdian et al., 2018). Three $\delta^{11}B_{SW}$ scenarios are used (*Greenop et al.*, 2017, *Lemarchand et al.*, 2002, *Raitzsch and Hönisch*, 2013). Uncertainty envelopes denote the maximum and minimum pH at the 17% and 83% confidence interval, independent of the $\delta^{11}B_{SW}$ scenario.

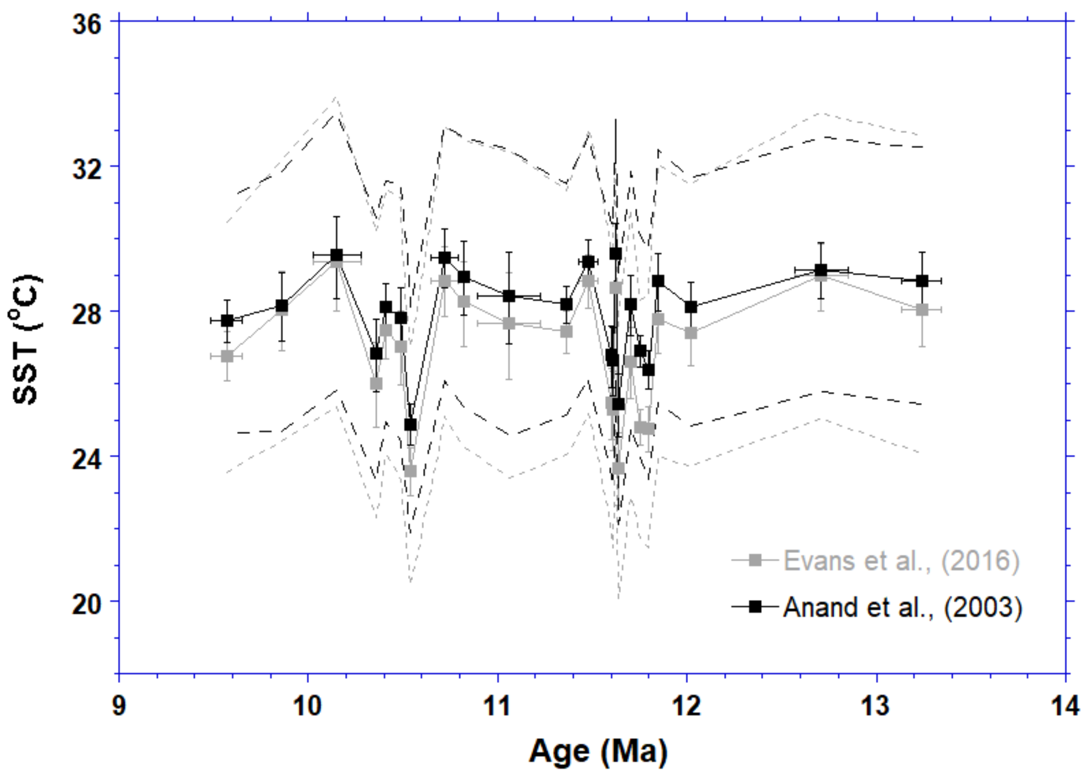

Figure S6. Sea surface temperature record at Sunbird-1 from LA-ICP-MS Mg/Ca using the preferred approach of *Anand et al.*(2003), without a pH correction (black squares), and the alternative approach of *Evans et al.* (2016) (grey squares). Vertical error bars denote the sample uncertainty (± 2SE) and horizontal error bars denote the age range of pooled samples. Dashed black and grey lines denote the full uncertainty on the temperature estimates, including that derived from the calibration uncertainty.

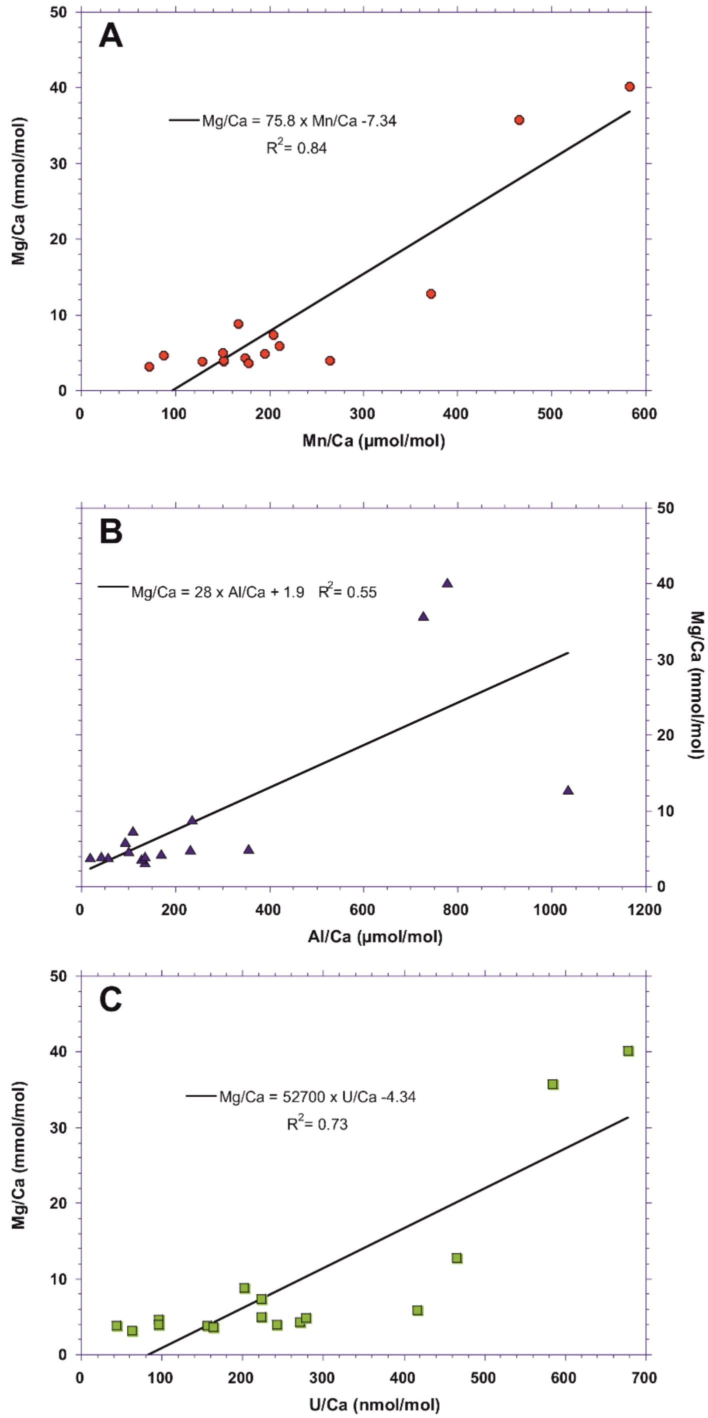

Figure S7. Covariance plots between *D. altispira* Mg/Ca and (a) Mn/Ca (red circles), (b) Al/Ca (blue triangles), and (c) U/Ca (green squares) from solution-based ICP-MS. R2 correlations for all plots are given.

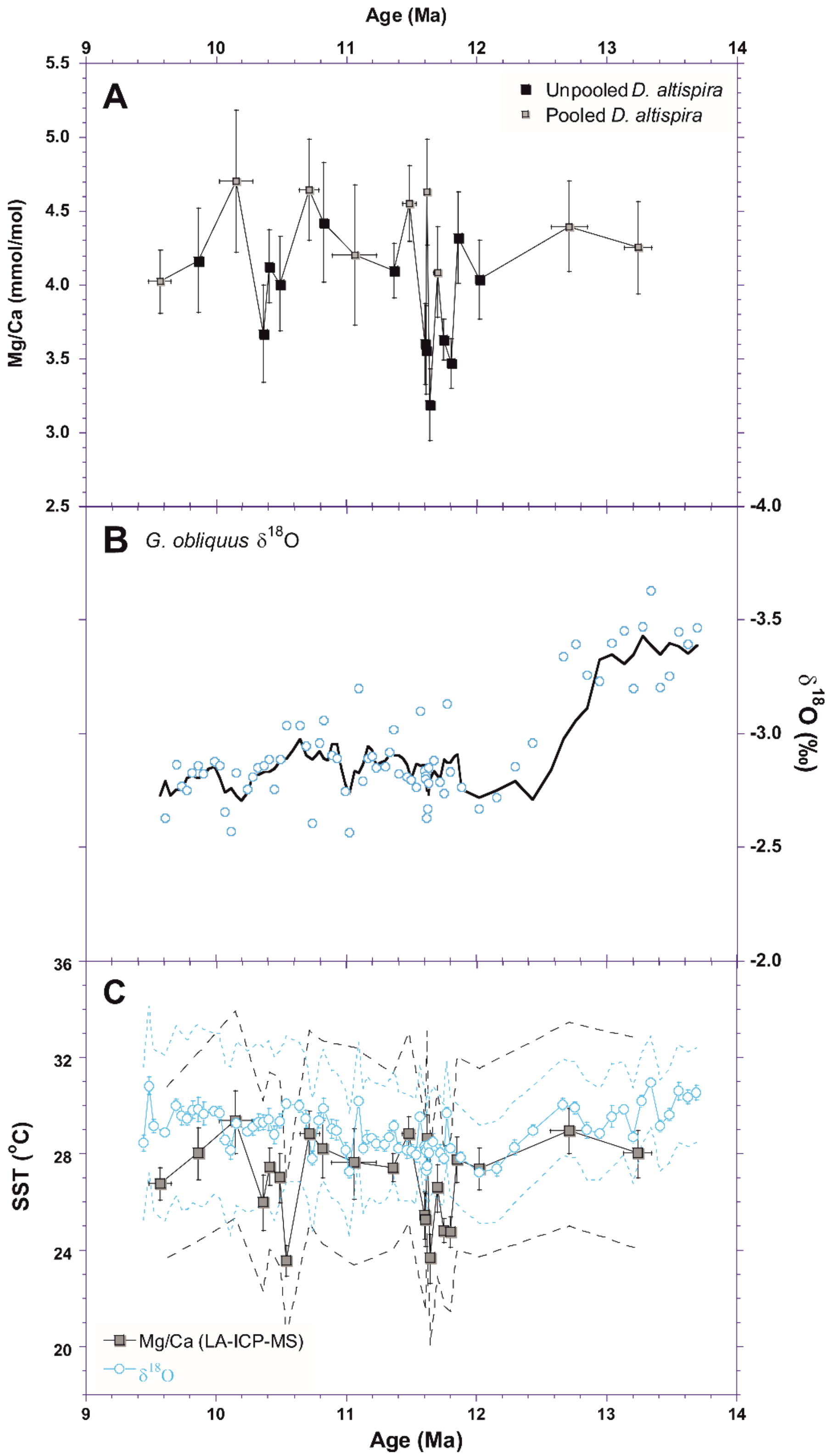

Figure S8. (a) Mean *D. altispira* LA-ICP-MS Mg/Ca ratios (mmol/mol) for unpooled (black squares) and pooled (grey squares) samples from Sunbird-1. Error bars denote the age range for pooled samples, and the ± 2SE of Mg/Ca from all depth profiles in the sample. (b) *G. obliquus* $\delta^{18}O$ from Sunbird-1. Solid line is a five-point moving average. (c) Sea surface temperature records at Sunbird-1 from planktic foraminiferal δ18O, and LA-ICP-MS Mg/Ca using the alternative approach of *Evans et al.* (2016). Symbols are the same as in (a) and (b). Error bars on the $\delta^{18}O$ record denote the analytical uncertainty (± 2SD), and error bars on the Mg/Ca record denote the sample uncertainty (± 2SE). As in (a), pooled Mg/Ca samples also have horizontal error bars denoting the sample age range. Dashed blue and black lines denote the full uncertainty on the temperature estimates, including that derived from the calibration uncertainty, for $\delta^{18}O$ and LA-ICP-MS Mg/Ca respectively. Figure 5 provides LA-ICP-MS Mg/Ca sea surface temperatures using the preferred approach of *Anand et al.* (2003) without a pH correction.

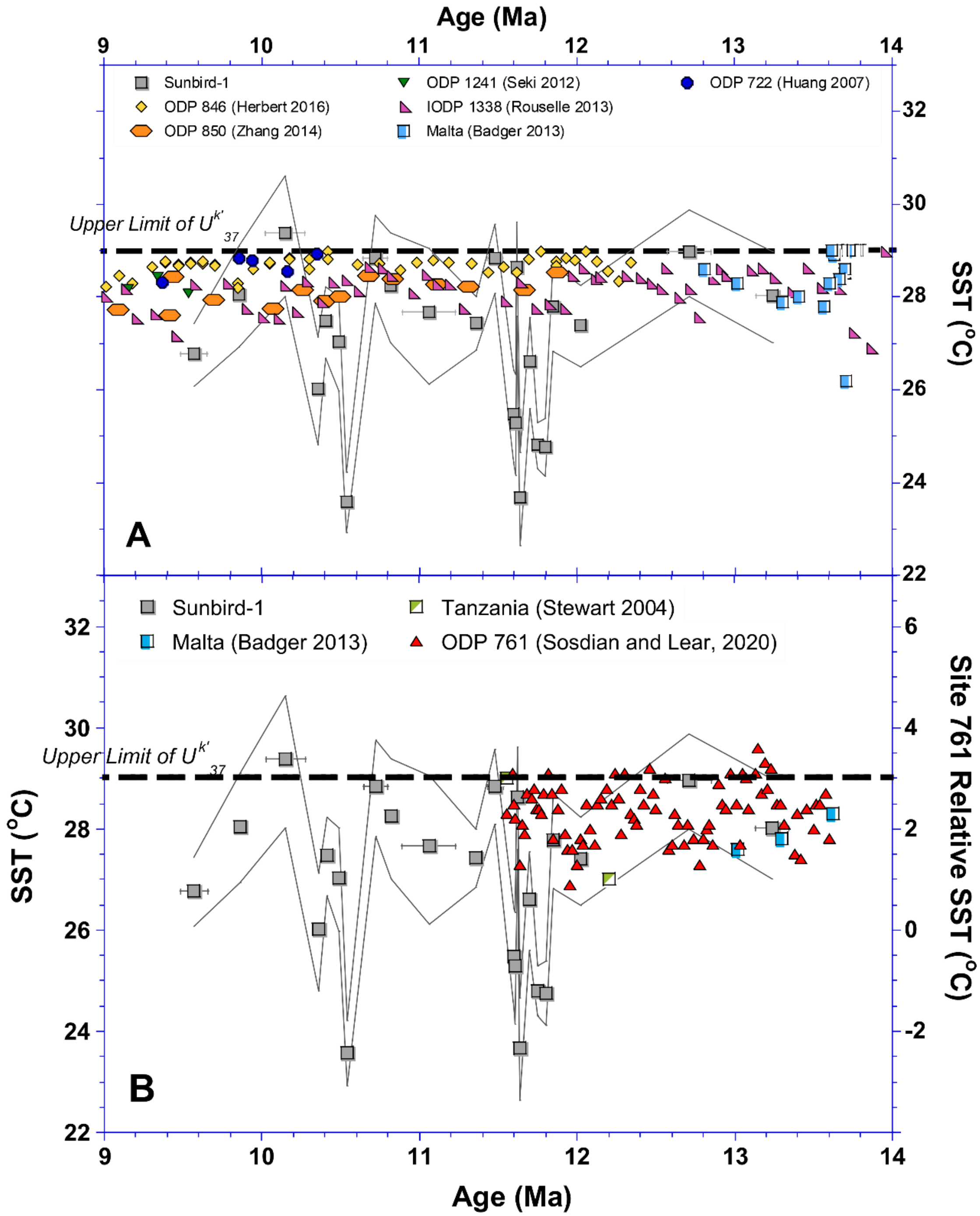

Figure S9. Sunbird-1 LA-ICP-MS Mg/Ca derived SST using the approach of *Evans et al.* (2016) compared to SST estimates at contemporaneous sites from (a) Uk37, and (b) foraminiferal geochemistry. Estimates applying Uk37 are from ODP Site 722 (*Huang et al.*, 2007) in the Arabian Sea, ODP & IODP Sites 846 (*Herbert et al.*, 2016), 850 (*Zhang et al.*, 2014), 1241 (*Seki et al.*, 2012), and U1338 (*Rousselle et al.*, 2013) in the Eastern Equatorial Pacific, and terrestrial outcrops in Malta (*Badger et al.*, 2013). Estimates applying the foraminiferal Mg/Ca proxy are from ODP Sites 761 (*Sosdian and Lear*, 2020) and terrestrial outcrops in Malta (*Badger et al.*, 2013). ODP Site 761 is displayed on an alternative axis as SST anomalies relative to the baseline average from 16.0 – 15.5 Ma. Two temperature estimates using the $\delta^{18}O$ of exceptionally preserved foraminifera from Tanzania are also shown (*Stewart et al.*, 2004). The upper limit for the Uk37 proxy (29⁰C) is marked by the thick dashed black line. All previously published records used for comparison are kept on their original age models.

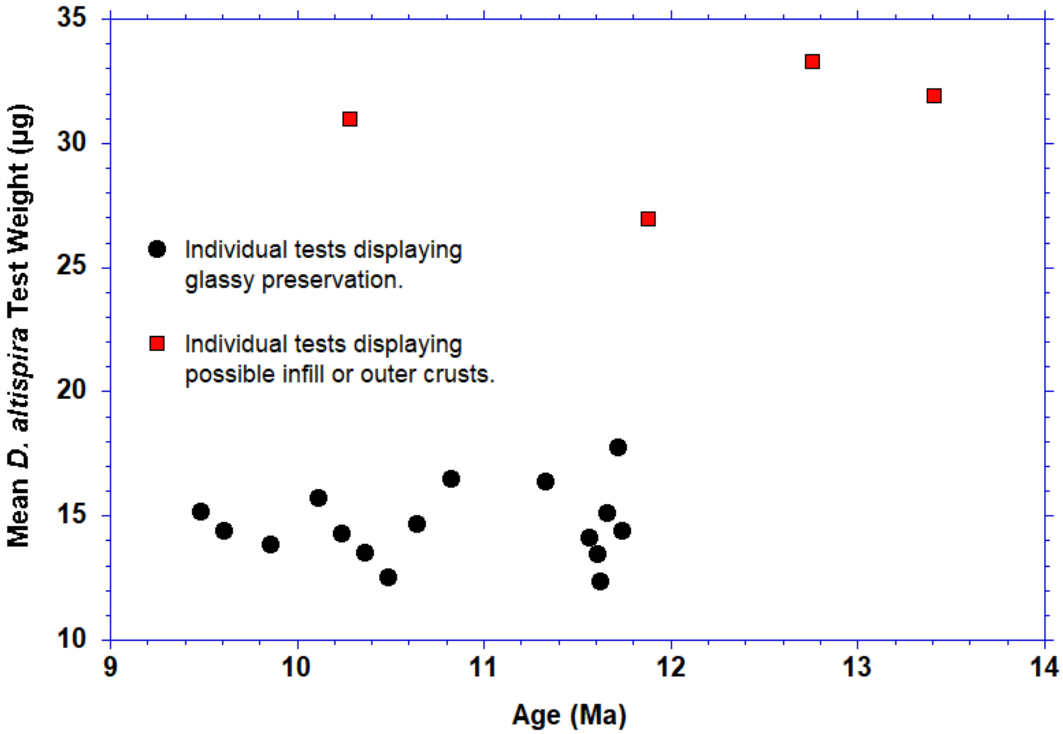

Figure S10. Mean *D. altispira* test weight (µg) for samples measured by solution ICP-MS (Supplementary Table S3) in the Sunbird-1 core. Samples noted to have individuals displaying either infill or outer crusts prior to chemical cleaning are displayed as red squares.

Table S1: Weighed coarse fraction (% >63µm) in the Sunbird-1 core. The 1353-1356m, 1356-1359m, and 1575-1578m samples (marked by an asterisk) were rejected due to the presence of concrete, emplaced by the drilling process, artificially raising the % coarse fraction.

Table S2: *Globigerinoides obliquus* $\delta^{18}O$ ratios in the Sunbird-1 core. Foraminiferal abundance from thirteen samples (marked with an asterisk) was insufficient for analysis.

Table S3: Solution-based *Dentoglobigerina altispira* trace metal/calcium ratios from Sunbird-1. We distinguish between those cleaned with and without the reductive cleaning step**.**

ICP-MS: Thermo Element XR

RF Power	1300 Watts
Torch Position (X, Y, Z)	2.5, -0.2, -4.5 mm
Argon Carrier Flow (optimised daily)	~0.90 l/min
Argon Coolant Flow	14 l/min
Argon Auxiliary Flow	0.80 l/min
Sweep Time	350 ms
Cones	Ni

Laser Ablation System: RESOlution S-155

Helium Flow	350 ml/min
N_2 Flow	4 ml/min
Spot Size	50 µm
Scan Speed	3 μms^{-1}
Fluence	3.5 Jcm^{-2}
Repetition Rate	2.0 Hz
ThO^+/Th^+	<0.4%
U^+/Th^+	~1

Table S4. Operating parameters of LA-ICP-MS for *Dentoglobigerina altispira* analyses. ICP-MS parameters were optimized daily during tuning, and typical operating values are stated.

Table S5. *Dentogloboquadrina altispira* LA-ICP-MS Mg/Ca ratios from the 1551-1554m sample in the Sunbird-1 core. Up to 10 profiles through 10 tests were analyzed for each species. Highlighted samples were excluded due to elevated Mn/Ca and/or Al/Ca ratios.

Table S6. Summary of *Dentogloboquadrina altispira* Mg/Ca ratios in the Sunbird-1 core from LA-ICP-MS analyses. Highlighted samples do not contain the required number of profiles for the Mg/Ca value to be considered representative for the sample.

Table S7. Age range and the number of samples, specimens, and profiles combined for each pooled sample of D. altispira from Sunbird-1.

Table S8. Summary of pooled and unpooled *Dentogloboquadrina altispira* mean Mg/Ca ratios in the Sunbird-1 core from LA-ICP-MS analyses. Minimum and maximum age refer to the age range of the pooled samples (Supplementary Table S7).

Table S9. Sea Surface Temperatures calculated from the unpooled and pooled *Dentogloboquadrina altispira* mean Mg/Ca ratios in the Sunbird-1 core from LA-ICP-MS analyses (Supplementary Table S8). Minimum and maximum age refer to the age range of the pooled samples (Supplementary Table S7). pH is calculated by linear interpolation between the pH measurements of *Sosdian et al.* (2018) (Supplementary Figure S5). pH corrected Mg/Ca is calculated using the multi-species calibration of *Evans et al*. (2016) (Equation 3). Seawater Mg/Ca is calculated from this study using Supplementary Figure S4. The pre-exponential (B) and exponential (A) constants of the Mg/Ca-temperature calibration are calculated using the calibration of *Evans et al.* (2016b), (Equation 4 and 5). Temperature is calculated as ln((Mg/Ca)/B)/A, using the values of B and A calculated in the previous columns. Maximum and Minimum temperatures refer to the full range of absolute temperatures derived incorporating the analytical and calibration uncertainty. Analytical Error Only Maximum and Minimum temperatures refer to the range of temperatures derived from the analytical and analytical uncertainty only.

Table S10. Supplementary Table S10: Sea Surface Temperatures calculated from *Globigerinoides obliqus* $\delta^{18}O$ ratios in the Sunbird-1 core (Supplementary Table S2) using the calibration of *Bemis et al.* (1998) (Equation 4). Calibration uncertainty includes ± 0.091 ‰ due to any potential influence of salinity (*LeGrande and Schmidt,* 2006) and seawater $\delta^{18}O$ (*Cramer et al.* 2011). This $\delta^{18}O_{SW}$ was converted from VSMOW to VPDB by incorporating a -0.27‰

correction (*Hut*, 1987). Maximum and Minimum temperatures refer to the full range of absolute temperatures derived incorporating the analytical and calibration uncertainty. Analytical Error Only Maximum and Minimum temperatures refer to the range of temperatures derived from the analytical uncertainty only**.**

Table S11. Supplementary Table S11: Mean *Dentoglobigerina altispira* test weight (µg) for samples measured by solution ICP-MS (Supplementary Table S3) in the Sunbird-1 core. Samples at 1413-1416m, 1566-1569m, 1587-1590m, and 1611-1614m depths (marked by an asterisk) were noted to have individuals displaying either infill or outer crusts, prior to chemical cleaning.